

Disrupters of the thymidylate synthase homodimer accelerate its proteasomal degradation and inhibit cancer growth.

Authors: Luca Costantino^{1‡}, Stefania Ferrari^{1‡}, Matteo Santucci^{1‡}, Outi M. H. Salo-Ahen^{3&}, Emanuele Carosati^{4,x}, Silvia Franchini¹, Angela Lauriola^{2±}, Cecilia Pozzi⁵, Gaetano Marverti², Matteo Trande^{1±}, Gaia Gozzi¹, Puneet Saxena^{1#}, Giuseppe Cannazza¹, Lorena Losi¹, Daniela Cardinale⁶, Alberto Venturelli^{1,£}, Antonio Quotadamo¹, Pasquale Linciano¹, Remo Guerrini⁷, Salvatore Pacifico⁷, Rosaria Luciani¹, Filippo Genovese¹, Stefan Henrich³, Silvia Alboni¹, Nuno Santarem⁸, Anabela da Silva Cordeiro^{8,9}, Elisa Giovannetti^{10,11}, Godefridus J Peters^{12^}, Paolo Pinton¹¹, Alessandro Rimessi¹¹, Gabriele Cruciani⁴, Robert M. Stroud^{13,†}, Rebecca C. Wade^{3,14,15,†}, Stefano Mangani^{5†}, Domenico D'Arca^{2*}, Glauco Ponterini^{1*} & Maria Paola Costi^{1*}.

Author	Contribution
Alboni Silvia	Performed the anticancer activity of hTS dimer disrupters and molecular biology studies: BS3 experiments, mutants experiments.
Cannazza Giuseppe	Performed the chromatographic enantioseparation of E7 enantiomers and determined the kinetic of racemization
Carosati Emanuele	Molecular modelling of small molecules (virtual screening)
Cordeiro Anabela	Preliminary PK on mice, living cells, FRET assays and general supervision of both experiments.
Costantino Luca	Conceived the chemistry work. Designed and synthesized the compounds.
Costi Maria Paola	Coordinate the work, conceived the work design and wrote the manuscript.
Cruciani Gabriele	Supervision of the small molecule modelling experiments.
Cardinale Daniela	Performed protein purification.
D'Arca Domenico	Conceived the molecular biology and chemical biology work. Supervised the anticancer activity of hTS dimer disrupters and molecular biology studies.
Ferrari Stefania	Coordinated the work together with MP Costi and wrote the manuscript.
Franchini Silvia	Performed the tethering experiments and analysed the mass-spectrometry data.

Genovese Filippo	Performed the tethering experiments and analysed the mass-spectrometry data
Giovannetti Elisa	Performed the pharmacology experiments with in vivo orthotopic pancreatic cancer.
Gozzi Gaia	Performed the anticancer activity of hTS dimer disrupters and molecular biology studies.
Guerrini Remo	Performed the synthesis of the E5 ligand conjugated with FITC probe.
Henrich Stefan	Performed the computational studies on tethered complexes.
Lauriola Angela	Performed the anticancer activity of hTS dimer disrupters and molecular biology studies.
Linciano Pasquale	Performed the synthesis, the characterization and the determination of the purity by HPLC analysis of the compounds.
Luciani Rosaria	Performed the hTS Enzymatic inhibition and FRET assays.
Mangani Stefano	Coordinate the x-ray crystallography work. Performed the x-ray crystal structures of the mutants.
Marverti Gaetano	Performed the anticancer activity of hTS dimer disrupters and molecular biology studies.
Rimessi Alessandro	Performed the pharmacology experiments with in vivo xenograft A2780 Cancer.
Pacifico Salvatore	Performed the synthesis of the main leads and the E5-FITC conjugate.
Peters Godefridus J.	Supervised the pharmacology experiments.
Pinton Paolo	Supervised the pharmacology experiments with xenograft A2780 cancer cells.
Ponterini Glauco	Conceived the kinetic and FRET study. Supervised the FRET experiment and performed the mechanistic analysis of dissociative inhibition.
Pozzi Cecilia	Performed the x-ray crystal structures of the mutants.
Quotadamo Antonio	Performed the synthesis in large-scale of the compounds for in vivo studies and the chromatographic enantioseparation of E7.
Rimessi Alessandro	Performed the pharmacology experiments with in vivo xenograft A2780 Cancer.
Salo-Ahen Outi M. H.	Molecular modelling: surface TS pocket identification.
Santarem Nuno	Performed the preclinical PK on mice and the living cells experiments
Santucci Matteo	Performed the hTS Enzymatic inhibition and FRET assays
Saxena Puneet	Performed the computational studies proposing the first docking model
Stroud Robert	Suggested the paper structure and supported the writing of the manuscript.
Trande Matteo	Performed the hTS Enzymatic inhibition and FRET assays
Venturelli Alberto	Performed the tethering experiments
Wade Rebecca C.	Designed and supervised the computational studies on the hTS interface pockets and tethering strategies and contributed to writing the manuscript

Supplementary Methods	pag.4
Computational studies for pocket identification	pag. 4
Site directed mutagenesis, protein purification and characterization	pag. 6
X-ray crystallography	pag.7
X-ray crystal structure determination of hTS-Y202C	pag. 8
X-ray crystal structure determination of hTS C195S-Y202C	pag. 10
X-ray crystal structure experiments of hTS-compound C series	pag. 11
Disulfide-compound library (A1-A55) design	pag. 12
Mass Spectrometry identification of tethered ligands	pag. 12
Details on mass spectrometry (MS) methods	pag. 13
Commercially available compound library (B1-B26) design and C3-C5 docking.	pag.16
Fluorescence experiments	pag.17
Synthesis of TPC, C1-C11, D1-D14, E1-E7, F1-F4, E5-(O ₂ Oc)-CAM-FITC	pag. 18
Enzyme purification	pag. 39
Inhibition assay of hTS and IC ₅₀ determination	pag. 40
Enantioseparation and racemization of E7	pag. 41
Analysis of combined equilibria and fitting to FRET data.	pag. 43
Analysis of a dissociative inhibition mechanism and fitting to data	pag. 45
Fluorescence microscopy	pag. 46
Biological experiments	pag. 47
Pharmacokinetic on BALB/c mice of E5 and E7.	pag. 50
<i>In vivo</i> cancer mouse model studies	pag. 51
Supplementary Figures	pag. 55
Supplementary Tables	pag. 77
SI references	pag.106

Supplementary methods

Computational studies for pocket identification.

In order to detect possible pockets for the tethering experiments at the hTS monomer-monomer interface, we examined the crystal structures of both the active (PDB-ID: 1HVY) and inactive (PDB-ID: 1YPV) hTS conformation (1). SYBYL 7.3 (Tripos Inc., St. Louis, MO) and PyMOL (version 1.8) were used for structure preparation and visualization of molecular structures. PASS (2), SiteIDTM (Tripos Inc., St. Louis, MO) and CASTp (3) were used to identify the pockets at the monomer interface as well as the surface crevices of dimeric hTS that extend into the interface. The GRID software (4) was used to calculate molecular interaction fields of different probes. The KYG server was used to predict the interface residues that could bind to RNA to avoid selecting interface pockets that would overlap with the predicted RNA binding site(s). We searched possible transient interface pockets by molecular dynamics (MD) simulations with the AMBER 8 simulation package (5). We used the ff03 force field (6); 7-ns long simulations were performed for the monomeric (active and inactive) hTS both in implicit (NPSA) (7) and explicit (TIP3P) (8) solvent. We performed shorter (4 ns) simulations for dimeric hTS, both active, with and without the dUMP substrate (from 1HVY), and inactive, with or without a phosphate ion in the active site (from 1YPV).

Detailed results description. The MD studies showed that, in general, the hTS structures and the energy of the simulations remained stable throughout the simulation time. The flexible regions (loops) of the inactive hTS were more mobile than in the active hTS structure and especially the modeled small domain was moving relatively much compared with the other loops. The dUMP-bound active dimeric hTS exhibited the smallest residue fluctuations. The identified interface pockets are reported in Table S1 and Fig. S1. We examined the interface pockets of the snapshot structures from the MD trajectories at every sharp nanosecond (Table S2). In all simulations, new pockets were formed while some disappeared and others reappeared. Table S2 shows the pockets along the active monomer simulation in explicit water (without dUMP). Finally, Y202 pocket was selected as the most promising target for tethering experiments since this pocket does not appear in the hTS dimer, it is

not predicted to be part of the mRNA region and it has the ability to interact with various functional groups. It is also of reasonable size and there are several smaller crevices around it that can fuse with it, as observed from the simulations.

Details on methods used in MD studies. The proteins and ligand preparation were carried out with the SYBYL 7.3 (Tripos Inc., St. Louis, MO) Biopolymer module; modified cysteines were reconstructed as normal cysteine residues, hydrogen atoms and missing side chains were added. The dimeric form of the inactive hTS was built with the Protein Quaternary Structure file server (9) and the missing small domain (residues 107-128) was modeled according to the 1HVY structure. The hydrogen of the sugar hydroxyl group in dUMP was directed toward the neighboring H256. The Antechamber tool of AMBER 8 was used to create the ligand parameters for the MD simulations. The ligand partial charges were modified manually: for the phosphate ion, the charge of phosphorus (P) atom was set to 1.216e (NPSA) or 1.4e (TIP3P) and the oxygen (O) atoms to -0.55e (NPSA) or -1.1e (TIP3P). The total charge of the phosphate ion in the NPSA model was -1e, and in the explicit water -3e. For dUMP, the charges were partly taken from the all_nucleic02.lib of AMBER 8: the uracil moiety from the RU unit and the sugar moiety from the DT3 unit. The phosphate group was set to have a total charge of -2e. Firstly, the systems were energy minimized, heated and equilibrated. For the implicit water (NPSA) simulations: 30 ps (10 K --> 100 K), 20 ps (100 K --> 200 K), 20 ps (200 K --> 300 K) and then 400 steps of minimization were carried out. For the explicit water simulations, an octahedral box extending 10 Å from the protein was filled with TIP3P water (including the crystallographic water sites) and neutralizing Na⁺ ions. Energy minimization was performed in six steps, decreasing the constraints on the protein stepwise from 5 to 0 kcal/molÅ². Each step was carried out for a maximum of 200 iterations. Equilibration: (i) restrained solute (5 kcal/mol restraint force constant, 10 K --> 100 K, 10 ps, constant volume, Langevin dynamics); (ii) free solute (10 K --> 100 K, 10 ps, constant volume, Langevin dynamics); (iii) free solute (100 K --> 200 K, 10 ps, constant volume, Langevin dynamics); (iv) free solute (200 K --> 300 K, 10 ps, constant volume, Langevin dynamics); (v) free solute (300 K, 10 ps, constant volume and

temperature, Langevin dynamics); (vi) free solute (300 K, 10 ps, constant pressure and temperature). The production simulations were performed at a constant temperature of 300 K and a pressure of 1 bar with Berendsen coupling constants of 5.0 and 2.0 ps, respectively (10).

Periodic boundary conditions, particle-mesh Ewald electrostatics (11) and a cut-off of 9 Å for non-bonded interactions were used. A time step of 2 fs was applied together with the SHAKE algorithm (12) to constrain the bonds to hydrogen atoms.

Site directed mutagenesis, protein purification and characterization, inhibition assay.

Bacterial cells expressing mutant (Y202C, C195S, C195S-Y202CC) hTS-His-tag (MRGSHHHHHHGS sequence added at the N-terminus) protein from Dr. Myllykallio (Ecole Polytechnique, 91128 Palaiseau, France) as already reported (13). The wt-hTS protein and the mutants were purified as reported SI pag.89. The hTS mutants were characterized through mass spectrometry and ESI-Q-ToF analysis (6520 Accurate-Mass Q-ToF – Agilent Technologies). MassHunter (B.02.00 – Agilent Technologies) was used as the deconvolution program (Maximum Entropy). For characterization of the mutants, the protein was digested with trypsin and mass spectra were acquired using both MALDI (4800 Plus MALDI TOF/TOF–Applied Biosystem) and nanoLC-ESI-Q-ToF (Agilent Technologies) mass spectrometers. MS and MS/MS spectra were analyzed by using the free Mascot software (www.matrixscience.com). Peptides containing the mutations were observed by MALDI and/or ESI-MS.

Protein characterization. For tethering experiment, Y202 was mutated to cysteine and the catalytic C195 was mutated to serine to avoid confusion due to covalent bonding the disulfide fragment compounds to the active site. The hTS C195S, hTS-Y202C and the hTS C195S-Y202C double mutant were obtained. While the hTS C195S-Y202C and the hTS-C195S mutants were catalytically inactive, the hTS-Y202C mutant was catalytically active, with a k_{cat} of 0.3 sec^{-1} , three times lower than WT-hTS ($k_{cat} = 0.9 \text{ sec}^{-1}$), and K_m values of $10 \mu\text{M}$ for both the dUMP substrate and the MTHF cofactor, similar to those of WT-hTS ($K_{m \text{ dUMP}} = 10 \mu\text{M}$ and $K_{m \text{ MTHF}} = 5 \mu\text{M}$). The specific activity (SA) of

the enzyme was 0.5 units per mg of purified protein. All experiments were repeated at least 3 times, standard error (SE) +/-20% of the displayed value. For the inhibition assays, varying concentrations of the compounds were mixed with hTS in 20 mM phosphate buffer, pH 6.9, at 25°C, incubated for 1 hour and aliquots of this mixture were assayed for TS activity under standard conditions.

X-ray crystallography.

Crystallization trials were performed at 24°C using the hanging drop vapor diffusion technique. Precipitant solutions at different pH values and ammonium sulfate concentrations were assayed in both the presence and absence of β -mercaptoethanol. Crystallization drops for the hTS Y202C mutant were prepared by mixing 3 μ L of precipitant solution and 6 μ L of a 5.0 mg/mL protein solution (buffer 0.1 M HEPES pH 7.5) and equilibrated against 600 μ L of a reservoir solution consisting of 20-35% saturated ammonium sulfate and 0.1 M TRIS buffer, pH 8.3. Two weeks later the drops were still clear with no sign of either crystals or precipitate. 1 μ L of a 200 mM β -mercaptoethanol solution was then added to half of the drops. Crystals appeared after almost 4 months in the drops where β -mercaptoethanol had been added and the precipitant solution consisted of 35% saturated ammonium sulfate and 0.1 M TRIS, pH 8.3. Crystallization drops for the hTS-C195S-Y202C mutant were prepared by mixing 3 μ L of precipitant solution and 3 μ L of an 11.2 mg/mL protein solution (in 0.1 M HEPES pH 7.5) and equilibrated over 600 μ L of a reservoir solution consisting of 25% saturated ammonium sulfate, 20 mM β -mercaptoethanol and 0.1 M TRIS buffer, pH 8.3. Crystals appeared in about one year. Before data collection, crystals were transferred to a cryoprotectant solution containing 20% ethylene glycol and 80% precipitant solution and then flash-frozen in liquid nitrogen. Complete data sets for the two mutants were collected at ESRF (European Synchrotron Radiation Facility, Grenoble, France) with the rotation technique. All data sets were processed with the program MOSFLM 7.0.4 (14) and scaled with SCALA (15) from the CCP4 suite (16). The structures were solved by the molecular replacement method, as implemented in the software MOLREP (17), using

one subunit of wild type hTS either in the inactive (PDB-ID code 3N5G) (18) or active (PDB-ID code 1HVY) (19) conformations as search model for the rotation and translation functions.

X-ray crystal structure determination of hTS-Y202C. The molecular replacement and refinement of the Y202C mutant were performed in the two possible space groups $P3_121$ and $P3_1$ in order to check if the two-fold symmetry axis present in the crystals of native hTS was maintained in the crystal of the mutant (13). The refinement quality indicated that the Y202C mutant crystallizes in the $P3_1$ space group with one protein dimer per asymmetric unit. The structure refinements were performed with the program REFMAC5 (20). The refinement protocol involved a sequence of iterative manual rebuilding of the model and maximum-likelihood refinement (20) using the TLS parameterization in the final cycles (21). The software Coot (22) was used to visualize the structures and for manual rebuilding and modeling of the missing atoms into the electron density maps. Water molecules were added using the program ARP/wARP (23) and checked both manually and with Coot.

The hTS Y202C mutant (hTS-Y202C) was crystallized under the same high salt conditions previously reported for the WT enzyme, in the space group $P3_1$ with an enzyme dimer (in the inactive conformation) in the asymmetric unit. Crystallographic data collection, structure determination and refinement are summarized in Table S3. Besides the 12 residues composing the His-tag, the first 25 N-terminal and the last three C-terminal residues of the WT sequence are not visible in the electron density maps and are not part of our model. Moreover, residues 107-130 and 103-130 in subunits A and B, respectively, were also excluded from the present model. The N-terminal region of hTS is usually highly flexible and has never been observed in the crystal structures of either active or inactive conformations of the enzyme. On the other hand, loop 107-128 and the last three C-terminal residues are disordered only in the structure of the hTS inactive conformation whereas they become ordered and completely visible in the active conformation. The structure of hTS-Y202C closely resembles that of the native enzyme in the inactive conformation as indicated by the 0.4 Å r.m.s. displacement obtained upon C α -atom matching, thus explaining the similar biochemical profiles of the two

proteins. The Fourier difference map clearly shows the replacement of the native Y202 by cysteine. Moreover, a positive extra electron density is found extending beyond the residue side chain, strongly indicating the reaction of the cysteine sulfur atom with β -mercaptoethanol (BME) in the crystallization solution, leading to a S,S-(2-hydroxyethyl)thiocysteine (CME) chemical modification of C202 (Fig. S2a,b,c). Out of the five native cysteine residues present in hTS-Y202C, only C210 is in the reduced, unmodified form, while the other cysteines are modified to either CME or S-methylthio-cysteine (SCH). Analysis of hTS-Y202C (inactive conformation) shows that the solvent accessibility of cysteine residues follows the trend shown in Table S4 (see also Figure S2). Only residue C43 is fully solvent accessible while shielding increases from C180 to C199 and C210, which are completely buried inside the hTS dimer. The reactivity of C180, C195 and C202 is understandable in terms of the thermal mobility of the residues that only partially shield these cysteines from the bulk solvent. More puzzling is the different chemical reactivity of C199 and C210, which are both completely buried under the protein surface. However, C199 lies at the bottom of the hTS cavity lined by W139 and Y230, which form H-bonds to the terminal OH group of CME199. A simple flip of W139 and/or Y230 side chains can expose C199 to the solvent allowing the reaction with BME to generate CME199. In the hTS-Y202C subunit A, the CME202 residue is stabilized by two H-bonds established between the hydroxyl group of CME and an ordered water molecule (Wat83), further linked to the carbonyl O of D173 and the NZ of K47 from the facing subunit (Fig. S2d). A second, ordered water molecule (Wat39) mediates the interactions of Wat83 with R175 NH1, belonging to the same subunit, and T55 OG1 and D254 OD2 of the facing subunit (Fig. S2d). In subunit B, the interactions of CME202 are conserved: the hydroxyl group of CME establishes two H-bonds with an ordered water molecule (Wat6), and with K47 NZ of the facing subunit (Fig. S2e). Furthermore, Wat6 is H-bonded to the carbonyl oxygen of both P172 and D174 and the backbone NH of V203 (the second ordered water molecule observed in subunit A is not found in the corresponding cavity of subunit B). C202 in the hTS-Y202C mutant is located in a pocket of the dimer interface considered important to maintain protein-protein interactions and exploitable for tethering with reactive

molecules aimed at disrupting the hTS dimer interface. Indeed, the CME modification can be viewed as a tethered compound of the parent cysteine although, due to the small dimensions of the S-hydroxyethyl moiety, the chemical modification of C202 does not affect the hTS quaternary structure. Comparison with the crystal structure of native hTS shows that in the Y202C variant the loop K47-T55 of the facing subunit is displaced, increasing the distances between the residues of the two partner subunits by 1.0-2.5 Å. As already suggested by the structural characterization of the native hTS in complex with the LR peptide (17), the structure of the hTS dimer allows small-to-medium-sized molecules, such as BME or the LR octapeptide, to access the dimer interface and to interact with the protein. The structural evidence indicates that the hTS dimer undergoes either monomer/dimer interconversion or “breathing” movements that allow the binding of exogenous molecules, such as the fragments of the disulfide library.

X-ray crystal structure determination of hTS C195S-Y202C. The crystal cell C195S-Y202C double mutant crystal cell has very close *a* and *b* parameters (Table S3). Indexing in the tetragonal P4₁2₁2 space group was attempted, but the figures of merit and the analysis of systematic absences showed that the true space group could be one of the orthorhombic space groups P2₁2₁2 or P2₁2₁2₁. Molecular replacement (MOLREP) (24) indicates that the true space group is P2₁2₁2₁ with two protein dimers per asymmetric unit. The refinement was carried out with the program PHENIX (25) and consisted of 14 cycles of maximum-likelihood refinement followed by manual rebuilding and modeling using the same procedures and software described for the single mutant. The stereochemical quality of the models was assessed using PROCHECK (26). The final coordinates and structure factors of hTS Y202C and hTS C195S-Y202C mutants were deposited in the Protein Data Bank under the accession codes **4O1U** and **4O1X**, respectively. Data collection and refinement statistics are summarized in Table S3. Figures were generated through the molecular visualization software CCP4MG (27).

The double mutant hTS C195S-Y202C was crystallized using the same high salt conditions applied for the crystallization of the Y202C variant. However, the crystal structure clearly reveals that all the

four independent subunits present in the crystal asymmetric unit are in the active conformation. The hTS-C195S-Y202C structure is the first example of hTS crystallized under high salt conditions showing the active conformation. Since the single Y202C mutant, crystallized under the same conditions of the double mutant, is in the inactive conformation, it appears that the active site C195S mutation is able to shift the hTS conformational equilibrium towards the active conformation. A possible explanation for this behavior is that the clustering of the four residues C180 and C195 from the two subunits of the dimer stabilizes the inactive conformation of hTS and hence the C195S mutation prevents this occurrence. All four independent subunits of hTS C195S-Y202C are fully visible in the electron density map, except for the 50-53 loop of the D subunit and for few residues at the N- and C-termini of all chains. Out of the five cysteine residues present in the protein, only C210 remains in the native state, while C180 in subunits B and D presents weak electron density extending beyond the sulfur atom indicating reaction with BME. However, the electron density is too undefined to allow modeling of extra atoms. All other cysteines have reacted with the BME present in the crystallization medium to give either CME or SCH derivative. The two mutants (C195S-Y202C and Y202C) have essentially the same behavior as regards thiol reactivity. CME202 in the double mutant maintains the same H-bond interactions already described for the single mutant (Fig.S2 h-j). The hTS C195S-Y202C structure validates the choice of Y202 as tethering mutation site since this residue is prone to react with thiol compounds independently of the conformation adopted by hTS.

X-ray crystal structure experiments of hTS-compounds C serie. Many attempts were made to obtain the co-crystal structure of hTS bound to compounds of the C series, and aiming to isolate the monomeric hTS-C compound complex. We started with 1-5 micromolar concentration of the enzyme treated with a 100-folds excess of the ligand in solution in order to shift the hTS monomer-dimer equilibrium towards the monomeric form. The solution was then concentrated in order to reach the crystallization conditions. However, all trials failed, always yielding the uncomplexed dimeric hTS structure.

Disulfide-compound library (A1-A55) design.

Version 8 of the ZINC archive (28) was screened to recover compounds containing a disulfide function. A preliminary search for S-S bonds was performed using the SMILES notation, finding 1066 molecules. Compounds with the disulfide bond within a cyclic structure (167/1066), and those with a disulfanyl group (SSH, 16/1066) or an oxidized sulphur atom (211/1066) were excluded. The remaining disulfides were subjected to a fragment-likeness analysis: molecular descriptors were calculated with VolSurf+ (29). LogP and molecular weight (MW) were used to filter out very large and flexible compounds, as well as too hydrophilic or too hydrophobic ones. Finally, multivariate statistical methods such as the Principal Component Analysis (PCA) were used for the final selection of 55 disulfides. The disulfide library is reported in Table S5.

Mass Spectrometry identification of tethered ligands.

Matrix-Assisted Laser Desorption/Ionization (MALDI) - Time of Flight (TOF) (Voyager-Pro MALDI-TOF (Applied Biosystems)) was chosen for a medium-throughput screening of the disulfide-compound library (A1-A55). The results obtained were validated using an Electron Spray Ionization Quadrupole - Time of Flight (ESI-QTOF) MS (Quadrupole - Time of Flight (ESI-QTOF) mass spectrometer (Agilent Technologies Inc.)). Both platforms allowed us to exclude any ionization-related issue in the ligand selection process. The screening approach was an iterative selection of the best ligands in a competitive environment obtained by arranging the ligands in pools properly chosen in order to avoid ambiguous mass peak assignments. Successive screening steps were performed in which the selected ligands from the previous screening were subjected to further screening using differently constituted pool. For the disulfide-compound library screening up to 3 ligands were pooled and mixed into a hTS-C195S-Y202C solution in a buffer containing 1 mM 2-mercaptoethanol and 20 mM K⁺ phosphate (pH 7.5). The reaction mixture was incubated at RT for 1 hour and then purified on a C4 ZipTip® (Millipore) to remove salts and unbound ligands. To identify the binding site of

these molecules, the protein-ligand complexes underwent enzymatic digestion in a classical bottom-up proteomic analysis using both ionization techniques for result evaluation.

Details on Mass Spectrometry (MS) methods.

MS-based disulphide library screening. A solution of each individual library member was prepared in dimethyl sulfoxide (DMSO) to a final concentration of 80 mM per ligand. 1 μ L of each ligand solution was then pooled to form groups of a maximum of 3 discrete compounds, having molecular weights that differed by at least 150 Da from one another; each pool was brought to a final volume of 10 μ L. 1 μ L of the desired ligand pool (8 mM) was added to 20 μ L of 19 μ M C195S/Y202C hTS double mutant solution in a buffer containing 1 mM 2-mercaptoethanol and 20 mM potassium phosphate (pH 7.5) to a final volume of 40 μ L. The protein was present at a concentration of 10 μ M while each of the disulphide library members was 0.2 mM. The reaction mixture was incubated at room temperature for 1 hour and then purified on a C4 ZipTip® (Millipore) to remove salts and unbound ligands. A solution of 10 mg/ml of sinapinic acid in acetonitrile/0.1% aqueous TFA in a 1:1 ratio was used to assist the ionization process. 1 μ L of the sample was deposited onto a MALDI sample plate and allowed to air-dry at room temperature; 0.5 μ L of matrix solution were then deposited on the same spot, resulting in a uniform layer of fine granular protein including matrix crystals. Mass spectra were recorded in positive-ion linear mode at an accelerating voltage of 20 kV and a delayed extraction time of 1200 ns. Each spectrum obtained was the mean of 100 laser shots. The ions were generated using the 337-nm laser beam from a nitrogen laser, having a pulse width of 3 ns. Data were obtained using the following parameters: 95% grid voltage, 0.08% guide wire voltage and a low mass gate of 15000 Da. An external calibration was performed based on the molecular weight of the untreated enzyme mutant previously reduced with DTT, alkylated with iodoacetamide and diluted 1:10 in TFA 0.1%. The software Data Explorer (Applied Biosystems) was used for mass spectral data processing; raw spectra were smoothed, and the baseline was corrected according to the normally observed peak broadness. Peak m/z values were annotated according to a peak detection algorithm

taking into account an average resolution of 3500. The identity of any library member bonded to the protein through a disulphide bond was determined by subtracting the mass of the free protein from the observed higher mass.

For ESI-QTOF measurement 0.5 μl of ligand (80 mM in DMSO) was added to 12 μl of 17 μM C195S/Y202C hTS mutant solution in a buffer containing 1 mM 2-mercaptoethanol and 20 mM potassium phosphate (pH 7.5) to a final volume of 20 μL . The protein was present at a concentration of 10 μM and the disulphide at 2mM. After equilibration at room temperature for 1 hour, 1 μl of the reaction mixture was diluted 1:10 with a solution of 5% formic acid in water/acetonitrile 95:5 and injected onto an HPLC-chip ESI-QTOF. The mobile phase composition was as follows: (A) 0.1%formic acid in a water/acetonitrile 98:2 solution and (B) 0.1%formic acid in a acetonitrile/water 98:2 solution. Chromatographic separations were performed at a flow rate of 400 nL/min with the following gradient: 15% B for 5 min, 15–85% B in 5 min, 85% B for 5 min, 85-15% B in 3 min. Under these conditions the protein-ligand complex was eluted between 6.5 and 8.0 min. The capillary voltage was set to 1600 V and the desolvating temperature was 350°C. Nitrogen was used as a drying gas (flow rate = 6 L/min). The mass spectrometer operated in positive mode in the scan range 200-3200 Da. An external calibration was performed based on the molecular weight of a multi-standard solution (ESI-L Low concentration tuning mixture - SUPELCO). During acquisition, some of these masses were constantly monitored and used for a fine calibration of the instrument. The multiply charged ions deriving from the free protein and the protein-ligand complex were deconvoluted with available software (MassHunter – Agilent Technologies Inc.). Results are reported in Table S6.

Analysis of the ligand-protein binding site by MS. To investigate the cysteine residue involved in the binding with the selected ligands, the protein-ligand complexes underwent enzymatic digestion in a classical bottom-up proteomic analysis using both ionization techniques for result evaluation.

In a typical experiment, 1 μL of the ligand (80 mM in DMSO) was added to 14 μL of the 29 μM hTS C195S-Y202C hTS mutant solution in a buffer containing 2 mM 2-mercaptoethanol and 20 mM phosphate buffer (pH 7.5) to a final volume of 20 μL . The reaction mixture was incubated at room

temperature for 1 hour. 6 μL of iodoacetamide (100 mM) was added and the reaction mixture was incubated in the dark, at room temperature, for 20 min in order to alkylate the unmodified cysteine residues. 3 μL of 0.1 $\mu\text{g}/\mu\text{L}$ sequencing grade modified trypsin (SIGMA) was added and the sample was incubated at 37 $^{\circ}\text{C}$. After 1 hour, a second aliquot of 3 μL of trypsin was added. The digestion was carried out at 37 $^{\circ}\text{C}$ overnight. 1 μL of trifluoroacetic acid (TFA) 0,1% was added and the reaction mixture was purified by a tip chromatography system (ZipTip C18, Millipore). The bound peptides were eluted from the tip stationary phase with 10 μL of acetonitrile 75%/TFA 0,1%. and 1 μL of the mixture was spotted onto a MALDI target for MS analysis. A saturated solution of *o*-cyano-4-hydroxycinnamic acid in 50% acetonitrile/0.1% trifluoroacetic acid (0.5 μL) was used to assist the ionization process. Mass spectra were recorded on a 4800plus MALDI TOF/TOF (Applied Biosystems) mass spectrometer, operating in positive ion reflector mode with an accelerating voltage of 20 KV and delayed extraction time of 300 ns. The MALDI ions were generated using a 355-nm Nd:YAG laser pulsed at 200 Hz with an intensity of 4600 (arbitrary units). Each spectrum was obtained by the accumulation of 1200-2500 laser shots. For MS/MS analysis the mass spectrometer was externally calibrated and the sample mixture was analyzed in the 750 - 3500 Da mass range. Fragmentation experiments were performed with and without a collision gas. Signals from 150 laser shots were averaged to increase the S/N ratio of each mass spectrum. Data Explorer (Applied Biosystems) was used for data processing (baseline correction, deisotoping, calibration and peak detection). Peptide mass lists were searched with the MASCOT server in a swiss-prot-based protein database including the mutant version of hTS.

In parallel, 1 μL of the reaction mixture was diluted 1:30 with a solution of 0.5% formic acid in water/acetonitrile 98:2 and 3 μL were injected onto an HPLC-chip ESI-QTOF. The mobile phase composition was as follows: (A) 0.1% formic acid in a water/acetonitrile 98:2 solution and (B) 0.1% formic acid in acetonitrile/water 98:2 solution. A chromatographic separation was performed at a flow rate of 400 nL/min with the following gradient: 3% B for 5 min, 3–30% B in 15 min, 30–40% B in 5 min, 40–85% B in 3 min, 85% B for 2 min, 85-3% B in 5 min. The capillary voltage was set

at 1600 V and the desolvating temperature was 350 °C. Nitrogen was used as a drying gas (flow rate = 6 L/min). The mass spectrometer operated in positive mode in the 200-3200 Da scan range. For MS/MS experiment up to three precursors were selected for each acquisition cycle. The precursor ion was automatically excluded for fragmentation if it was present in two consecutive spectra, or if it persisted for more than 0.12 min. An external calibration was performed based on the molecular weight of a multi-standard solution (ESI-L Low concentration tuning mixture - SUPELCO). During the acquisition, some of these masses were constantly monitored and used for a fine calibration of the instrument. The multiply charged ions deriving from the free protein and the protein-ligand complex were deconvoluted with available software (MassHunter – Agilent Technologies Inc.). The results of the trypsin digestion are reported in Table S7. To investigate which of the three cysteine of the D186-R215 peptide (Fig. 2) was involved in the binding with the ligand, MS/MS experiments were performed. Unfortunately, the MS/MS spectra did not allow the identification of the corresponding fragment due to (i) the low abundance of the ligand bound-D186-R215 peptide and (ii) ion suppression effects. However, molecular dynamics and x-ray crystallography highlighted that among the three cysteine residues, cysteine 202 was the one exposed to the solvent and thus available for tethering.

Commercially available compound library (B1-B26) design and C3-C5 docking.

A dataset of 331,600 compounds, commercially available from Specs, was downloaded from the ZINC website (www.zinc.org; ZINC version 8) (28). We retained 242,590 compounds with a MW between 300 and 500 amu. Then we used SMARTS ([openbabel, http://openbabel.org/wiki/Main_Page](http://openbabel.org/wiki/Main_Page)) to search for the presence of specific fragments (Fig. 3): 97% of compounds were filtered out. Then, a library of 5,774 compounds was screened against WT-hTS (1HVY) focusing on the subunit-subunit interface close to Y202. We used FLAP (30) to build two receptor-based pharmacophore models, to screen the library versus these receptor-models, and to dock the most interesting candidates into the binding pockets. Each molecule was subjected to a

conformational analysis and the Molecular Interaction Fields (MIF) were generated with the GRID probes DRY, O, N1 and H. Out of compounds with the highest overall scores (> 0.60 for both receptor-based pharmacophore models), we selected a subset of 26 compounds, available for purchase at the time of study, and displaying reasonable structural diversity (Table S8). Compounds **C3**, **C4** and **C5** were docked against wt-hTS (1HVY) focusing on the subunit-subunit interface close to Y202, using Autodock, version 4.2, software (31).

Fluorescence experiments.

To investigate the dimer/monomer equilibrium modulation by the selected compounds, we employed a previously developed FRET assay in which hTS was tagged with fluorescein (F, excitation energy donor) and tetramethylrhodamine (T, acceptor) probes as described in (32). Tagging yielded samples with spectrophotometrically determined F:T:protein-dimer concentration ratios near the expected 1:1:1 values. Absorption spectra were measured on a Varian Cary 100 UV-vis spectrophotometer. Fluorescence spectra were measured on a Spex-JobinYvon Fluoromax2 spectrofluorometer. Usually, samples with spectrophotometrically determined protein and probe concentrations in the range 50-490 nM in phosphate buffer at pH 7.5 were excited at 450 nm, a wavelength at which the F/T excitation ratio is very high and T emission is almost negligible (32). All measurements were performed at 20 ± 3 °C. The value of the observed FRET efficiency, Φ_{FRET} , was determined from the emission intensities at 580 nm, I_{580} , the maximum of T emission, and at 520 nm, the maximum of F emission, I_{F} , as described in⁹. Measurement of residual F emission and of sensitized T emission following almost selective F excitation (Fig. 4a) enables Φ_{FRET} to be evaluated (32). In the unperturbed dimer such an efficiency is near 1 because a distance that is roughly half the critical Förster distance for the F/T pair separates the C43 and C43' residues of the two subunits (25Å). On the other hand, it is zero when the protein is fully dissociated. Developed on a spectrofluorometer, the assay has later been adapted to a medium-throughput format. In short, 1 or 2 μL of a 10 mM DMSO solution of each inhibitor was distributed in a 96 well multiplate to a final concentration of

10 or 20 μM together with 300 nM hTS properly derivatized with the two fluorescent probes (at this concentration, in the absence of inhibitors, the more than 95% of the protein is in the dimer form). Control wells contained only hTS, either alone or with 2 μL of DMSO. Each sample was assayed in duplicate. The Tecan GeniusPRO equipment was employed to read the fluorescence emission from each well at both 535 nm (fluorescein signal) and 590 nm (fluorescein and tetramethylrhodamine signals) following excitation at 470 nm. From the I_{590}/I_{535} ratio, the FRET efficiency in each well and its difference with respect to the control wells were determined.

Synthesis of TPC, C1-C11, D1-D14, E1-E7, F1-F4. and E5-(O₂Oc)-CAM-FITC

General. All commercial chemicals and solvents were reagent grade and were used without further purification. The compound purchased from NCI and ChemBridge were used without purification. Reaction progress was monitored by TLC on pre-coated silica gel 60 F254 plates (Merck) and visualization was accomplished with UV light (254 nm). ¹H and ¹³C NMR spectra were recorded on a Bruker DPX200 or a Bruker FT-NMR AVANCE 400 spectrometers. Chemical shifts are reported as δ values (ppm) referenced to residual solvent (CHCl₃ at δ 7.26 ppm, DMSO at δ 2.50 ppm, MeOD at δ 3.31 ppm, CD₃OCD₃ at δ 2.05 ppm); *J* values were given in Hz. When peak multiplicities are given the following abbreviations are used: s, singlet; d, doublet; t, triplet; q, quartet; m, multiplet; br, broadened signal. Two-dimensional NMR techniques (heteronuclear single quantum coherence and heteronuclear multiple bond correlation) were used to aid the assignment of signals in ¹H and ¹³C spectra. Silica gel Merck (60-230 mesh) was used for column chromatography. Purity of the compounds was assayed by means of TLC (Merck F-254 silica gel). Analysis on compound purity was determined through liquid chromatography UV/Vis using Jasco LC system equipped with a Jasco PU-2080 Plus pump, coupled with a Jasco PU-2075 Plus UV/Vis detector. LC separation was performed on an Agilent Poroshell 120 50 mm \times 3.0 mm analytical column, packed with EC-C18 2.7 μM as stationary phase (Agilent Technologies, Milan, Italy). 10 μL of a 100 $\mu\text{g}/\text{mL}$ solution of compound in methanol was injected. A gradient was delivered at 0.2 mL/min using (A) 0.1% FA in

water and (B) ACN. Samples were eluted with 5% B (0.00–5.00 min); 1–95% B (5.00–20.00 min); 95% B (20.00–300.00 min) and 5% B (30.00–40.00 min). The eluted was detected with UV detection at $\lambda = 220$ nm. All the compounds showed a level of purity above 95%. MS spectra were recorded by means of a Q-TOF Accurate-Mass G6520AA (Agilent Technologies). Microanalyses were carried out in the Microanalysis Laboratory of the Department of Life Sciences, Modena University.

Synthesis of TPC (Fig. S3). N-(4-toluenesulfonyl)-D-proline (3). A solution of *p*-toluene sulfonyl chloride **1** (1.64 g, 8.6 mmol) in diethyl ether (16 mL) was added to a cold (0°C) solution of D-proline (**2**) (0.99 g, 8.6 mmol) in NaOH 2M (8.6 mL, 17.4 mmol). The reaction was stirred 4h at room temperature (RT). The mixture was treated with concentrated HCl until pH 2. The aqueous solution was then extracted with ethyl acetate (6 x 10 mL), the organic layer was washed with brine (4 x 10 mL), dried (Na₂SO₄) and the solvent was removed under reduced pressure to yield a colorless glue. Yield 1.79 g, 77%; ¹H NMR (CDCl₃, 200 MHz) δ 2.12-1.72 (H-7 and H-8, m, 4H), 2.44 (H-1, s, 3H), 3.29 (H-9B, m, 1H), 3.50 (H-9A, m, 1H), 4.29 (H-6, dd, *J* 3.9, *J* 4.0, 1H), 7.33 (H-3, d, *J* 7.9, 2H), 7.77 (H-4, *J* 8.2, 2H).

N-N'-[D-prolyl-N-(4-toluenesulfonyl)]-cistamine (TPC). A solution of compound **3** (0.16 g, 0.6 mmol) in dichloromethane (5 mL), N,N'-dicyclohexylcarbodiimide (DCC) (0.16 g, 0.8 mmol) were added in succession and the solution was stirred at RT for 30 min; after cooling at 0°C, the suspended cystamine·2HCl (**4**) (0.068 g, 0.3 mmol) in dichloromethane (8 mL) and TEA (0.083 mL, 0.6 mmol) was added dropwise over 5 min. The reaction mixture was stirred at RT overnight, then filtered, and the solution was washed with NaHCO₃ (2 x 5 mL), NH₄Cl (2 x 5 mL) and H₂O (2 x 5 mL). The organic layer was dried over Na₂SO₄, the solvent was evaporated at reduced pressure to produce the product that was purified by column chromatography (EtOAc/CHCl₃ 2:8). Yield g. 0.087, 44% (oil); ¹H NMR (DMSO-d₆, 200 MHz) δ 1.58-1.97 (m, 8H), 2.25 (s, 6H), 2.62 (t, 4H, *j* 5.90), 3.10 (m, 2H), 3.35 (m, 5H), 3.95 (m, 3H), 7.36 (m, 4H), 7.68 (m, 4H), 8.05 (t, 2H, *J* 5.90); ¹³C NMR (DMSO-d₆, 50 MHz) δ 20.9, 23.2, 30.0, 37.9, 39.2, 42.0, 62.9, 129.5, 129.9, 133.5, 144.7, 174.3. ESI-HRMS

calcd for C₂₈H₃₉N₄O₆S₄: 655.1752 (M+H⁺), found 655.1723. Anal. Calc. for C₂₈H₃₈N₄O₆S₄: C 51.35, H 5.85, N 8.56, found, C, 51.66, H, 5.90, N, 8.40.

Synthesis of compounds C1-C5, C11, D5-D8, D11-D14 (Figure S4). Synthesis of 2-Bromo-N-(substituted-phenyl)acetamide derivatives (H1b, H6b). General procedure. To a solution of o-chloroaniline (**H1a**) or 8-aminoquinoline (**H6a**) (10.0 mmol) and TEA (11.0 mmol) in anhydrous CH₂Cl₂ (30 mL), under stirring at 0°C under N₂ atmosphere, a solution of bromoacetyl bromide (10.0 mmol) in anhydrous CH₂Cl₂ (20 mL) was added dropwise. The suspension thus obtained was stirred at RT for 1 hour, then it was diluted with CH₂Cl₂, washed with a saturated solution of NH₄Cl; afterwards, the organic phase was dried (Na₂SO₄) and the solvent removed under reduced pressure. The residue thus obtained was purified by means of column chromatography as described.

2-Bromo-N-(2-chlorophenyl)acetamide (H1b): Yield 2.49 g (96%), m.p. 83-85°C (column chromatography cyclohexane/EtOAc 17.5:2.5), ¹H-NMR (DMSO-d₆, 200 MHz) (δ) (ppm): 9.90 (1H, broad s), 7.70 (1H, dd, *J* 7.9, *J* 1.7), 7.50 (1H, dd, *J* 7.9, *J* 1.7), 7.35 (1H, dt, *J* 7.6, *J* 1.6), 7.25 (1H, dt, *J* 7.7, *J* 1.7), 4.15 (2H, s); ¹³C-NMR (DMSO-d₆, 50 MHz) (δ) (ppm): 165.77, 135.00, 130.05, 127.99, 127.25, 126.42, 30.13.

2-Bromo-N-(quinolin-8-yl)acetamide (H6b): Yield 2.40 g (91%), m.p. 93-96°C C (column chromatography cyclohexane/EtOAc 8:2), ¹H-NMR (DMSO-d₆, 200 MHz) (δ) (ppm): 10.70 (1H, broad s), 8.90-8.60 (2H, m), 8.15 (1H, dd, *J* 8.3, *J* 1.7), 7.65-7.40 (3H, m), 4.10 (1H, s); ¹³C-NMR (DMSO-d₆, 50 MHz) (δ) (ppm): 148.54, 138.61, 136.31, 127.92, 127.15, 122.43, 121.74, 116.59, 29.68.

Synthesis of Bromo-N-(carboxy- or 4-carboxymethyl- phenyl)-acetamide derivatives (H2b, H3b, H5b). General procedure. These compounds were synthesized according to the published procedure (64-65). To a solution of the appropriate aminobenzoic acid (**H2a** or **H3a** for the synthesis of **H2b** and **H3b**, respectively) or p-aminophenylacetic acid (**H5a**) for the synthesis of (**H5b**) (19.87 mmol) and Na₂CO₃ (56.60 mmol) in water (60 mL) at 0°C under stirring, a solution of

bromoacetyl bromide (27.81 mmol) in anhydrous CH₃CN was added dropwise during 10 min. The suspension thus obtained was stirred at 0°C for another 10 min, then at RT for 10 min. Afterwards, the suspension was acidified (HCl 1 N, pH 1), and the precipitate thus obtained collected and washed with water. The products were then purified by trituration with anhydrous diethyl ether.

Bromo-N-(3-carboxyphenyl)acetamide (H2b). Yield 1.20 g (43%), m.p. 213-216°C (dec.), ¹H-NMR (DMSO-d₆, 200 MHz) (δ) (ppm): 10.51 (1H, broad s), 8.22 (1H, s), 7.79 (1H, m), 7.66 (1H, d, *J* 8.0), 7.45 (1H, t, *J* 7.6), 4.05 (2H, s); ¹³C-NMR (DMSO-d₆, 50 MHz) (δ) (ppm): 167.44, 165.50, 139.27, 131.90, 129.61, 125.06, 123.79, 120.43, 30.71.

Bromo-N-(4-carboxyphenyl)acetamide (H3b). Yield 82%, m.p. 223-226°C (dec.), ¹H-NMR (DMSO-d₆, 200 MHz) (δ) (ppm): 10.65 (1H, broad s), 7.90 (2H, m), 7.70 (2H, m), 4.05 (2H, s); ¹³C-NMR (DMSO-d₆, 50 MHz) (δ) (ppm): 167.26, 165.73, 143.02, 130.91, 126.23, 119.04, 30.72.

Bromo-N-(4-carboxymethylphenyl)acetamide (H5b). Yield 86%, m.p. 130-132°C (dec.), ¹H-NMR (DMSO-d₆, 400 MHz) (δ) (ppm): 12.50 (1H, broad s), 10.50 (1H, s), 7.68 (2H, m), 7.37 (2H, m), 4.19 (2H, s), 3.68 (2H, s); ¹³C-NMR (DMSO-d₆, 100 MHz) (δ) (ppm): 173.18, 165.15, 137.63, 130.93, 130.22, 119.63, 40.60, 30.89.

Bromo-N-(2-carboxyphenyl)acetamide (H4b). The compound was synthesized according to the procedure reported (66). To a solution of anthranilic acid (**H4a**) (1.50 g, 10.9 mmol) in anhydrous DMF (5 mL) and dioxane (5 mL), at -5°C under stirring under N₂ atmosphere, bromoacetyl bromide (2.76 g, 13.67 mmol) was added dropwise. The suspension thus obtained was stirred at RT for 12 hours, then ice (50 mL) was added to the reaction mixture; the solid thus obtained was collected and washed with water. Yield 2.52 g (89%), m.p. 163-166°C, ¹H-NMR (DMSO-d₆, 200 MHz) (δ) (ppm): 11.55 (1H, broad s), 8.45 (1H, d, *J* 8.6), 8.00 (1H, d, *J* 7.8, *J* 1.2), 7.60 (1H, m), 7.20 (1H, m), 4.25 (2H, s); ¹³C-NMR (DMSO-d₆, 50 MHz) (δ) (ppm): 169.65, 165.47, 140.42, 134.48, 131.57, 123.89, 120.51, 117.62, 31.10.

2-(Substituted aryl- or heteroarylthio)-N-(substituted phenyl)acetamide derivatives C2-C5, D5-D8, D11-D14. General procedure. To a suspension of K₂CO₃ (3.0 eq.) in anhydrous acetone (20

mL) at RT under stirring in a N₂ atmosphere, the appropriate mercaptoderivative (1.0 eq.) was added, followed by the appropriate (carboxyphenyl)-amidomethyl bromides (1 eq.). The suspension was stirred at RT for 12 hours, then the mixture was cooled, acidified (HCl 1N, pH 1.0) and the solid thus obtained was collected by filtration and washed with water. The crude product was purified by crystallization or column chromatography as reported below.

2-(4-Nitrophenylthio)-N-(3-carboxyphenyl)acetamide (C2): Yield 0.20 g (26%), m.p. 250-252°C (column chromatography CH₂Cl₂: CH₃OH 9:1)., ¹H-NMR (DMSO-d₆, 400 MHz) (δ) (ppm): 13.20 (1H, broad s), 10.70 (1H, broad s), 8.37 (1H, s), 8.32 (2H, m), 7.93 (1H, m), 7.80 (1H, d, *J* 7.9), 7.75 (2H, m), 7.60 (1H, m), 4.25 (2H, s); ¹³C-NMR (DMSO-d₆, 100 MHz) (δ) (ppm): 166.50, 166.71, 147.27, 145.19, 139.40, 131.86, 129.61, 126.91, 124.90, 124.38, 123.75, 120.38, 36.45; ESI-HRMS calcd for C₁₅H₁₃N₂O₅S (M+H⁺) 333.0545, found 333.0544. HPLC-UV/Vis *k* (retention time): 11.76. Anal. Calc. for C₁₅H₁₂N₂O₅S, C, 54.21, H, 3.64, N, 8.43; found, C, 54.43, H, 3.69, N, 8.19.

2-(4-Nitrophenylthio)-N-(4-carboxyphenyl)acetamide (C3): Yield 0.28 g (36%), m.p. 234-236°C (column chromatography CH₂Cl₂: CH₃OH 9:1), ¹H-NMR (DMSO-d₆, 400 MHz) (δ) (ppm): 12.89 (1H, broad s), 10.80 (1H, broad s), 8.31 (2H, m), 8.06 (2H, m), 7.83 (2H, m), 7.74 (2H, m), 4.28 (2H, s); ¹³C-NMR (DMSO-d₆, 100 MHz) (δ) (ppm): 167.30, 166.97, 147.19, 145.21, 143.16, 130.94, 126.92, 126.03, 124.38, 118.99, 36.56; ESI-HRMS calcd for C₁₅H₁₃N₂O₅S (M+H⁺) 333.0545, found 333.0526 HPLC-UV/Vis *k*: 11.77. Anal. Calc. for C₁₅H₁₂N₂O₅S, C, 54.21, H, 3.64, N, 8.43; found, C, 54.13, H, 3.66, N, 8.55.

2-(4-Nitrophenylthio)-N-(2-carboxyphenyl)acetamide (C4): Yield 0.60 (77%), m.p. 203-206°C (column chromatography CH₂Cl₂: CH₃OH 9:1), ¹H-NMR (DMSO-d₆, 400 MHz) (δ) (ppm): 13.79 (1H, broad s), 11.83 (1H, broad s), 8.61 (1H, d, *J* 8.2), 8.30 (2H, m), 8.10 (1H, dd, *J* 7.9, *J* 1.2), 7.76-7.70 (3H, m), 7.32 (1H, m), 4.40 (2H, s); ¹³C-NMR (DMSO-d₆, 100 MHz) (δ) (ppm): 169.61, 166.88, 146.47, 145.35, 140.52, 134.50, 131.57, 126.97, 124.47, 123.73, 120.63, 117.49, 36.85; ESI-HRMS

calcd for C₁₅H₁₃N₂O₅S (M+H⁺) 333.0545, found 333.0548. HPLC-UV/Vis *k*: 12.71. Anal. Calc. for C₁₅H₁₂N₂O₅S, C, 54.21, H, 3.64, N, 8.43; found, C, 54.33, H, 3.45, N, 8.55.

2-(4-Nitrophenylthio)-N-(4-carboxymethylphenyl)acetamide (C5). Yield 64%, m.p. 142-144°C (column chromatography CH₂Cl₂/CH₃OH 9:1), ¹H-NMR (DMSO-d₆, 400 MHz) (δ) (ppm): 12.20 (1H, broad s), 10.30 (1H, s), 8.18 (2H, m), 7.60 (2H, m), 7.55 (2H, m), 7.20 (2H, m), 4.09 (2H, s), 3.50 (2H, s); ¹³C-NMR (DMSO-d₆, 100 MHz) (δ) (ppm): 173.22, 166.29, 147.42, 145.16, 137.70, 130.82, 130.21, 126.88, 124.36, 119.62, 49.06, 36.45. ESI-HRMS calc. for C₁₆H₁₅N₂O₅S (M+H⁺) 347.0702, found 347.0709. . HPLC-UV/Vis *k*: 11.59. Anal. Calc. for C₁₆H₁₄N₂O₅S, C, 55.48, H, 4.07, N, 8.09; found, C, 55.33, H, 3.95, N, 8.44.

2-(4-Carboxyphenylthio)-N-(2-carboxyphenyl)acetamide (D5). Yield 53%, m.p. 244-245°C (trituration with Et₂O), ¹H-NMR (DMSO-d₆, 200 MHz) (δ) (ppm): 13.26 (1 H, broad s), 11.72 (1 H, s), 8.48 (1 H, d, J 8.2), 7.96 (2 H, m), 7.85 (2 H, m), 7.58 (2H, m), 7.43 (2 H, m), 7.15 (1 H, t, J 8.2); ¹³C-NMR (DMSO-d₆, 50 MHz) (δ) (ppm): 169.56, 167.31, 167.28, 142.20, 140.60, 134.45, 131.54, 130.32, 128.40, 126.85, 123.58, 120.48, 117.35, 37.23. ESI-HRMS calc. for C₁₆H₁₄NO₅S (M+H⁺) 332.0593, found 332.0590. HPLC-UV/Vis *k*: 11.01. Anal. Calc. for C₁₆H₁₃NO₅S, C, 58.00, H, 3.95, N, 4.23; found, C, 58.33, H, 3.85, N, 4.55.

2-(4-Carboxyphenylthio)-N-(4-carboxyphenyl)acetamide (D6). Yield 50%, m.p. 294-296°C (DMF/H₂O), ¹H-NMR (DMSO-d₆, 400 MHz) (δ) (ppm): 12.80 (2H, broad s), 10.60 (1H, s), 7.88 (4H, m), 7.68 (2H, m), 7.48 (2H, m), 4.05 (2H, s); ¹³C-NMR (DMSO-d₆, 100 MHz) (δ) (ppm): 167.37, 167.31, 143.21, 142.96, 130.94, 130.24, 128.08, 127.75, 125.91, 118.93, 36.77. ESI-HRMS calc. for C₁₆H₁₄NO₅S (M+H⁺) 332.0593, found 332.0578. HPLC-UV/Vis *k*: 10.06. Anal. Calc. for C₁₆H₁₃NO₅S: C 58.00, H 3.95, N 4.23, found, C, 57.96, H, 3.68, N, 4.71.

2-(Benzoxazol-2-ylthio)-N-(4-carboxyphenyl)acetamide (D7). Yield 77%, m.p. 229-230°C (CH₃OH), ¹H-NMR (DMSO-d₆, 400 MHz) (δ) (ppm): 12.70 (1H, broad s), 10.70 (1H, s), 7.91 (2H, m), 7.75-7.55 (4H, m), 7.32 (2H, m), 4.40 (2H, s); ¹³C-NMR (DMSO-d₆, 100 MHz) (δ) (ppm): 167.28, 165.99, 164.22, 151.81, 143.13, 141.67, 130.94, 126.04, 125.12, 124.81, 118.97, 118.71,

110.67, 37.28. ESI-HRMS calc. for $C_{16}H_{13}N_2O_4S$ ($M+H^+$) 329.0596, found 329.0592; HPLC-UV/Vis k : 11.83. Anal. Calc. for $C_{16}H_{12}N_2O_4S$: C 58.53, H 3.68, N 8.53, found, C, 58.87, H, 3.44, N, 8.47.

2-(Benzothiazol-2ylthio)-N-(4-carboxyphenyl)acetamide (D8). Yield 75%, m.p. 220-222°C (CH₃OH), ¹H-NMR (DMSO-d₆, 400 MHz) (δ) (ppm): 12.78 (1H, broad s), 10.81 (1H, s), 8.03 (1H, d, J 8.0, J 0.6), 7.93 (2H, m), 7.83 (1H, d, J 8.0), 7.73 (2H, m), 7.47 (1H, dt, J 7.4, J 1.2), 7.37 (1H, dt, J 8.2, J 1.1), 4.44 (2H, s); ¹³C-NMR (DMSO-d₆, 100 MHz) (δ) (ppm): 167.31, 166.41, 166.27, 152.97, 143.21, 135.26, 130.97, 126.89, 126.00, 125.03, 122.37, 121.56, 118.95, 38.27. ESI-HRMS calc. for $C_{16}H_{13}N_2O_3S_2$ ($M+H^+$) 345.0368, found 345.0366. HPLC-UV/Vis k : 12.31. Anal. Calc. for $C_{16}H_{12}N_2O_3S_2$, C, 55.80, H, 3.51, N, 8.13; found, C, 55.53, H, 3.45, N, 8.38.

2-(2-Carboxyphenylthio)-N-(4-carboxyphenyl)acetamide (D11). Yield 59%, m.p. 265-266°C (DMF/H₂O), ¹H-NMR (DMSO-d₆, 400 MHz) (δ) (ppm): 11.05 (2H, broad s), 9.10 (1H, s), 6.75 (3H, m), 6.56 (2H, m), 6.42 (2H, m), 6.15 (1H, m), 4.01 (2H, s); ¹³C-NMR (DMSO-d₆, 100 MHz) (δ) (ppm): 167.89, 167.87, 167.30, 143.31, 140.83, 132.90, 131.42, 130.89, 128.41, 126.21, 125.90, 124.78, 118.93, 37.18. ESI-HRMS calc. for $C_{16}H_{14}NO_5S$ ($M+H^+$) 332.0593, found 332.0581. HPLC-UV/Vis k : 10.09. Anal. Calc. for $C_{16}H_{13}NO_5S$: C 58.00, H 3.95, N 4.23, found, C, 58.19, H, 3.85, N, 4.58.

2-(Pyrimidin-2ylthio)-N-(4-carboxyphenyl)acetamide (D12). Yield 72%, m.p. 208-210 °C (CH₃OH/Et₂O), ¹H-NMR (DMSO-d₆, 200 MHz) (δ) (ppm): 12.60 (1H, broad s), 10.51 (1H, s), 8.64 (2H, d, J 9.2), 7.88 (2H, m), 7.68 (2H, m), 7.23 (1H, t, J 9.2), 4.10 (2H, s); ¹³C-NMR (DMSO-d₆, 50 MHz) (δ) (ppm): 167.31, 167.15, 158.25, 143.43, 130.87, 125.75, 118.86, 117.91, 36.00. ESI-HRMS calc. for $C_{13}H_{12}N_3O_3S$ ($M+H^+$) 290.0599, found 290.0594. HPLC-UV/Vis k : 9.04. Anal. Calc. for $C_{13}H_{11}N_3O_3S$, C, 53.97, H, 3.83, N, 14.52; found, C, 54.13, H, 3.85, N, 14.55.

2-(4-Acetylaminothio)-N-(4-carboxyphenyl)acetamide (D13). Yield 81%, m.p. 262-264°C (CH₃OH), ¹H-NMR (DMSO-d₆, 400 MHz) (δ) (ppm): 12.71 (1H, broad s), 10.40 (1H, s), 9.90 (1H, s), 7.88 (2H, m), 7.66 (2H, m), 7.53 (2H, m), 7.35 (2H, m), 3.80 (2H, s), 2.00 (3H, s); ¹³C-NMR (DMSO-d₆, 100 MHz) (δ) (ppm): 168.75, 167.97, 167.29, 143.31, 138.75, 130.94, 130.86, 129.00, 125.85, 120.02, 118.92, 39.38, 36.00. ESI-HRMS calc. for $C_{17}H_{17}N_2O_4S$ ($M+H^+$) 345.0909, found

345.0907. HPLC-UV/Vis *k*: 9.68. Anal. Calc. for C₁₇H₁₆N₂O₄S, C, 59.29, H, 4.68, N, 8.13; found, C, 59.55, H, 4.45, N, 8.35.

2-(5-Sulfamoylpyridin-2-ylthio)-N-(2-carboxyphenyl)acetamide (D14). Yield 72%, m.p. 268-270°C (CH₃OH/Et₂O), ¹H-NMR (DMSO-d₆, 200 MHz) (δ) (ppm): 12.65 (1H, s), 10.60 (1H, s), 8.78 (1 H, d, *J* 1.4), 7.95 (1 H, dd, *J* 1.4, *J* 8.6), 7.88 (2 H, m), 7.69 (2 H, m), 7.60 (1 H, d, *J* 8.6), 7.49 (2 H, s), 4.23 (2 H, s); ¹³C-NMR (DMSO-d₆, 50 MHz) (δ) (ppm): 167.30, 167.08, 162.49, 146.57, 143.37, 136.89, 134.29, 130.89, 125.83, 121.92, 118.89, 40.05. ESI-HRMS calc. for C₁₄H₁₄N₃O₅S₂ (M+H⁺) 368.0375, found 368.0368. HPLC-UV/Vis *k*: 9.29. Anal. Calc. for C₁₄H₁₃N₃O₅S₂, C, 45.77, H, 3.57, N, 11.44; found, C, 45.50, H, 3.45, N, 11.57.

2-(4-Nitrophenylthio)-N-(substituted)acetamide derivatives (C1) and (C12). General procedure. To a solution of (**H1b**) or (**H6b**) respectively (2.0 mmol) and TEA (3.0 mmol) in anhydrous THF (30 mL), 4-nitrothiophenol (**J1**) (2.0 mmol) in anhydrous THF (20 mL) was added under stirring at RT under a N₂ atmosphere, and the solution thus obtained was stirred for 2 hours; at the end of the reaction, the solution was diluted with CH₂Cl₂, washed with 1N HCl (20 mL); the organic phase was dried (Na₂SO₄) and the solvent removed under reduced pressure. The residue thus obtained was purified by means of column chromatography (cyclohexane:EtOAc 8:2 then 100% EtOAc).

2-(4-Nitrophenylthio)-N-(2-chlorophenyl)acetamide (C1): Yield 0.44g (67%), m.p. 144-146°C, ¹H-NMR (DMSO-d₆, 400 MHz) (δ) (ppm): 10.10 (1H, broad s), 8.32 (2H, m), 7.87 (1H, d, *J* 7.7), 7.76 (2H, m), 7.65 (1H, d, *J* 8.1), 7.47 (1H, m), 7.35 (1H, m), 4.40 (2H, s); ¹³C-NMR (DMSO-d₆, 100 MHz) (δ) (ppm): 166.9, 147.15, 145.25, 134.89, 130.02, 128.00, 127.08, 126.99, 126.77, 126.29, 124.37, 35.86; ESI-HRMS calcd for C₁₄H₁₂ClN₂O₃S (M+H⁺) 323.0257, found 323.0261; HPLC-UV/Vis *k*: 13.87. Anal. Calc. for C₁₄H₁₁ClN₂O₃S, C, 52.10, H, 3.44, N, 8.68; found C, 52.33, H, 3.22, N, 8.80.

2-(4-Nitrophenylthio)-N-(quinolin-8-yl)acetamide (C10): Yield 0.30 g (39%), m.p. 160-161°C, ¹H-NMR (DMSO-d₆, 400 MHz) (δ) (ppm): 10.90 (1H, broad s), 9.08 (1H, dd, *J* 4.1, *J* 1.6) 8.75 (1H, dd, *J* 7.7, *J* 0.9), 8.56 (1H, dd, *J* 8.4, *J* 1.6), 8.30 (2H, m), 7.87-7.77 (4H, m), 7.73 (1H, m), 4.55 (2H, s); ¹³C-NMR (DMSO-d₆, 100 MHz) (δ) (ppm): 166.99, 149.50, 146.85, 145.33, 138.59, 137.11, 134.56, 128.33, 127.40, 127.13, 124.43, 122.87, 122.73, 117.18, 35.59; ESI-HRMS calcd for C₁₇H₁₄N₃O₃S (M+H⁺) 340.0756, found 340.0754. HPLC-UV/Vis *k*: 14.37. Anal. Calc. for C₁₇H₁₃N₃O₃S, C, 60.17, H, 3.86, N, 12.38; found, C 60.57, H, 3.60, N, 12.20.

2-(4-Aminophenylthio)-N-(4-carboxyphenyl)- (D9) and 2-(4-aminophenylthio)-N-(2-carboxyphenyl)acetamide(D10). General procedure. (Figure S5) The compounds were obtained by means of catalytic reduction of the corresponding nitroderivatives (**C3**) and (**C4**), respectively. A solution of **C3** and **C4** (1.77 mmol) in CH₃OH (100 mL) was hydrogenated on Pd/C 5% (0.26 g) at 2 atm for 6 hours. At the end of the reaction, the catalyst was filtered and the solvent removed under reduced pressure.

2-(4-Aminophenylthio)-N-(4-carboxyphenyl)acetamide (D9). Yield 68%, m.p. 238-240°C (dec.) (CH₃OH/EtOAc), ¹H-NMR (DMSO-d₆, 400 MHz) (δ) (ppm): 10.93 (1H, s), 7.88 (2H, m), 7.68 (2H, m), 7.46 (2H, m), 7.23 (2H, m), 3.90 (2H, s); ¹³C-NMR (DMSO-d₆, 100 MHz) (δ) (ppm): 167.78, 167.32, 143.40, 134.38, 133.01, 132.39, 130.84, 130.16, 125.82, 123.29, 118.93, 112.81, 38.17. ESI-HRMS calc. for C₁₅H₁₅N₂O₃S (M+H⁺) 303.0803, found 303.0808. HPLC-UV/Vis *k*: 8.36. Anal. Calc. for C₁₅H₁₄N₂O₃S, C, 59.59, H, 4.67, N, 9.27; found, C, 59.77, H, 4.60, N, 9.08.

2-(4-Aminophenylthio)-N-(2-carboxyphenyl)acetamide (D10). Yield 0.587 g (90%), m.p. 154-155°C, ¹H-NMR (DMSO-d₆, 200 MHz) (δ) (ppm): 11.88 (1H, s), 8.50 (1H, d, *J* 8.4), 7.93 (1H, d, *J* 7.7), 7.55 (1H, t, *J* 7.9), 7.15 (3H, m), 6.50 (2H, m), 3.80 (2H, s); ¹³C-NMR (DMSO-d₆, 50 MHz) (δ) (ppm): 169.66, 168.39, 148.73, 140.95, 134.46, 133.83, 131.57, 123.25, 120.11, 118.68, 116.94, 115.26, 42.25. ESI-HRMS calc. for C₁₅H₁₅N₂O₃S (M+H⁺) 303.0803, found 303.0801. HPLC-UV/Vis *k*: 9.46. Anal. Calc. for C₁₅H₁₄N₂O₃S, C, 59.59, H, 4.67, N, 9.27; found, C, 59.80, H, 4.66, N, 9.55.

Synthesis of compounds C6-C9, C11, E1-E7 (Figure S6). Synthesis of methyl- or ethyl-2-[(4-nitrophenylthio)]acetate derivatives (K1a-K1d esters). General procedure. To a suspension of 4-nitrothiophenol (3.87 mmol) and K_2CO_3 (5.79 mmol) in anhydrous acetone (20 mL) under N_2 atmosphere under stirring at RT, the appropriate bromoacetate (**K1a-K1d**) (4.25 mmol) was added dropwise, and the suspension was stirred for 1 hour; in the case of (**K1b**), the reaction time was 12 hours. At the end of the reaction, water was added (40 mL) and the mixture was extracted with EtOAc (3x10 mL); the organic phase was dried (Na_2SO_4) and the solvent removed under reduced pressure.

Ethyl-[2-(4-nitrophenylthio)]propionate (K1a ester). Yield 90%, oil (column chromatography cyclohexane/EtOAc 8:2), 1H -NMR ($CDCl_3$, 400 MHz) (δ) (ppm): 8.16 (2H, m), 7.52 (2H, m), 4.20 (2H, q, J 7.2), 4.05 (1H, q, J 7.2), 1.60 (3H, d, J 7.2), 1.25 (3H, t, J 7.2); ^{13}C -NMR ($CDCl_3$, 100 MHz) (δ) (ppm): 171.82, 146.08, 144.61, 128.94, 126.43, 124.45, 123.93, 61.99, 43.73, 17.26, 14.21.

Ethyl-[2-methyl(4-nitrophenylthio)]propionate (K1b ester). Yield 92%, oil (column chromatography cyclohexane/EtOAc 7.5:2.5), 1H -NMR ($CDCl_3$, 400 MHz) (δ) (ppm): 8.15 (2H, m), 7.60 (2H, m), 4.15 (2H, q, J 7.2), 1.60 (6H, s), 1.28 (3H, t, J 7.2); ^{13}C -NMR ($CDCl_3$, 100 MHz) (δ) (ppm): 173.46, 147.71, 141.41, 135.16, 123.53, 61.63, 51.54, 26.08, 14.08.

Ethyl-[2-phenyl(4-nitrophenylthio)]acetate (K1c ester). Yield 77%, oil, 1H -NMR ($CDCl_3$, 400 MHz) (δ) (ppm): 8.11 (2H, m), 7.54 (2H, dd, J 8.0, J 2.0), 7.40 (5H, m), 4.20 (3H, m), 1.33 (3H, t, J 7.2); ^{13}C -NMR ($CDCl_3$, 100 MHz) (δ) (ppm): 169.50, 146.18, 144.57, 134.33, 129.07, 128.95, 128.91, 128.44, 123.98, 62.37, 54.61, 14.04.

Methyl-2-[(4-nitrophenylthio)]acetate (K1d ester). Yield 82%, m.p. 47-49°C, 1H -NMR ($DMSO-d_6$, 200 MHz) (δ) (ppm): 8.15 (2H, m), 7.50 (2H, m), 4.15 (2H, s), 3.65 (3H, s); ^{13}C -NMR ($DMSO-d_6$, 50 MHz) (δ) (ppm): 169.53, 146.46, 145.30, 135.23, 126.90, 124.39, 124.34, 52.97, 33.58.

2-[(4-Nitrophenylthio)] acetic acid derivatives (K1a-K1d acids). General procedure. To a solution of the appropriate ester (**K1a-K1d esters**) (6.87 mmol) in ethanol (43 ml) aqueous NaOH 2 M (10.31 mmol) was added and the solution thus obtained was stirred elm at RT under N_2 for 1h, then the solvent was removed under reduced pressure. The residue thus obtained was dissolved in

EtOAc, and the organic phase was washed with HCl 0.5N; then the organic phase was dried (Na₂SO₄) and the solvent removed under reduced pressure; the product was then purified as reported below.

[2-(4-Nitrophenylthio)]propionic acid (K1a acid). Yield 70%, m.p. 110-111°C (trituration with isopropyl ether), ¹H-NMR (DMSO-d₆, 400 MHz) (δ) (ppm): 8.16 (2H, m), 7.52 (2H, m), 4.05 (1H, q, J 7.2), 1.60 (3H, d, J 7.2); ¹³C-NMR (DMSO-d₆, 100 MHz) (δ) (ppm): 171.82, 146.08, 144.61, 128.94, 126.43, 124.45, 123.93, 43.73, 17.26.

[2-Methyl-(4-nitrophenylthio)]propionic acid (K1b acid). Yield 59%, m.p. 105-107°C (trituration with diethyl ether), ¹H-NMR (CDCl₃, 400 MHz) (δ) (ppm): 8.15 (2H, m), 7.60 (2H, m), 1.60 (6H, s); ¹³C-NMR (CDCl₃, 100 MHz) (δ) (ppm): 173.46, 147.71, 141.41, 135.16, 123.53, 26.08.

[2-Phenyl(4-nitrophenylthio)]acetic acid (K1c acid). Yield 66%, m.p. 126-128°C (trituration with isopropyl ether), ¹H-NMR (DMSO-d₆, 400 MHz) (δ) (ppm): 8.27 (2H, m), 7.74-7.66 (4H, m), 7.55-7.45 (3H, m), 5.79 (1H, s); ¹³C-NMR (DMSO-d₆, 100 MHz) (δ) (ppm): 171.08, 145.73, 145.59, 135.91, 129.28, 128.87, 128.24, 124.35, 53.22.

[(4-Nitrophenyl)thio]acetic acid (K1d acid). Yield 68%, m.p. 140-142°C (acetone/petrol ether b.p. 40-60°C), ¹H-NMR (DMSO-d₆, 200 MHz) (δ) (ppm): 12.90 (1H, broad s), 8.15 (2H, m), 7.95 (2H, m), 4.0 (2H, s); ¹³C-NMR (DMSO-d₆, 50 MHz) (δ) (ppm): 170.29, 147.07, 145.12, 126.71, 124.30, 34.10.

2-(4-Nitrophenylthio)-N-(aryl- or heteroaryl)-acetamide derivatives C6, C7, C9, C11, E1-E6:

General procedure. To a solution of the appropriate carboxylic acid (**K1a-K1d acids**) (4.69 mmol) in anhydrous THF (17 mL) and anhydrous DMF (0.033 mL) at 0°C under elm stirring in a N₂ atmosphere, oxalylchloride (7.18 mmol) was added dropwise, then the mixture was stirred for 1 hour at RT. At the end of the reaction, the solvent was removed under reduced pressure and coevaporated with anhydrous CH₂Cl₂ three times. The oily material was used in the next step without purification. The solution of the acyl chloride thus obtained in CH₂Cl₂ (10 mL) was added dropwise to the solution of the appropriate amine derivative (1.2 eq) in anhydrous CH₂Cl₂ (20 mL), TEA (1.2 eq. in the case of (**E5**) and (**E6**), in the other cases 2.2 eq.) and anhydrous DMF (2-4 mL) at 0°C under stirring in a

N₂ atmosphere. After 12 hours, solvents were evaporated under reduced pressure, water was added to the residue, pH was adjusted to 1.00 (HCl 1N) and the precipitate thus obtained was collected and washed with water. The crude product thus obtained was purified as reported below.

2-(4-Nitrophenylthio)-N-(indol-6-yl)acetamide (C6): Yield 0.167 g (40%), m.p. 192-194°C (column chromatography (cyclohexane:EtOAc 4:6), ¹H-NMR (DMSO-d₆, 400 MHz) (δ) (ppm): 11.00 (1H, broad s), 10.25 (1H, broad s), 8.18 (2H, m), 7.94 (1H, s), 7.63 (2H, m), 7.46 (1H, d, J 8.3), 7.27 (1H, m), 7.03 (1H, dd, J 8.6, J 1.7), 6.36 (1H, s), 4.10 (2H, s); ¹³C-NMR (DMSO-d₆, 100 MHz) (δ) (ppm): 165.82, 147.63, 145.13, 136.28, 133.27, 126.90, 125.64, 124.65, 124.35, 120.38, 112.64, 102.76, 101.42, 36.60; ESI-HRMS calcd for C₁₆H₁₄N₃O₃S (M+H⁺) 328.0756, found 328.0740. HPLC-UV/Vis *k*: 12.82. Anal. Calc. for C₁₆H₁₃N₃O₃S, C, 58.70, H, 4.00, N, 12.84; found, C, 58.77, H, 4.11, N, 12.89.

2-(4-Nitrophenylthio)-N-(acetylaminosulfonylphen-4-yl)acetamide (C7): The reaction was carried out as described in the general procedure, using a suspension of sodium sulfacetamide (0.54 g, 2.30 mmol) in anhydrous DMF (6 mL) and TEA (0.26 g, 2.53 mmol). Yield 0.37 g (39%), m.p. 227-228°C (methanol), ¹H-NMR (DMSO-d₆, 400 MHz) (δ) (ppm): 12.10 (1H, broad s), 10.90 (1H, broad s), 8.31 (2H, m), 8.15 (2H, m), 7.93 (2H, m), 7.74 (2H, m), 4.30 (2H, s), 2.05 (3H, s); ¹³C-NMR (DMSO-d₆, 100 MHz) (δ) (ppm): 169.13, 167.24, 147.06, 145.25, 143.64, 133.91, 129.45, 126.96, 124.39, 119.24, 36.53, 23.65; ESI-HRMS calcd for C₁₆H₁₆N₃O₆S₂ (M+H⁺) 410.0480, found 410.0479. HPLC-UV/Vis *k*: 11.74. Anal. Calc. for C₁₆H₁₅N₃O₆S₂, C, 46.94, H, 3.69, N, 10.26; found, C, 46.66, H, 3.80, N, 10.33.

2-(4-Nitrophenylthio)-N-(2-chlorobenzyl)acetamide (C9): Yield 0.40 g (85%), m.p. 122-123°C (column chromatography cyclohexane:EtOAc 8:2)., ¹H-NMR (DMSO-d₆, 400 MHz) (δ) (ppm): 8.90 (1H, t, J 5.5), 8.28 (2H, m), 7.72-7.70 (2H, m), 7.57 (1H, m), 7.43-7.41 (3H, m), 4.50 (2H, d, J 5.5), 4.11 (2H, s); ¹³C-NMR (DMSO-d₆, 100 MHz) (δ) (ppm): 167.80, 147.41, 145.15, 136.30, 132.62, 129.62, 129.46, 129.26, 127.56, 126.99, 124.28, 40.97, 35.27; ESI-HRMS calcd for C₁₅H₁₄ClN₂O₃S

(M+H⁺) 337.0413, found 337.0403. HPLC-UV/Vis *k*: 13.33. Anal. Calc. for C₁₅H₁₃ClN₂O₃S, C, 53.49, H, 3.89, N, 8.32; found, C, 53.66, H, 3.96, N, 8.20.

2-(4-Nitrophenylthio)-N-(3-carboxypyridin-2-yl)acetamide (C11). Yield 21%, m.p. 194-196°C (H₂O), ¹H-NMR (DMSO-d₆, 400 MHz) (δ) (ppm): 11.11 (1H, s), 8.53 (1H, dd, J 7.1, J 1.9), 8.22 (1H, dd, J 8.2, J 2.3), 8.15 (2H, m), 7.56 (2H, m), 7.28 (1H, dd, J 8.2, J 7.1), 4.30 (2H, s); ¹³C-NMR (DMSO-d₆, 100 MHz) (δ) (ppm): 167.92, 167.31, 151.56, 150.12, 147.26, 147.00, 140.26, 126.97, 126.73, 124.31, 120.29, 36.86. ESI-HRMS calc. for C₁₄H₁₂N₃O₅S (M+H⁺) 334.0498, found 334.0490. HPLC-UV/Vis *k*: 9.05. Anal. Calc. for C₁₄H₁₁N₃O₅S, C, 50.45, H, 3.33, N, 12.61; found, C, 50.33, H, 3.45, N, 12.85.

2-(4-Nitrophenylthio)-N-(4-carboxyphenyl)propionamide (E1). Yield 74%, m.p. 232-234°C (trituration with diethyl ether), ¹H-NMR (DMSO-d₆, 400 MHz) (δ) (ppm): 12.80 (1H, broad s), 10.66 (1H, s), 8.18 (2H, m), 7.92 (2H, m), 7.70 (2H, m), 7.61 (2H, m), 4.43 1H, q, J 6.9), 1.58 (3H, d, J 6.9); ¹³C-NMR (DMSO-d₆, 100 MHz) (δ) (ppm): 170.07, 167.29, 145.78, 145.32, 143.06, 130.90, 128.82, 126.15, 124.52, 119.22, 45.58, 18.33. ESI-HRMS calc. for C₁₆H₁₅N₂O₅S (M+H⁺) 347.0702, found 347.0701. HPLC-UV/Vis *k*: 12.31. Anal. Calc. for C₁₆H₁₄N₂O₅S, C, 55.48, H, 4.07, N, 8.09; found, C, 55.23, H, 3.95, N, 8.55.

2-Methyl-2-(4-nitrophenylthio)-N-(4-carboxyphenyl)propionamide (E2). Yield 20%, m.p. 215-217°C (column chromatography CH₂Cl₂/CH₃OH 9.5:0.5), ¹H-NMR (DMSO-d₆, 400 MHz) (δ) (ppm): 12.80 (1H, broad s), 10.11 (1H, s), 18.18 (2H, m), 7.90 (2H, m), 7.75 (2H, m), 7.5r8 (2H, m), 1.70 (6H, s); ¹³C-NMR (DMSO-d₆, 100 MHz) (δ) (ppm): 170.28, 167.00, 148.20, 144.10, 143.21, 130.42, 130.15, 126.52, 120.44, 120.00, 50.42, 26.51. ESI-HRMS calc. for C₁₇H₁₇N₂O₅S (M+H⁺) 361.0858, found 361.0844. HPLC-UV/Vis *k*: 13.02. Anal. Calc. for C₁₇H₁₆N₂O₅S, C, 56.66, H, 4.47, N, 7.77; found, C, 56.39, H, 4.45, N, 8.00.

2-Phenyl-2-(4-nitrophenylthio)-N-(4-carboxyphenyl)carboxylic acid (E3). Yield 40%, m.p. 219-221°C (column chromatography CH₂Cl₂/CH₃OH 9.5:0.5), ¹H-NMR (DMSO-d₆, 400 MHz) (δ) (ppm): 12.80 (1H, broad s), 8.18 (2H, m), 7.90 (2H, m), 7.69 (2H, m) 7.64 (2H, m), 7.55 (2H, m),

7.40 (2H, m), 7.35 (1H, m), 5.75 (1H, s); ¹³C-NMR (DMSO-d₆, 100 MHz) (δ) (ppm): 167.63, 167.23, 145.72, 145.66, 142.80, 136.15, 130.93, 129.34, 128.99, 128.74, 128.13, 126.41, 124.60, 119.30, 54.98. ESI-HRMS calc. for C₂₁H₁₇N₂O₅S (M+H⁺) 409.0858, found 409.0867. HPLC-UV/Vis *k*: 13.63. Anal. Calc. for C₂₁H₁₆N₂O₅S, C, 61.76, H, 3.95, N, 6.86; found, C, 61.70, H, 3.70, N, 6.95.

2-Phenyl-2-(4-nitrophenylthio)-N-(3-hydroxy-4-carboxyphenyl)acetamide (E4). Yield 23%, m.p. 218-220°C (column chromatography CH₂Cl₂/CH₃OH 8.5:1.5), ¹H-NMR (DMSO-d₆, 400 MHz) (δ) (ppm) 15.80 (1H, broad s), 10.58 (1H, s), 8.18 (2H, s), 7.63 (3H, m), 7.52 (2H, m), 7.44-7.30 (3H, m), 6.99 (1H, d, J 1.9), 6.82 (1H, dd, J 8.4, J 1.9), 5.71 (1H, s); ¹³C-NMR (DMSO-d₆, 100 MHz) (δ) (ppm): 167.07, 163.59, 145.2, 145.62, 141.97, 136.47, 131.02, 129.28, 128.88, 128.69, 127.99, 124.57, 116.23, 108.31, 106.70, 54.96. ESI-HRMS calc. for C₂₁H₁₇N₂O₆S (M+H⁺) 425.0807, found 425.0793. HPLC-UV/Vis *k*: 13.89. Anal. Calc. for C₂₁H₁₆N₂O₆S, C, 59.43, H, 3.80, N, 6.60; found, C, 59.59, H, 3.95, N, 6.55.

2-Phenyl-2-(4-nitrophenylthio)-N-(4-carboxamidophenyl)acetamide (E5). Yield 59%, m.p. 228-230°C, ¹H-NMR (DMSO-d₆, 400 MHz) (δ) (ppm): 10.90 (1H, s), 8.31 (2H, m), 8.00 (3H, m), 7.80 (4H, m), 7.70 (2H, m), 7.60-7.45 (2H, m), 7.40 (2H, s), 5.81 (1H, s); ¹³C-NMR (DMSO-d₆, 100 MHz) (δ) (ppm): 167.64, 167.43, 145.70, 141.34, 136.20, 130.08, 129.34, 128.95, 128.73, 128.11, 124.61, 119.10, 55.04. ESI-HRMS calc. for C₂₁H₁₈N₃O₄S (M+H⁺) 408.1018, found 408.1038. HPLC-UV/Vis *k*: 12.73. Anal. Calc. for C₂₁H₁₇N₃O₄S, C, 61.90, H, 4.21, N, 10.31; found, C, 61.56, H, 3.99, N, 10.50.

2-(4-Nitrophenylthio)-N-(3-carbomethoxypyridin-6-yl)acetamide (E6). Methyl (6-amino)nicotinate (**L3**), starting material for the synthesis of (**E6**), was obtained via esterification of 6-amino-nicotinic acid in MeOH saturated with HCl_g, prepared in situ adding HCl_g to a suspension of the nicotinic acid (0.730 g, 5.29 mmol) in MeOH (50 ml) at 0°C. Then the reaction mixture was refluxed at 100°C under stirring in a N₂ atmosphere for 3 hours. The solvent was removed under reduced pressure and Na₂CO₃ was added up to pH=9. A white powder was collected. Yield 87%. Compound **E6** was thus obtained following the general procedure described above. Yield 65%, m.p.

138-140°C (EtOH), ¹H-NMR (DMSO-d₆, 400 MHz) (δ) (ppm): 11.64 (1H, s), 8.90 (1H, s), 8.29 (1H, dd, J 8.7, J 2.3), 8.15 (3H, m), 7.63 (2H, m), 7.55 (2H, m), 7.45-7.35 (3H, m), 5.90 (1H, s) 3.94 (3H, s); ¹³C-NMR (DMSO-d₆, 100 MHz) (δ) (ppm): 168.60, 165.16, 154.97, 150.07, 145.78, 145.38, 140.10, 135.87, 129.42, 129.11, 128.77, 128.12, 124.65, 122.07, 113.26, 54.32, 52.65. ESI-HRMS calc. for C₂₁H₁₈N₃O₅S (M+H⁺) 424.0967, found 424.0964. HPLC-UV/Vis *k*: 15.00. Anal. Calc. for C₂₁H₁₇N₃O₅S, C, 59.57, H, 4.05, N, 9.92; found, C, 59.66, H, 3.98, N, 9.75.

2-(4-Nitrophenylthio)- and phenyl-2-(4-nitrophenylthio)-N-(6-methanesulfonylbenzothiazol-2-yl)acetamide (C8) and (E7). General procedure. To a solution of (**K1d acid**) and (**K1c acid**) respectively (0.50 g, 2.35 mmol) in anhydrous DMF (10 mL) under stirring at RT in a N₂ atmosphere, 1-ethyl-3-(3-dimethylaminopropyl)carbodiimide (WSC) (0.45 g, 2.35 mmol), 2-amino-6-methanesulphonylbenzothiazole (L4) (0.54 g, 2.35 mmol) and HOBt (0.32 g, 2.35 mmol) were added in sequence. After 12 hours at RT the mixture was treated with water (2 x 10 mL) and the residue thus obtained was purified by trituration with EtOAc.

2-(4-Nitrophenylthio)-N-(6-methanesulfonylbenzothiazol-2-yl)acetamide (C8): Yield 35%, m.p. 217-218°C (ethyl acetate). ¹H-NMR (DMSO-d₆, 400 MHz) (δ) (ppm): 13.00 (1H, broad s), 8.64 (1H, s), 8.18 (2H, m), 7.97 (2H, s), 7.61 (2H, m), 4.30 (2H, s), 3.22 (3H, s); ¹³C-NMR (DMSO-d₆, 100 MHz) (δ) (ppm): 168.48, 162.22, 152.43, 146.42, 145.41, 136.09, 132.48, 127.12, 125.39, 124.45, 122.65, 121.49, 44.48, 35.33. ESI-HRMS calc. for C₁₆H₁₄N₃O₅S₃ (M+H⁺) 424.0096, found 424.0096. HPLC-UV/Vis *k*: 12.44. Anal. Calc. for C₁₆H₁₃N₃O₅S₃, C, 45.38, H, 3.09, N, 9.92; found, C, 45.65, H, 3.25, N, 9.75.

Phenyl[2-(4-nitrophenylthio)-N-(6-methanesulfonylbenzothiazol-2-yl)]acetamide (E7): Yield 18%, m.p. 95°C (dec.) (column chromatography CH₂Cl₂:CH₃OH 9.5:0.5, then trituration with diisopropyl ether). ¹H-NMR (DMSO-d₆, 200 MHz) (δ) (ppm): 13.30 (1H, broad s), 8.66 (1H, s), 8.12 (2H, m), 7.95 (2H, s), 7.70-7.30 (7H, m), 5.83 (1H, s), 3.20 (3H, s); ¹³C-NMR (DMSO-d₆, 50 MHz) (δ) (ppm): 174.01, 168.10, 152.09, 146.03, 136.30, 134.99, 129.52, 129.35, 128.93, 128.67, 125.44, 124.67, 122.72, 121.62, 53.98, 44.46. ESI-HRMS calc. for C₂₂H₁₈N₃O₅S₃ (M+H⁺) 500.0409, found

500.0404. HPLC-UV/Vis *k*: 14.16. Anal. Calc. for C₂₂H₁₇N₃O₅S₃, C, 52.89, H, 3.43, N, 8.41; found, C, 52.65, H, 3.35, N, 8.65.

Synthesis of compounds D1-D4 (Figure S7). **General procedure.** To a solution of aminobenzoic acid (**M1**) or (**M2**) (3.56 mmol) and TEA (6.52 mmol) in anhydrous CH₂Cl₂ (20 mL) was added, during 10 min, a solution of the opportune acyl chloride (**N1**)-(N3) (2.96 mmol) in anhydrous CH₂Cl₂ (6 mL) under stirring elm at 0°C in a N₂ atmosphere. The solution was stirred for 12 hours at RT, then the solvent was removed under reduced pressure, the residue was diluted with water/ice, acidified (HCl 0.5N) and the precipitate was collected and washed with water.

3-phenyl-N-(4-carboxyphenyl)propionamide (D1). Yield 0.156 g (20%) (CH₃OH), m.p. 240-242°C, ¹H-NMR (DMSO-d₆, 400 MHz) (δ) (ppm): 12.80 (1H, broad s), 10.21 (1H, s), 7.89 (2H, m), 7.70 (2H, m), 7.30-7.15 (5H, m), 2.93 (2H, t, J 8.0), 2.68 (2H, t, J 8.0); ¹³C-NMR (DMSO-d₆, 100 MHz) (δ) (ppm): 171.40, 167.39, 143.70, 141.52, 130.85, 128.80, 128.71, 126.44, 125.40, 118.73, 38.50, 31.00. ESI-HRMS calc. for C₁₆H₁₆NO₃ (M+H⁺) 270.1130, found 270.1127. HPLC-UV/Vis *k*: 11.87. Anal. Calc. for C₁₆H₁₅NO₃, C, 71.36, H, 5.61, N, 5.20; found, C, 71.45, H, 5.65, N, 5.35.

3-phenyl-N-(3-carboxyphenyl)propionamide (D2). Yield 63%, m.p. 214-216°C (CH₃OH), ¹H-NMR (DMSO-d₆, 200 MHz) (δ) (ppm): 12.90 (1H, broad s), 10.05 (1H, s), 8.22 (1H, s), 7.82 1H, d, J 8.2), 7.60 (1H, d, J 8.2), 7.40 (1H, t, J 8.2), 7.30-7.10 (5H, m), 2.90 (2H, t, 8.0), 2.50 (2H, t, J 8.0); ¹³C-NMR (DMSO-d₆, 50 MHz) (δ) (ppm): 171.09, 167,62, 141.57, 139.88, 131.73, 129.37, 128.78, 128.69, 126.40, 124.30, 123.60, 120.28, 38.39, 31.20. ESI-HRMS calc. for C₁₆H₁₆NO₃ (M+H⁺) 270.1130, found 270.1124. HPLC-UV/Vis *k*: 11.55. Anal. Calc. for C₁₆H₁₅NO₃: C 71.36, H 5.61, N 5.20, found, C, 71.28, H, 5.58, N, 5.24.

3-(4-Nitrophenyl)-N-(3-carboxyphenyl)prop-2-enamide (D3). Yield 43%, m.p. 295-297°C (CH₃OH), ¹H-NMR (DMSO-d₆, 200 MHz) (δ) (ppm): 12.90 (1H, broad s), 10.65 (1H, s), 8.28 (3H, m), 7.90 (3H, m), 7.68 (1H, d, J 8.0), 7.65 (1H, d, J 15.5), 7.45 (1H, t, J 8.0), 6.98 (1H, d, J 15.5); ¹³C-NMR (DMSO-d₆, 50 MHz) (δ) (ppm): 165.53, 163.48, 148.18, 141.65, 139.70, 138.48, 131.89, 129.58, 129.26, 126.79, 124.87, 124.61, 123.85, 120.52. ESI-HRMS calc. for C₁₆H₁₃N₂O₅ (M+H⁺)

313.0824, found 313.0812. HPLC-UV/Vis *k*: 12.04. Anal. Calc. for C₁₆H₁₂N₂O₅: C 61.54, H 3.87, N 8.97, found, C, 61.34, H, 4.00, N, 8.77.

3-(4-Nitrophenyl)-N-(4-carboxyphenyl)propionamide (D4). Yield 0.072 (10%), m.p. 292-294°C (trituration with CH₂Cl₂), ¹H-NMR (DMSO-d₆, 400 MHz) (δ) (ppm): 12.80 (1H, broad s), 10.40 (1H, broad s), 8.31 (2H, m), 8.02 (2H, m), 7.83 (2H, m), 7.70 (2H, m), 3.21 (2H, m), 2.90 (2H, m); ¹³C-NMR (DMSO-d₆, 100 MHz) (δ) (ppm): 170.91, 167.36, 150.05, 146.46, 143.58, 130.85, 130.10, 125.48, 123.93, 118.76, 37.56, 30.78; ESI-HRMS calcd for C₁₆H₁₅N₂O₅ (M+H⁺) 315.0981, found 315.0980. HPLC-UV/Vis *k*: 11.60. Anal. Calc. for C₁₆H₁₄N₂O₅, C, 61.14, H, 4.49, N, 8.91; found, C, 61.50, H, 4.33, N, 8.89.

Synthesis of compounds F1-F4 (Figures S8 and S9). **Methyl 2-[(quinolin-8-ylsulphonyl)amino]benzoate (F1b)**: To a solution of methyl anthranilate (0.63 g, 4.18 mmol) in anhydrous CH₂Cl₂ (10 mL) at RT were added 8-quinolinesulfonyl chloride (**F1a**) (1.00 g, 4.39 mmol), pyridine (0.99 g, 12.5 mmol), and DMAP (0.03 g, 0.21 mmol) under elm stirring at RT in N₂ atmosphere. The mixture was stirred at RT for 12 hours, then the solvent was removed under reduced pressure. Water was added to the residue thus obtained and the mixture was extracted with EtOAc (2 x 20 mL); the organic phase was dried (Na₂SO₄) and the solvent removed under reduced pressure. This material was used in the next step without further purification. Yield 1.40 g (98%), m.p. 206-209°C, ¹H-NMR (DMSO-d₆, 200 MHz) (δ) (ppm): 11.05 (1H, broad s), 8.98 (1H, m), 8.60-8.20 (3H, m), 7.80-7.55 (4H, m), 7.42 (1H, m), 6.95 (1H, m), 3.90 (1H, s); ¹³C-NMR (DMSO-d₆, 50 MHz) (δ) (ppm): 167.57, 151.99, 139.75, 137.54, 135.33, 134.88, 133.08, 131.41, 128.81, 126.10, 123.28, 123.24, 117.73, 116.57, 53.09.

2-[(Quinolin-8-ylsulphonyl)amino]benzoic acid (F1c): A suspension of (**F1b**) (1.26 g, 3.67 mmol) and aqueous LiOH 2M (7.1 mL) in THF (8.5 mL) was stirred at RT for 12 hours. The solution thus obtained was cooled with ice and HCl 0.5 N (20 mL) was added until pH 2. The residue thus obtained was filtered and washed with water. Yield 1.10g (92%), m.p. 253-259°C (dec.), ¹H-NMR (DMSO-

d₆, 200 MHz) (δ) (ppm): 11.50 (1H, broad s), 8.95 (1H, m), 8.60-8.40 (2H, m), 8.25 (1H, d, *J* 8.2), 7.85-7.50 (4H, m), 7.50-7.30 (1H, m), 7.0-6.80 (1H, m); ¹³C-NMR (DMSO-d₆, 50 MHz) (δ) (ppm): 169.36, 151.87, 142.84, 140.19, 137.43, 135.20, 134.74, 134.51, 133.04, 131.82, 128.81, 126.06, 123.18, 122.91, 117.19, 117.09.

1-[[Quinoline-8-yl-sulfonyl]amino]benzoylmorpholine (F1): To a solution of (F1c) (0.3 g, 0.91 mmol) in anhydrous THF (5 mL) and DMF (0.01 mL) at 0°C, oxalylchloride (0.13 g, 1.35 mmol) was added dropwise, then the mixture was stirred for 1 hour at RT. At the end of the reaction, the solvent was removed under reduced pressure. The solid thus obtained was coevaporated with anhydrous CH₂Cl₂ three times, and the compound (F1d) thus obtained was used in the next step without purification. To a solution of (F1d) (0.32 g, 0.91 mmol) and TEA (0.23 g, 2.28 mmol) in anhydrous CH₂Cl₂ (20 mL) morpholine (0.07 g, 0.82 mmol) was added and the solution thus obtained was stirred at RT for 6 hours. Then the solvent was removed under pressure and the residue thus obtained was purified by column chromatography (EtOAc 100%). Yield 0.099 g (31%), m.p. 191-194°C, ¹H-NMR (DMSO-d₆, 400 MHz) (δ) (ppm): 9.50 (1H, broad s), 9.25 (1H, d, *J* 2.9), 8.75 (1H, d, *J* 7.9), 8.45 (2H, m), 7.91 (2H, m), 7.63 (1H, m), 7.48 (1H, m), 7.27 (2H, m), 3.8-3.0 (8H, m); ¹³C-NMR (DMSO-d₆, 100 MHz) (δ) (ppm): 167.39, 152.16, 142.85, 137.76, 135.59, 134.78, 131.34, 130.89, 128.96, 128.49, 127.47, 126.27, 124.99, 123.94, 123.34, 66.04, 65.38, 47.60, 42.30, 15.63; ESI-HRMS calcd for C₂₀H₂₀N₃O₄S (M+H⁺) 398.1174, found 398.1189. HPLC-UV/Vis *k*: 10.97.

Substituted (isatoic anhydrides) (1b) and (2b). General procedure. To a solution of the appropriate (substituted)-2-aminobenzoic acid (1a, 2a) (5.10 mmol) in anhydrous THF (25 mL), triphosgene (2.20 mmol) was added at RT under stirring elm. The suspension thus obtained was stirred for 24 hours; then, water was added and the solution was extracted with EtOAc (2 x 50 mL); the organic phase was dried (Na₂SO₄) and the solvent removed under reduced pressure.

5,6-Dimethoxy isatoic anhydride (1b): Yield 1.03 g (91%), m.p. 260-261°C (dec.), ¹H-NMR (DMSO-d₆, 200 MHz) (δ) (ppm): 11.5 (1H, broad s), 7.20 (1H, s), 6.60 (1H, s), 3.80 (6H, s); ¹³C-

NMR (DMSO- d_6 , 50 MHz) (δ) (ppm): 159.78, 157.01, 147.83, 146.13, 138.06, 109.06, 101.62, 98.14, 56.53, 56.34.

5-Methoxycarbonyl isatoic anhydride (2b): Yield 1.00 g (88%), m.p. 192-194°C, $^1\text{H-NMR}$ (DMSO- d_6 , 200 MHz) (δ) (ppm): 11.85 (1H, broad s), 8.0 (1H, d, J 8.1), 7.70 (2H, m), 3.9 (3H, s); $^{13}\text{C-NMR}$ (DMSO- d_6 , 50 MHz) (δ) (ppm): 165.31, 147.28, 141.94, 136.86, 130.03, 123.64, 116.39, 114.37, 53.31.

Substituted quinolines (1c) and (2c). General procedure. To a suspension of the appropriate (substituted)isatoic anhydride (**1b**) or (**2b**) (4.6 mmol) in anhydrous DMF (30 mL) morpholine (4.6 mmol) and DMAP (0.46 mmol) were added under stirring at RT in a N_2 atmosphere. The solution was stirred for 8 hours at RT, then, water was added to the reaction mixture and the product was extracted with EtOAc, the organic phase was dried (Na_2SO_4) and the solvent removed under reduced pressure.

1-(2-Amino-4,5-dimethoxybenzoyl)morpholine (1c): Yield 0.36g (30%), m.p. 100-102°C, $^1\text{H-NMR}$ (DMSO- d_6 , 200 MHz) (δ) (ppm): 6.60 (1H, s), 6.35 (1H, s), 4.95 (2H, s), 3.70 (3H, s), 3.65 (3H, s), 3.58 (4H, m), 3.45 (4H, m); $^{13}\text{C-NMR}$ (DMSO- d_6 , 50 MHz) (δ) (ppm): 168.00, 151.62, 142.04, 113.53, 100.76, 66.63, 56.93, 55.66.

1-[(2-Amino-4-methoxycarbonyl)benzoyl]morpholine (2c): Yield 0.65 g (54%), m.p. 112-113°C, $^1\text{H-NMR}$ (DMSO- d_6 , 200 MHz) (δ) (ppm): 7.35(1H, s), 7.10 (2H, s), 5.45 (2H, s), 3.80 (3H, s), 3.7-3.3 (8H, m); $^{13}\text{C-NMR}$ (DMSO- d_6 , 50 MHz) (δ) (ppm): 168.04, 166.66, 146.07, 131.36, 128.47, 123.83, 116.46, 116.42, 66.53, 52.48.

1-[[Quinoline-8-yl-sulfonyl]amino]-3,4-dimethoxybenzoyl]morpholine (F2): To a solution of (**1c**) (0.33 g, 1.25 mmol) in anhydrous CH_2Cl_2 (10 mL) under stirring at RT, 8-quinolinesulfonylchloride (0.28 g, 1.26 mmol), pyridine (0.30 g, 3.75 mmol) and DMAP (8 mg, 0.06 mmol) were added. The mixture was stirred at RT for 12 hours, then the solvent was removed under pressure; water and ice were added to the oily residue, and the solid thus formed was filtered, washed

with water, dried and purified by trituration with anh. diethyl ether (4 mL). Yield 0.57 g 100%, m.p. 166-168°C, ¹H-NMR (DMSO-d₆, 400 MHz) (δ) (ppm): 9.42 (1H, broad s), 9.25 (1H, m), 8.82-8.68 (1H, m), 8.55-8.33 (2H, m), 8.02-7.78 (2H, m), 7.15 (1H, m), 6.80 (1H, m), 3.80 (6H, m), 3.70-2.70 (8H, m); ¹³C-NMR (DMSO-d₆, 100 MHz) (δ) (ppm): 167.26, 152.14, 150.60, 145.99, 142.88, 137.64, 135.46, 134.74, 131.60, 129.10, 128.89, 126.26, 123.34, 119.89, 111.37, 108.68, 81.154, 65.92, 56.194, 55.93; ESI-HRMS calcd for C₂₂H₂₄N₃O₆S (M+H⁺) 458.1386, found 458.1386. HPLC-UV/Vis *k*: 10.54.

Methyl 3-[(quinoline-8-yl-sulfonyl)amino]-4-[(morpholin-1-yl)oxo] benzoate (F3): To a solution of (2c) (0.59 g, 2.22 mmol) in anhydrous CH₂Cl₂ (15 mL) at RT under stirring elm, were added 8-quinolinesulfonylchloride (0.56 g, 2.44 mmol), pyridine (0.53 g, 6.66 mmol) and DMAP (0.014 g, 0.11 mmol). The solution was stirred at RT for 12 hours, then the solvent was removed under reduced pressure. A mixture of water and ice (10 mL), then EtOAc (4 mL) was added to the oily residue; the precipitate thus obtained was filtered, washed with water, dried and purified by trituration with diethyl ether. Yield 1.00 g (99%), m.p. 174-176°C, ¹H-NMR (DMSO-d₆, 400 MHz) (δ) (ppm): 9.65 (1H, broad s), 9.26 (1H, dd, *J* 4.3, *J* 1.8), 8.77 (1H, dd, *J* 8.4, *J* 1.4), 8.50 (1H, m), 8.43 (1H, dd, *J* 7.3, *J* 1.2), 8.19 (1H, d, *J* 1.4), 7.95 (1H, m), 7.88 (1H, m), 7.82 (1H, dd, *J* 7.9, *J* 1.6), 7.59 (1H, d, *J* 8.1), 4.00 (3H, s), 3.70-3.2 (8H, m); ¹³C-NMR (DMSO-d₆, 100 MHz) (δ) (ppm): 166.24, 165.55, 152.21, 142.79, 137.80, 135.65, 135.58, 134.97, 132.24, 131.59, 131.25, 128.99, 126.31, 125.71, 124.87, 123.44; ESI-HRMS calcd for C₂₂H₂₂N₃O₆S (M+H⁺) 456.1229, found 456.1227. HPLC-UV/Vis *k*: 11.37.

1-[[Quinoline-8-yl-sulfonyl)amino]-4-carboxybenzoyl]morpholine (F4): A suspension of (2c) (0.25 g, 0.59 mmol) in THF (3 mL) and aqueous LiOH 2M (1.15 mL) was stirred at RT for 12 hours. The solution thus obtained was cooled with ice and HCl 0.5 N (20 mL) was added until pH 2.0. The solid thus obtained was filtered and washed with water. Yield 0.22 g (91%), m.p. 255-258°C, ¹H-NMR (DMSO-d₆, 400 MHz) (δ) (ppm): 13.40 (1H, broad, s), 9.60 (1H, broad, s), 9.25 (1H, dd, *J* 4.3,

J 1.8), 8.76 (1H, dd, *J* 8.4, *J* 1.6), 8.49 (1H, dd, 8.4, *J* 1.2), 8.43 (1H, dd, *J* 7.3, *J* 1.4), 8.18 (1H, d, *J* 1.4), 7.95 (1H, m), 7.92-7.85 (1H, m), 7.83-7.77 (1H, dd, *J* 7.9, *J* 1.6), 7.46 (1H, d, *J* 7.9), 3.70-3.10 (8H, m); ¹³C-NMR (DMSO-d₆, 100 MHz) (δ) (ppm): 166.56, 166.43, 152.20, 142.79, 137.78, 135.60, 135.57, 134.93, 132.88, 131.74, 131.23, 128.70, 128.83, 126.03, 125.79, 124.90, 123.42, 66.00; ESI-HRMS calcd for C₂₁H₂₀N₃O₆S (M+H⁺) 442.1073, found 442.1068. HPLC-UV/Vis *k*: 9.85.

Synthesis of E5-(O₂Oc)-CAM (Fig. S10): The Cysteamine (CAM) 2-chlorotrityl resin (0.079 mmol) was swelled in DMF and suspended in a solution of Fmoc-amino-3,6 dioxaoctanoic acid (Fmoc-O₂Oc-OH) (0.316 mmol), N,N'-Diisopropylcarbodiimide (DIC) (0.316 mmol) and hydroxybenzotriazole (HOBT) (0.316 mmol) in DMF (2 mL). This suspension was shaken for 30 minutes. After this time the solid phase was filtered and washed with DMF (3x2mL). The polymer was successively suspended in a 40% solution of piperidine in DMF (3x2 mL) and shaken for 5 minutes. The resin was filtered and washed with DMF (3x2 mL). In the final step the solid support was suspended in a solution of **E3**, (0.158 mmol), (1-[Bis(dimethylamino)methylene]-1H-1,2,3-triazolo[4,5-b]pyridinium 3-oxid hexafluorophosphate (HATU) (0.237 mmol) and diisopropylethylamine (DIPEA) (0.237 mmol) in DMF and shaken for 3 hours. The functionalized resin was washed with DMF (3x2mL) and the desired molecule was released after a treatment with a mixture of trifluoroacetic acid (TFA)/H₂O/phenol/triisopropylsilane 88:5:5:2 v/v (10 mL per 0.2 g of resin) for 30 minutes at room temperature. After filtration of the resin, the solvent was concentrated in vacuo and the residue triturated with ethyl ether. The crude of reaction was purified by preparative HPLC giving, after lyophilization, the E3-(O₂Oc)-CAM as a pale yellow amorphous solid (49% yield). ESI-HRMS calcd for C₂₉H₃₃N₄O₇S₂⁺ (M+H⁺): 613.1785 (Fig.S11); found: 613.7175.

Synthesis of E5-(O₂Oc)-CAM-FITC (Figure S10): To a stirred solution of **E5-(O₂Oc)-CAM** (0.0277 mmol) in CH₃CN (0,5 mL), Fluorescein-5-Maleimide (FITC) (0.00156 mmol) solubilized in CH₃CN/H₂O (250μL/250μL) was added followed by 20 μL of 5% solution of NaHCO₃. The reaction was stirred in the dark and the MS monitoring showed a complete consumption of the fluorescent probe in about 5 minutes. After this time the reaction solution the product was purified directly by

preparative HPLC using the same experimental conditions as for the purification of E3-(O₂Oc)-CAM. After lyophilization in the dark, a yellow amorphous solid was obtained in quantitative yield and with a purity grade > 95%. ESI-HRMS calcd for C₅₃H₄₆N₅O₁₄S₂⁺ (M+H⁺): 1040.2477 (Fig.S13); found: 1040.3098.

Enzyme purification

Bacterial cells were grown at 37 °C overnight in LB agar medium (40 g/L) supplemented with 100 µg/mL ampicillin. When absorbance at 600 nm reached 0.7 protein expression was induced by adding isopropyl-β-D-thiogalactopyranoside, to a final concentration of 1 mM. After incubation of 3-4 hours at 37°C, the bacteria were pelleted, washed, lysed, then centrifuged and the supernatant was filtered with a 0.45 µm filter. Protein purification was obtained by anionic exchange chromatography, affinity chromatography (Nickel-Sepharose 6 Fast Flow (Amersham Biosciences) column; equilibration with a solution of 20 mM K⁺ phosphate (pH 7.5), 30 mM NaCl and 20 mM imidazole at 4°C with continuous stirring for 90 min; washing with 4 V of equilibration buffer; elution with increasing concentration of imidazole, (100-500 mM) in 20 mM K⁺ phosphate (pH 7.5) and 30 mM NaCl); then gel-filtration on a HiTrap® desalting column (Amersham Biosciences) pre-packed with Sephadex G-25 superfine resin using a FPLC AKTA prime system (GE-Healthcare). The purified protein was tested for enzymatic activity and stored at -80°C. The protein purity was assessed by SDS-PAGE on a 4-15% polyacrylamide gradient gel under reducing conditions.

Inhibition assay of hTS and IC₅₀ determination.

All compounds were tested against the hTS enzyme and IC₅₀ was measured spectrophotometrically using Spectramax 190 UV/Vis spectrophotometer, 96 wells multiplate reader. The inhibition reactions were conducted following the classical method (31). The compounds were all tested in two different modes: without incubation and after 60' incubation time. The incubation time was selected after incubation time optimization studies. The reaction was followed at λ=340 nm for 180 seconds in triplicates. Each inhibitor was firstly dissolved in DMSO in a 10mM stock solution. At least 8

concentration were evaluated considering the compounds solubility (1-100 μ M) at 37°C. The reaction mixture included the following reagents solutions (a-e) added in the proper order: a, TES buffer 50% v/v (TES/water) (where TES=2-[[1,3-dihydroxy-2-(hydroxymethyl)propan-2-yl]amino]ethane sulfonic acid), 100mM; MgCl₂ 50mM; Ethylenediaminetetraacetic acid (EDTA) 2mM; β -mercapto ethanol-(BME) 150mM; pH 7.4); b, hTS enzyme (0.37 μ M); c, the inhibitor at the appropriate concentration; d. MTHF cofactor (55 μ M). e. dUMP is added as last reagent to start the reaction. For incubation studies: a, b and c solutions were added to each well. After 1-hour incubation, solution d and e were added and the reaction monitoring started. For both experimental conditions, the final DMSO concentration into the experimental cuvette (for each assayed concentration) was less than 1% v/v in order to remove a potential DMSO interfering inhibition effect on the catalytic activity of the target enzyme protein. The IC₅₀ value was obtained from the nonlinear regression analysis of the experimental data. All data showed an experimental standard error within the 20%. Compounds showing interesting activities were re-tested in further assays.

Enantioseparation and racemization of E7

Materials. The columns used were Chiralcel OD-RH [cellulose tris (3,5-dimethylphenylcarbamate); 250 \times 4.6 mm I.D.; 5 μ m], Chiralcel OD [cellulose tris (3,5-dimethylphenylcarbamate); 250 \times 10 mm I.D., 10 μ m] purchased from Chiral Technologies Europe, Illkirch, France. HPLC analyses were performed on an Agilent Technologies (Waldbronn, Germany) modular model 1200 system, consisting of a vacuum degasser, a binary pump, an autosampler, a thermostated column compartment and a variable ultraviolet detector (UV). Chromatograms were acquired at 254 nm. HPLC-grade acetonitrile and water were obtained from Baker.

Analytical and semipreparative enantioseparation. The analytical enantioseparation of chiral **E7** was performed in reversed phase using a Chiralcel OD-RH column with mobile phases of water:acetonitrile mixtures at different percentages. The separation was carried out isocratically at 25

°C. The racemic compound mixture was dissolved in acetonitrile and subsequently diluted 1:10 (v/v) with the mobile phase at a final concentration of 100 µg/mL. The injection volume was 6 µL. The detector was set at 254 nm. The retention factors (k_1 and k_2) were calculated as $k_1 = (t_1 - t_0)/t_0$ where t_1 and t_2 are the retention times of the first and second eluted enantiomers and the separation factor (α) as k_2/k_1 . The resolution factor (R_s) was calculated as $R_s = 2(t_2 - t_1)/(w_1 + w_2)$, where w_1 and w_2 are the peak widths at the base for the two eluted enantiomers. The dead time of the columns (t_0) was determined by injection of 1,3,5-tri-*tert*-butylbenzene. Among the mobile phases used, water:acetonitrile 2:98 (v/v) was chosen for the subsequent semipreparative separation because it gave a good baseline enantiomeric resolution, with $k_1 = 0.36$, $k_2 = 0.62$ and $R_s = 4.76$ (Fig. S13).

Semipreparative enantioseparation of (\pm)-**E7** was carried out on Chiralcel® OD employing water:acetonitrile 2:98 (v/v) as the mobile phase at 5 mL/min. By injecting 15 mg of the racemic mixture, the single enantiomers were collected with acceptable enantiomeric excess (99.0% and 80.1% e.e. for the first and second eluted enantiomer, respectively, Fig. S14). 8.8 mg of the first enantiomer and 4.4 mg of the second one was obtained and were sufficient for further stability studies. The specific rotation in acetonitrile of first and second eluted enantiomers were acquired on a Perkin-Elmer 241 Polarimeter resulting in $[\alpha]_D^{20} = +7.95^\circ$ (c 0.00088 g/ml; acetonitrile) and $[\alpha]_D^{20} = -9.10^\circ$ (0.00044 g/ml, acetonitrile), respectively.

Racemization. Racemization is the conversion of an enantiomer into a racemic mixture and is associated with a loss in optical activity of the chiral compound over time. The rate constant of racemization k_{rac} refers to this first-order kinetic process and can be calculated from the linear plot of the logarithmic values of the enantiomeric excess (\ln (e.e.)) *versus* time, according to Eq. (S1):

$$(S1) \quad \ln(\text{e.e.}) = -k_{rac} \cdot t$$

The half-life of racemization ($t_{1/2\text{rac}}$) is the time during which the enantiomeric purity of a chiral compound reduces to 50% of its original e.e. For a first-order racemization, the half-life can be calculated from Eq. (S2):

$$(S2) \quad t_{1/2\text{rac}} = \ln 2 / k_{\text{rac}}$$

Single enantiomers of (\pm)-**E7** were dissolved in acetonitrile [1 mg/ml] and then diluted 1:100 with buffer solution at final concentration of [0.1 $\mu\text{g/mL}$]. The solution was thermostated at 37.5 °C and racemization was monitored by injecting the solution at fixed times on a Chiralcel OD-RH column using water and acetonitrile 2:98 (v/v) as mobile phase. Four repeats of each experiment were carried out.

Racemization kinetics. The previously obtained single enantiomers of (\pm)-**E7** were solubilized in buffer solutions to simulate *in vitro* test conditions and then incubated for a set of times at 37.5 °C. After the selected times, they were injected in a Chiralcel OD-RH column (water:acetonitrile 2:98 (v/v)) to evaluate racemization rates. The data were analyzed. The kinetic parameters were calculated from the corresponding peak areas according to Eqs. S1 and S2 (Table S13).

Enantiomers and racemate inhibition of hTS.

The capability of (\pm) **E7** compound to inhibit the kinetic activity of hTS protein enzyme was spectrophotometrically evaluated using the JASCO V730 UV/Vis spectrophotometer. *The reaction was* monitored by following the absorption change of MTHF substrate at 340 nm for 180 seconds. The method was the same reported in the previous section. “Inhibition assay of hTS and IC50 detection.”

Inhibition Potency Evaluation of (+)-E7 compound

The (+)-**E7** compound does not show activity at time zero (% of enzyme inhibition below 10%) at the two 10 and 20 μM ; after one hour of incubation with hTS, (+)-**E7** is able to inhibit the enzyme activity at the 34% and 39% at 10 and 20 μM respectively with respect to the non-inhibited enzyme. (-)-**E7** enantiomer shows the same potency of (+)-**E7** compound at time zero (30%-48% at 10-20 μM) and, after 1 hour, it doubles the efficacy to 51 and 67% at the same assayed concentrations. Regarding

to E7 racemic compound, the compound results to be active just at time zero (26% and 40%, 10-20uM) and it also maintains unaltered the efficacy after 1 hour of incubation (25%-52%, 10-20uM). We did not analyze the data further at this stage.

Analysis of combined equilibria and fitting to FRET data. E_T is the total concentration of enzyme dimers:

$$E_T = \frac{K'_D K''_I}{2K''_D [I]} [M] + \frac{K''_I}{K''_D [I]} [MI]^2 + \frac{[MI]}{2} + \frac{K'_D{}^2 K''_I{}^2 [MI]^2}{K_D K''_D{}^2 [I]^2} + \frac{[MI]^2}{K''_D}$$

where M represents an enzyme monomer and I an inhibitor molecule. Φ , the FRET efficiency, is near one for M_2 ; if we assume the same for M_2I and M_2I_2 , i.e., that binding of the inhibitor does not cause a structural change able to significantly reduce the efficiency of FRET, then the observed efficiency, Φ_{FRET} , will coincide with the total fraction of dimeric protein:

$$\Phi_{\text{FRET}} = \frac{[M_2] + [M_2I] + [M_2I_2]}{E_T} = \frac{[E_T] - \frac{1}{2}([M] + [MI])}{E_T} = 1 - \frac{([M] + [MI])}{2[E_T]}$$

Our goal is to express [M] and [MI] in terms of E_T , I_T (the total inhibitor concentration) and the pertinent equilibrium constants.

$$[I_T] = [I] + [MI] + [M_2I] + 2[M_2I_2]$$

$$K_D = \frac{[M]^2}{[M_2]} \quad K'_D = \frac{[M][MI]}{[M_2I]} \quad K''_D = \frac{[MI]^2}{[M_2I_2]} \quad K_I = \frac{[I][M]}{[MI]} \quad K'_I = \frac{[I][M_2]}{[M_2I]} \quad K''_I = \frac{[I][M_2I]}{[M_2I_2]}$$

Because $I_T \gg E_T$, we simplify $[I] \approx I_T$, and rewrite:

$$\Phi_{\text{FRET}} = 1 - \frac{([M] + [MI])}{2E_T} = 1 - \frac{1}{2E_T} \left(\frac{K_i}{[I]} + 1 \right) [MI] = 1 - \frac{1}{2E_T} \left(\frac{K_i}{I_T} + 1 \right) [MI]$$

[MI] is calculated from the positive root of the quadratic equation obtained by expressing each term contributing to E_T in terms of [MI], [I] and the Ks, and replacing $[I] \approx I_T$:

$$E_T = \frac{K'_D K''_I}{2K''_D [I]} [MI] + \frac{K''_I}{K''_D [I]} [MI]^2 + \frac{[MI]}{2} + \frac{K'_D{}^2 K''_I{}^2 [MI]^2}{K_D K''_D{}^2 [I]^2} + \frac{[MI]^2}{K''_D}$$

$$\left(\frac{1}{K''_D} + \frac{K''_I}{K''_D I_T} + \frac{K'_D{}^2 K''_I{}^2}{K_D K''_D{}^2} \frac{1}{I_T^2} \right) [MI]^2 + \left(\frac{1}{2} + \frac{K'_D K''_I}{2 K''_D I_T} \right) [MI] - E_T = a[MI]^2 + 2b[MI] - E_T = 0$$

$$\phi_{\text{FRET}} = 1 - \frac{1}{2E_T} \left(\frac{K_i}{I_T} + 1 \right) \left(\frac{-b \pm \sqrt{b^2 + aE_T}}{a} \right)$$

Eq. S3

The dependence of ϕ_{obs} on I_T for the three inhibitors was fitted to eq. S3 (Fig. 4b in the main text). To narrow the amount of fitting parameters, K_D was kept fixed at the value obtained from FRET measurements without inhibitors (6×10^{-8} M) and K'_D was estimated by assuming that the effect of each inhibitor molecule on the standard free energy for the enzyme dimer dissociation was constant: $\Delta G^{\circ\prime}_D = (\Delta G^{\circ}_D + \Delta G^{\circ\prime\prime}_D)/2$. From the above value of K_D and the K''_D obtained from the limit values of ϕ_{obs} at high $[C3]$, $K''_D = 3.3 \times 10^{-7}$ M (paragraph Mechanistic analysis of dissociative inhibition, main text), we estimated $K'_D = 1.5 \times 10^{-7}$ M and used this value in the fitting procedure. K''_D values were obtained from the high I_T behavior of ϕ_{obs} , while K_I and K''_I were adjusted to fit the low and intermediate I_T data.

Analysis of a dissociative inhibition mechanism and fitting to data. Here, to test the suitability of the proposed mechanism to fit the experimental inhibition results, rather than searching for linear plots, we aim at expressing the dependence of the observed reaction rate on the total substrate concentration, S_T , at different total inhibitor, I_T , and total enzyme, E_T , concentrations.

$$v = k[M_2][S] + k' [M_2I][S] + k'' [M_2I_2][S] = k \frac{[M_2][S]}{K_1} + k' \frac{[M_2I][S]}{K_2} + k'' \frac{[M_2I_2][S]}{K_3} =$$

$$= k \frac{[M_2][S]}{K_1} + k' \frac{[M_2][I][S]}{K_2 K'_I} + k'' \frac{[M_2][I]^2[S]}{K_3 K'_I K''_I}$$

So, $v = [M_2][S]D$ with

$$D = \left(\frac{k}{K_1} + \frac{k'[I]}{K_2K'_1} + \frac{k''[I]^2}{K_3K'_1K''_1} \right)$$

We now express E_T in terms of v , $[I]$ and $[S]$:

$$\begin{aligned} E_T &= \frac{[M]}{2} + \frac{[MI]}{2} + [M_2] + [M_2I] + [M_2I_2] + [M_2S] + [M_2IS] + [M_2I_2S] = \\ &= \frac{1}{2}(K_D[M_2])^{1/2} \left(1 + \frac{[I]}{K_1}\right) + [M_2] \left(1 + \frac{[I]}{K'_1} + \frac{[I]^2}{K'_1K''_1}\right) + [M_2][S] \left(\frac{1}{K_1} + \frac{[I]}{K_2K'_1} + \frac{[I]^2}{K_3K'_1K''_1}\right) \end{aligned}$$

Because $S_T, I_T \gg E_T$, we approximate $[S] = S_T$ and $[I] = I_T$. Calling 2a, b and c the coefficients that multiply $[M_2]^{1/2}$, $[M_2]$ and $[M_2][S]$ in the three terms and writing $x = [M_2]^{1/2}$, we obtain the second-degree equation:

$$(b + cS_T)x^2 + 2ax - E_T = 0$$

whose positive root, x_r , yields the desired value of v : $v = x_r^2 S_T D$.

So, given the experimental values of E_T , S_T and I_T , we can calculate v using the equilibrium and rate constants in the scheme in Fig. 4e of the main text. In the fitting analysis, we kept K_D fixed at 6×10^{-8} M, as obtained from dilution experiments in the absence of inhibitors. We also kept the equilibrium constant for the binding of mTHF to hTS saturated with dUMP, K_1 , fixed to the value obtained in the absence of inhibitors, 10^{-5} M. Also, K_I was taken equal to 10^{-6} M for the three inhibitors from the results of the fitting of FRET data. The other equilibrium constants were explored subject to the conditions imposed by the combined equilibria in Fig. 4e of the main text, i.e.: $K_D/K_I = K'_D/K'_I$ and $K'_D/K_I = K''_D/K''_I$. So, K'_I and K''_I were kept one order of magnitude larger than K_I , i.e., 10^{-5} M. Finally, the catalytic rate constant, k , was fixed at its value with no inhibitor, 0.9 s^{-1} ; k' and k'' were variable fitting parameters.

Fluorescence microscopy. HT-29 cells were plated at $4 \times 10^4/\text{cm}^2$ in IBIDI 15 μ -Slide 8 Well plates for 24 hours and maintained at 37°C, 5% CO₂. Then they were transfected with 500 ng/well of either TS-TC or wtTS using the Lipofectamine 3000 transfection Kit (Invitrogen) and following the manufacturer's recommendations. 24 hours later the medium was removed and 50 μM E5-FITC was added to the cells for 6 hours. Subsequently, the compound was removed, cells were washed with Opti-MEM reduced Serum Medium (Gibco), stained with the TC-ReAsh II in-cell Tetracysteine Tag Detection Kit (Life Technologies Corporation) according to the manufacturer's recommendations for 60 minutes. Then, the cells were washed three times with Opti-MEM, twice with BAL and placed in Opti-MEM until visualization. The image acquisition was done on a Leica SP8 confocal microscope. Subsequent FRET analysis was performed using PixFRET (Version 1.5.0) within ImageJ (Version 1.52e). Each dot represents the total FRET area of an individual field with at least 10 cells. The statistical analysis was performed using unpaired two tailed t-test (P value $>0,0001$) using Prism 8 for windows (version 3.1.1).

Biological experiments.

Cell lines. The human ovarian cancer cell lines IGROV-1, TOV112D, 2008, C13*, A2780 and A2780/CP were grown as monolayers in RPMI 1640 medium. The C13* and A2780-CP human ovarian carcinoma cell lines are 9- to 15-fold resistant to cisplatin (cDDP) and derived from the parent 2008 and A2780 cell lines (33,34). The HT29, HCT116, and LoVo cell lines were cultured in DMEM medium (Euroclone, Devon, UK). Cell culture media were supplemented with 10% heat-inactivated fetal bovine serum (Euroclone) and 1% Pen/Strep (Euroclone). The PDAC primary cell cultures were established from patients undergoing pancreaticoduodenectomy, as described previously (35). All experiments in the present study utilized cells collected during passages 5 to 8. Cultures were equilibrated with humidified 5% CO₂ in air at 37 °C. All studies were performed in Mycoplasma negative cells, as routinely determined with the MycoAlert Mycoplasma detection kit (Lonza, Walkersville, MD, USA).

Cell density. Cell growth was determined using a modified crystal violet assay (36). After 72-h treatment with **E5**, **E7** and **5FU**, the cell monolayer was fixed and stained with 0.2% crystal violet solution in 20% methanol for at least 30 minutes. After washing to remove excess dye, the incorporated dye, proportional to the cell number, was solubilized in acidified isopropanol (1N HCl: 2-propanol, 1:10) and determined spectrophotometrically at 540 nm. The percentage of cytotoxicity was calculated by comparing the absorbance of cultures exposed to the drug with un-exposed (control) cultures. The PDAC cell growth was evaluated using the sulforhodamine B assay after exposure for 72 hr (35).

Half-life using cycloheximide. A2780 cells were analysed for hTS protein half-life using cycloheximide (90 µg/ml; for 0, 3, 6, 9, 12 and 22 hrs).

Treatment of cancer cells with cycloheximide. Cells were treated with **E5** or **E7** at concentrations corresponding to their IC₅₀ values or 2xIC₅₀ and harvested at different times (0, 1, 2 and 3 hrs) in the presence of medium containing 90 µg/ml of cycloheximide. The A2780 cells were treated with E7 and then with a proteasome inhibitor (MG132 10 µM) for 5h.

HCT116 cell transfection and cycloheximide treatment. HCT116 cells were transfected by the reverse transfection, using MirusIT-X2 reagent. The reverse transfection increases the % of transfection and makes it homogeneous. The complexes were made with a ratio of 1:3 between DNA and reagent (2.5ug of TS-MYC-DDK-WT or TS-MYC-DDK-F59A and 7.5 ul of the reagent). The complexes were incubated 20 min at RT and in the meantime the cells were counted to be seeded (500.000 cells/well of a 6-well). After 24 hours from transfection the cells were treated with cycloheximide (CHX, 60 ug/ml) for 0, 6 and 10 hours to evaluate the hTS degradation.

Cellular TS catalytic assay. Extracts from exponentially growing cells were used for the TS catalytic assay, by measuring the amounts of ³H released during the TS-catalyzed conversion of [5-³H]dUMP to dTMP, as previously reported (36). Briefly, the enzyme and 650 µM MTHF were contained in a final volume of 50 µl of the assay buffer. The reaction was started by adding [5-³H]dUMP (1 µM

final concentration, specific activity 5 mCi/mol), followed by incubation at 37°C for 60 min, and was stopped by adding 50 µl of ice-cold 35% trichloroacetic acid. Residual [5-³H]dUMP was removed by adding 250 µl of 10% neutral activated charcoal. The charcoal was removed by centrifugation at 14,000g for 15 min at 4°C, and a 150-µl sample of the supernatant was assayed for tritium radioactivity in the liquid scintillation analyzer Tri-Carb 2100 (Packard).

Western blotting. Cells were harvested and washed in ice-cold PBS and suspended in RIPA buffer supplemented with protease and phosphatase inhibitors (Sigma Aldrich). The insoluble debris was removed by centrifugation at 14,000g for 30 min. Cellular extracts were resolved using 12% SDS-PAGE and transferred to PVDF membranes (Hybond-P, Amersham). Immunoblot analysis was performed using anti-hTS (clone TS106, Millipore, 1:500 dilution), anti-hDHFR (clone 872442, Millipore, 1:1000) and anti-FLAG M2 (clone M2, F1804, Sigma-Aldrich, 1:1000 dilution), anti-β-Actin (clone AC-15, Santa Cruz Biotechnology, 1:1500 dilution). Horseradish peroxidase-conjugated secondary antibody (GE Healthcare UK Limited) was used to detect the bound primary antibody. Immune complexes were visualized by enhanced chemiluminescence (Amersham™ ECL™ Prime Western blotting reagent) following the manufacturer's instructions. Band density was calculated using Image J software or an image analyzer (GS-690 BIORAD).

Treatment of A2780 with E7 and cross-linking experiments. The human ovarian cancer cell line A2780 were exposed to **E7** (stock solution 20 mM) at the final concentrations of 20 µM or vehicle (DMSO 0.1%) for 3 hours. The **E7** dose was decided based on the IC₅₀ of this compound in these cells. Proteic extracts from human A2780 cells exposed to **E7** or vehicle (DMSO) were cross-linked for 1 h at room temperature with Bis(sulfosuccinimidyl)suberate (BS³) (3mM) (Sigma) on a rocker and then processed with the standard procedure (see western-blotting section) (37).

RNA Extraction and qPCR. Total RNA was isolated from the cells using TRIzol Reagent (Invitrogen). Reverse transcription was performed with 0.5 µg or 0.25 µg of total RNA using SuperScript first-strand synthesis for RT-PCR (Invitrogen). RT-PCR was performed with 50 ng of cDNA using SsoAdvanced Universal SYBR Green Supermix (Bio-Rad Laboratories). Samples were amplified by

an initial denaturation at 95°C for 30 s, followed by 40 cycles of denaturation at 95°C for 10 s, primer annealing at 60°C for 30 s, in CFX Connect Real-Time PCR machine (Bio-Rad Laboratories). The amplified were analyzed by the CFX maestro software (Bio-Rad Laboratories). The amount of target expressed was normalized with GAPDH. 24 hours after transfection, total RNA was isolated from HCT116 tranfected with hTS-Myc-DDK-F59A mutant and hTS-Myc-DDK tagged wild type vectors (N= 6 for each vectors from two independent experiment) and analyzed as previously described. Two primer pairs were designed for hTS target, one pair to amplify the total hTS mRNA and one pair for the exogenous hTS mRNA: FW_hTS1, GCCCAAGTCCCCTTCTTCTC; REV_hTS, AGCGAGAACCCAGACCTTTC; FW_hTS2, AGCGAGAACCCAGAC CTT TC; REV-FLAG, TCATTTGCTGCCAGATCCTCTT. For the reference target: GAPDH primer forward (hGAPDH1 fw) (Sigma Genosys 1062, 3174-083): 5'-CAAGGTCATCCATGACAACCTTTG-3', reverse: 5'-GGGCCATCCACAGTCTTCTG-3' (hGAPDH1 rw) (Sigma Genosys 1062, 3174-084). The expressions levels of total (endogenous plus exogenous) and exogenous hTS mRNAs were not significantly different (t= 0.248, p= 0.809 and t= 1.583, p= 0.145 respectively).

hTS mutants generation. Human thymidylate synthase (TYMS)-Myc-DDK-tagged vector (Origene RC204814) was used to generate a hTS-F59A mutant. hTS mutations were introduced by PCR, using the GENEART® Site-Directed Mutagenesis System (Invitrogen). The mutagenic oligonucleotides used were: FW_hTS-F59A: GGC ACC CTG TGC GTA GCC GGC ATG CAG GCG CG; REV_hTS-F59A: CAC GCC TGC ATG CCG GCT ACC GAC AGG GTG CC. PCRs for single amino acid mutations were run for 18 cycles of 20 seconds at 94°C and 30 seconds at 57°C, followed by 3 minutes and 40 seconds at 68°C. Then, the products were analyzed on a 0.8% agarose gel, the recombination reaction was performed and DH5 α -T1 competent cells were transformed. The resulting mutated plasmid were verified by DNA sequencing. After sequencing, 0.5 ug of hTS-MYC-DDK and hTS-MYC-DDK-F59A vectors were loaded on the agarose gel to determine the purity of DNA isolation.

Apoptosis. After treatment, cells were stained with AnnexinV and PI according to the manufacturer's protocol (Immunological Sciences, IK-11130). Then, apoptotic cells percentage was evaluated by flow cytometry. 1×10^6 cells were washed with PBS, and stained with 2 μ l of Annexin V and 2 μ l of PI in $1 \times$ binding buffer for 15 min at room temperature in the dark. Early apoptotic cells (Annexin V-positive, PI-negative), late apoptotic cells (Annexin V-positive and PI positive) and necrotic cells (Annexin V-negative, PI-positive) were included in cell death measurements (Fig.S20). Staurosporine treatment was used as a positive control (FACSCoulter Epics XL flow cytometer).

Pharmacokinetic studies on BALB/c mice of E5 and E7.

We tested both compounds in a preliminary pharmacokinetic study (Snapshot-PK) (38) Female BALB/c mice were purchased from Charles River Laboratories and maintained at IBMC Animal Facilities, in sterile IVC cabinets, with food and water available ad libitum. All animals used in experiments were aged from six to eight weeks. The mice were randomized into four groups of six and then treated with **E7** or **E5** evaluating two independent administration routes, oral or intra-venous (IV). The doses administered were 1 mg/kg for I.V. (administered in 100 μ l in the tail vein) and 20 mg/kg for per os (oral gavage with 100 μ l). Blood samples were taken from the tail vein at specific time points to heparinized tubes (two animals for each time point were used with around 20 μ l of total blood recovered), plasma was recovered by centrifugation and stored at -20°C until quantification by UHPLC-MS/MS ESI+. In particular, plasma samples from 6 BALB/c mice treated with (1m/kg/IV or 20 mg/kg/oral) compound **E5** or **E7** recovered at 0, 5, 15, 30, 45, 60, 120, 300 min and 24, 48 or 72 hours post administration for IV or 0, 30,45,60,120,180, 300 min and 24, 48 and 72 hours post administration. The detection of the compounds in the plasma was done by UHPLC-MS/MS ESI+ (Acquity Quattro Premier WATERS, column Acquity BEH HILIC 1,7 μ m (2,1 x 100 mm). All data are reported in Table S16) All animal experiments were carried out in accordance with the IBMC.INEB Animal Ethics Committees and the Portuguese National Authorities for Animal Health guidelines, according to the statements on the Directive 2010/63/EU of the European Parliament and

of the Council. NS and ACS have an accreditation for animal research given by the Portuguese Veterinary Direction (Ministerial Directive 1005/92).

***In vivo* cancer mouse model studies**

Orthotopic model. The orthotopic pancreatic ductal adenocarcinoma (PDAC) cancer mouse model was generated via direct injection of the primary PDAC-2 cells, transduced with a lentiviral vector containing Gaussia luciferase (G-luc), in the pancreas of female nude mice (age 6–8 weeks) anesthetized with isoflurane, as described previously (39). Pre-/post-operative pain was counteracted by administering Temgesic (0.05-0.1 mg/kg SC). Frozen tumors from PDAC-2 mice treated with E7 or 5FU (24 hours before their sacrifice) were used for RNA and protein extraction, as described above, in order to evaluate the mRNA expression of hTS, compared with untreated control mice using already validated primers for Real-time PCR (FW: 5'-CAGATTATTCAGGACAGGGAGTT-3'; RW: 5'-CATCAGAGGAAGATCTCTTGGAT T-3'). Immunohistochemical (IHC) stainings were performed according to standard procedures. Sections of 3 µm pancreatic slices were cut from paraffin-embedded specimens. IHC was performed with the anti-hTS antibody described above (dilution 1:100). Visualization was obtained with BenchMark Special Stain Automation system (Ventana Medical Systems, inc., USA).

Antitumor activity. Orthotropic PDAC models were generated via injection of 10⁶ primary cells into the pancreas of six six/eight weeks old female athymic nude mice (Charles River). Tumor growth was monitored using bioluminescence imaging (BLI) of Gaussian luciferase (G-luc) reporter. Five days after surgery, mice were stratified on the basis of BLI intensities into three groups with comparable G-luc activity. Six mice per group were treated with 10 mg/kg **E7** 3 times/week (every 2 days) every 3 weeks (administered intraperitoneally, i.p.), or 100 mg/kg **5FU** i.p. once per week for 3 weeks (or q7dx3) (38), whereas six control mice were treated only with sterile saline. Mice were sacrificed upon discomfort or >10% weight loss, and the log-rank test was used to evaluate significant differences in survival. Pancreas and internal organs were removed and frozen or fixed in 4%

paraformaldehyde. To evaluate the modulation of hTS *in vivo*, two mice of the control group were exposed to a single dose of **E7** or **5FU** 24 hours before their sacrifice. qPCR and immunohistochemical studies were performed as described above. Animal experiments were approved by the Committees on Animal Experiments of the VU University Amsterdam, The Netherlands and of the University of Pisa, Pisa, Italy, and were performed in accordance with institutional guidelines and international law and policies.

Xenograft model. Athymic Nude-Foxn1nu female mice aged 7 weeks (Envigo RMS Srl, Udine, Italy) were housed and handled under aseptic conditions, in accordance with the University of Ferrara Institutional Animal Care and Use Committee guidelines.

Antitumor activity. Tumor xenografts in mice were obtained by subcutaneously implanting (s.c.) with 2×10^6 of A2780 cells suspended in 100 μ l of PBS and 100 μ l of Matrigel (BD Biosciences). When tumor mass became palpable in successfully engrafted mice (around 7 days after the injection), animals were weighed and randomly divided into three groups to be subjected to various treatments as indicated in the Fig.S21. Treatments administrated via intraperitoneal injection were **E7**, 5FU and vehicle solutions. **E7** was administrated 10 mg/Kg three times a week while 5FU (100mg/Kg) one time a week. During the course of the experiment there was no difference in body weight between control and treatment groups. Tumor growth was monitored daily, and tumor diameters were measured with calipers every two days. The tumor volume was calculated using the following equation: $\text{volume} = \pi/6 \times (a \times b^2)$, where **a** is the major diameter and **b** is the minor diameter. All mice that reached the endpoint of the experiment were euthanized and, subsequently, tumors were excised.

Supplementary Figures

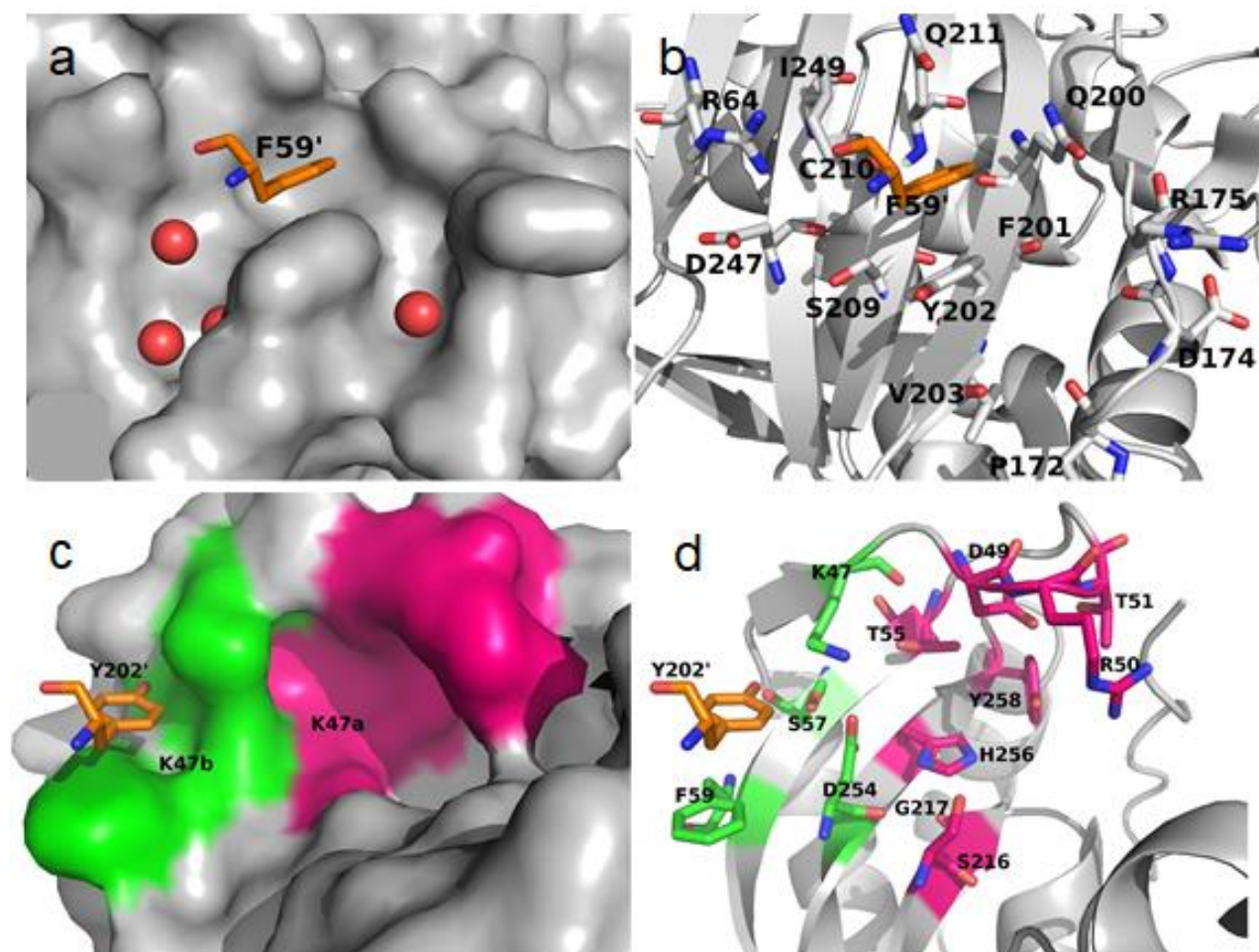


Figure S1. Y202 and K47 pockets at the hTS monomer-monomer interface (PDB ID: 1HVY, A chain). **a**, Surface presentation of the hTS monomer, with residue F59' (in orange, shown as sticks) from the opposite monomer binding in the Y202 pocket (PDB ID: 1HVY, chain A). Crystallographic water molecules found in the Y202 pocket region are shown as red spheres. **b**, Cartoon representation of the hTS monomer with F59' (in orange, shown as sticks) from the opposite monomer binding in the Y202 pocket (PDB ID: 1HVY, chain A). Residues forming the Y202 pocket are shown in sticks. Atom colour code: carbon – grey/orange; nitrogen – blue; oxygen – red. **c**, Surface representation of the K47 pocket region in the hTS monomer (PDB ID: 1HVY, chain A), with residue Y202' (in orange, shown as sticks) from the opposite monomer, binding in the K47 subpocket K47b (green) adjacent to the K47a subpocket (pink). **d**, Cartoon and sticks presentation of the K47 pocket region in the hTS monomer with residue Y202' (in orange, shown as sticks) from the opposite monomer, binding in the K47b subpocket (PDB ID: 1HVY, chain A). Residues K47, S57 and D254 form a dividing wall that is part of both sub-pockets K47a (pink) and K47b (green), (see also Table S1). Atom color code: carbon – grey/orange/green/pink; nitrogen – blue; oxygen – red.

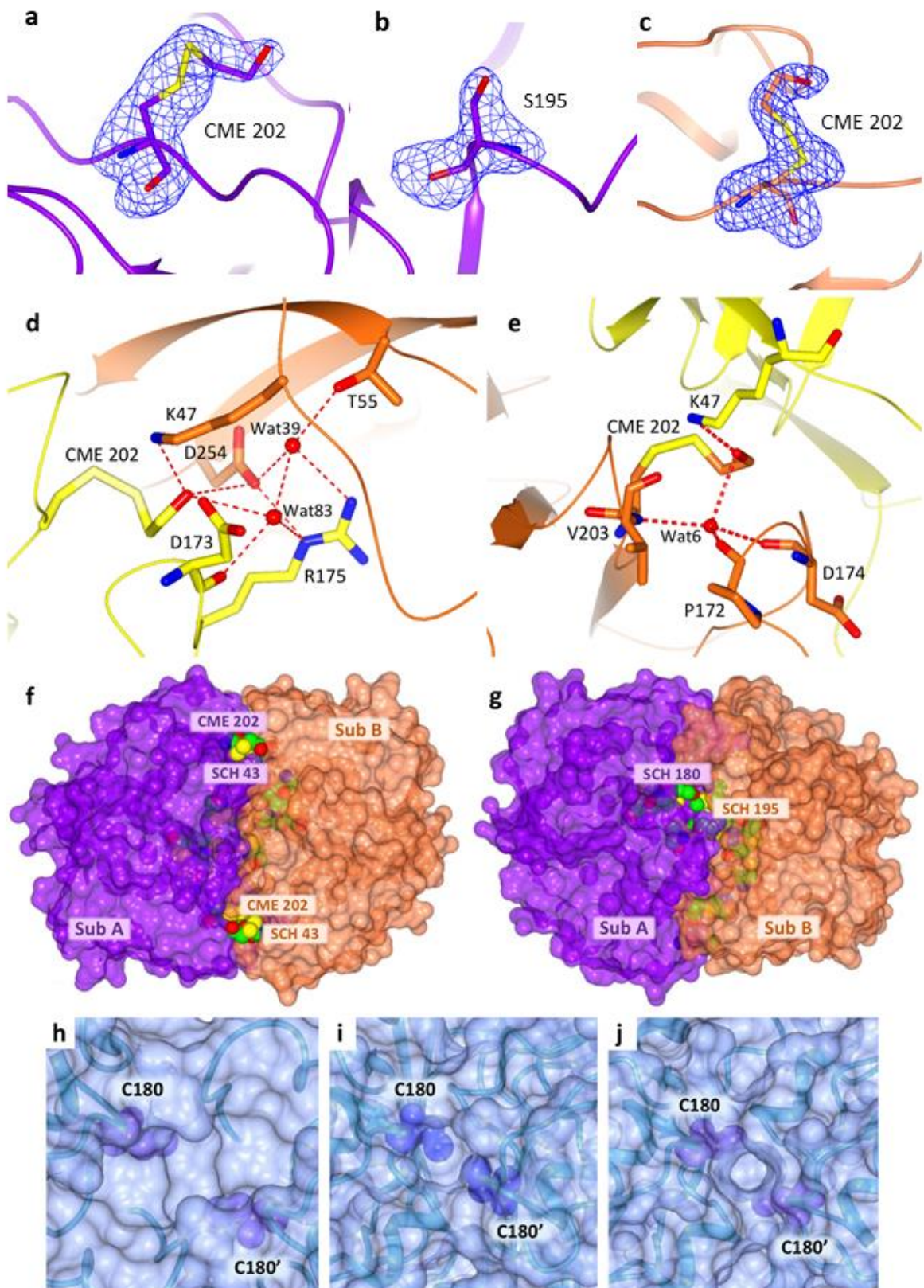


Figure S2. X-ray crystallographic structure of hTS-Y202C and hTS C195S-Y202C. a-c, Unbiased omit map (blue wired map contoured at 3.0σ), showing the S,S(2-hydroxyethyl)cysteine (CME) chemical modification occurring at the mutated residue C202 (panel **a**), and the mutated residue S195 (panel **b**) in the hTS double mutant C195S-Y202C. Panel **c** reports the omit map (contoured at 3.0σ) showing the S,S(2-hydroxyethyl)cysteine (CME) chemical modification occurring at the mutated residue C202 in the single hTS Y202C mutant. The mutated serine and the CME residues are represented as sticks. The hTS C195S-Y202C structure is drawn in violet whereas the single mutant structure is coloured in orange (cartoon representation). **d-e,** H-bond interactions (represented as dashed lines) involving the CME202 residue in hTS Y202C subunits A (panel **d**) and B (panel **e**). Interacting residues are represented as sticks and water molecules as red spheres. Residues belonging to the A subunit are coloured in yellow while those of the B subunit are coloured in orange. **f-g,** two views of the surface of the hTS Y202C dimer. The two symmetry-related subunits are shown in violet (subunit A) and orange (subunit B), while the CME and S-methyl-thio-cysteine (SCH) residues are represented as spheres. Only SCH43 (panel **f**), appears fully solvent accessible, with CME202, partially visible in its pocket, just below SCH43. Panel **g**, shows that SCH180 is partially solvent accessible, while SCH195, CME199 and C210 are buried to different extents below the hTS surface. **h-j,** surface representations showing the solvent accessibility of C180 residues in wt hTS and hTS double mutant (C195S-Y202C). The protein is shown in a transparent surface and the C180-C180' residues from two facing subunits are represented by labeled blue-violet spheres. **h,** wt hTS dimer in inactive conformation (PDB ID: 3N5G); **i,** wt hTS in active conformation (PDB ID: 2RDA); **j,** C195S-Y202C hTS mutant in active conformation (PDB ID: 4O1X). PISA server analysis (76) indicates that C180-C180' are buried in all three structures. However, as it can be appreciated by comparing the three figures, the active conformation increases the shielding of the facing C180-C180' residues from solvent as their buried surface goes from about 30 \AA^2 (**h**) to $50\text{-}68 \text{ \AA}^2$ (**i-j**). Also the crevice between subunits is much larger in inactive vs. active conformation (from about $15 \times 6 \text{ \AA}$ in inactive to about $5 \times 5 \text{ \AA}$ in active conformation).

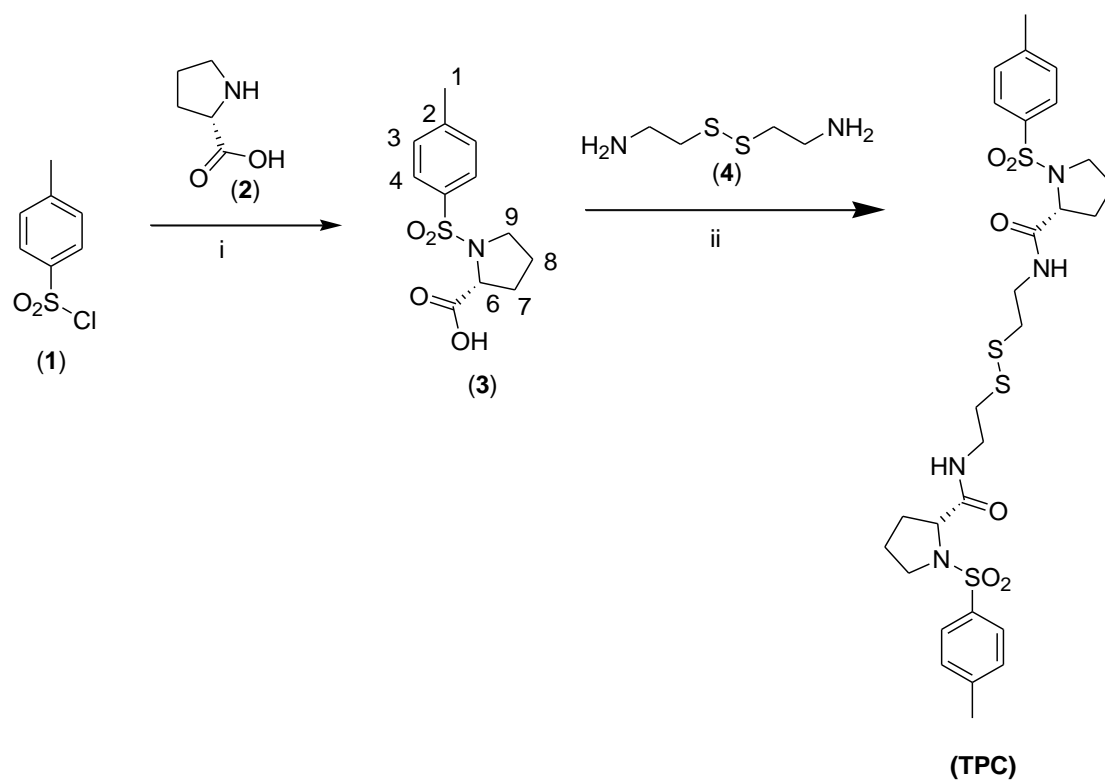
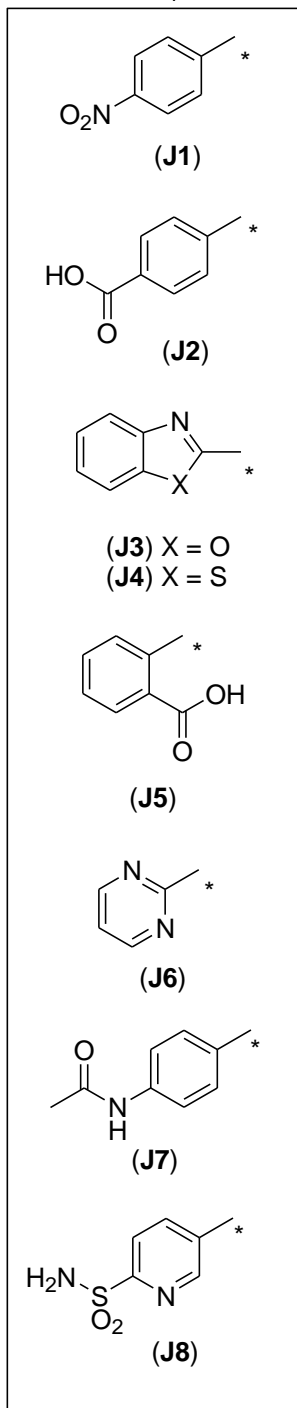
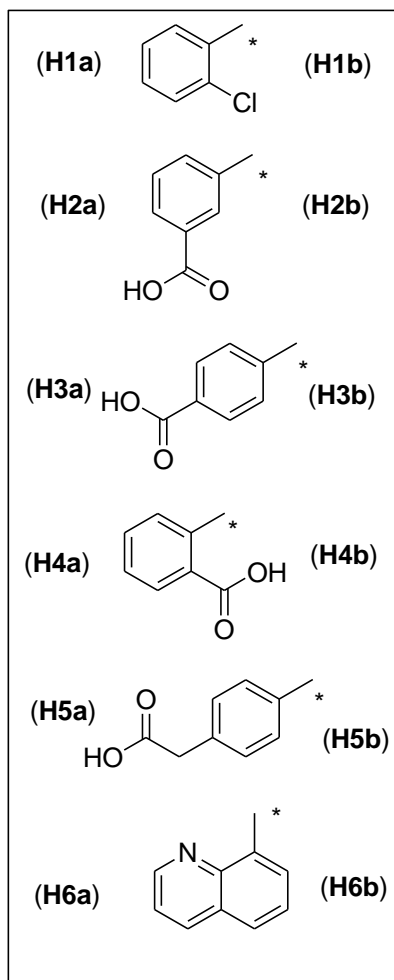
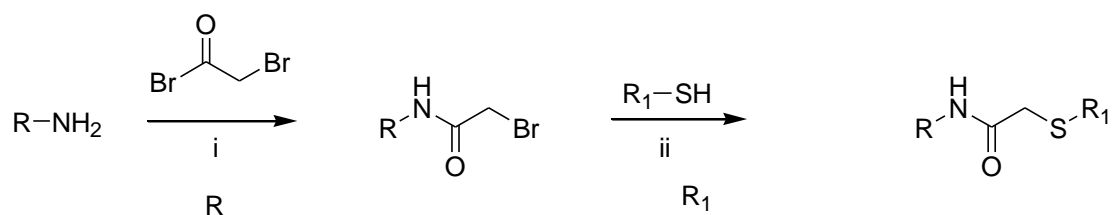


Figure S3. Synthesis of TPC. (i) diethyl ether, NaOH 2M, RT, 4h; HCl conc.; (ii) HOBT, EDAC, TEA, DCC.



C1 (from **H1b** and **J1**)
C2 (from **H2b** and **J1**)
C3 (from **H3b** and **J1**)
C4 (from **H4b** and **J1**)
C5 (from **H5b** and **J1**)
C10 (from **H6b** and **J1**)
D5 (from **H4b** and **J2**)
D6 (from **H3b** and **J2**)
D7 (from **H3b** and **J3**)
D8 (from **H3b** and **J4**)
D11 (from **H3b** and **J5**)
D12 (from **H3b** and **J6**)
D13 (from **H3b** and **J7**)
D14 (from **H3b** and **J8**)

Figure S4. Synthesis of compounds C1-C5, C10, D5-D8, D11-D14 . (i): TEA/CH₂Cl₂ (for H1b, H2b) or Na₂CO₃/H₂O (for H2b, H3b, H5b, H6b); (ii): K₂CO₃/acetone for C2-C5, D5-D8, D11-D14) or TEA/THF (for C1, C10).

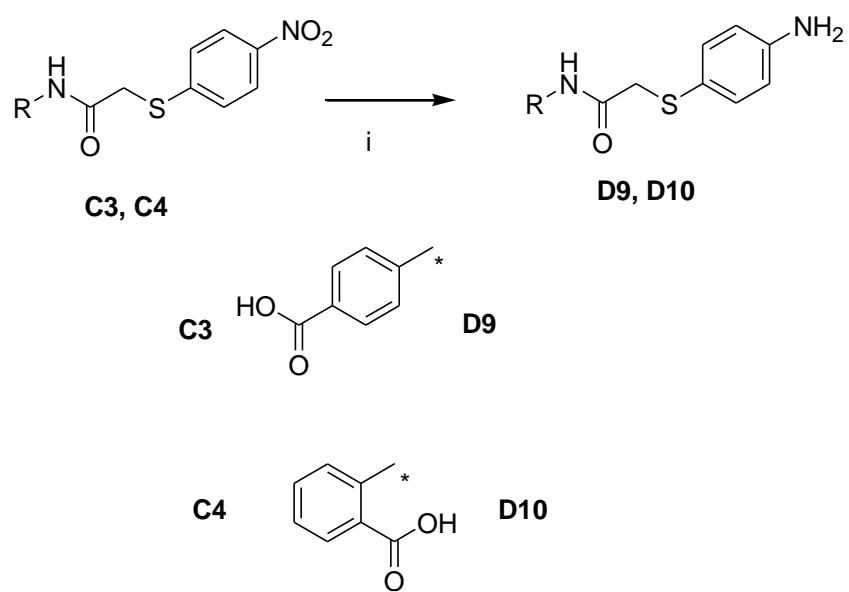
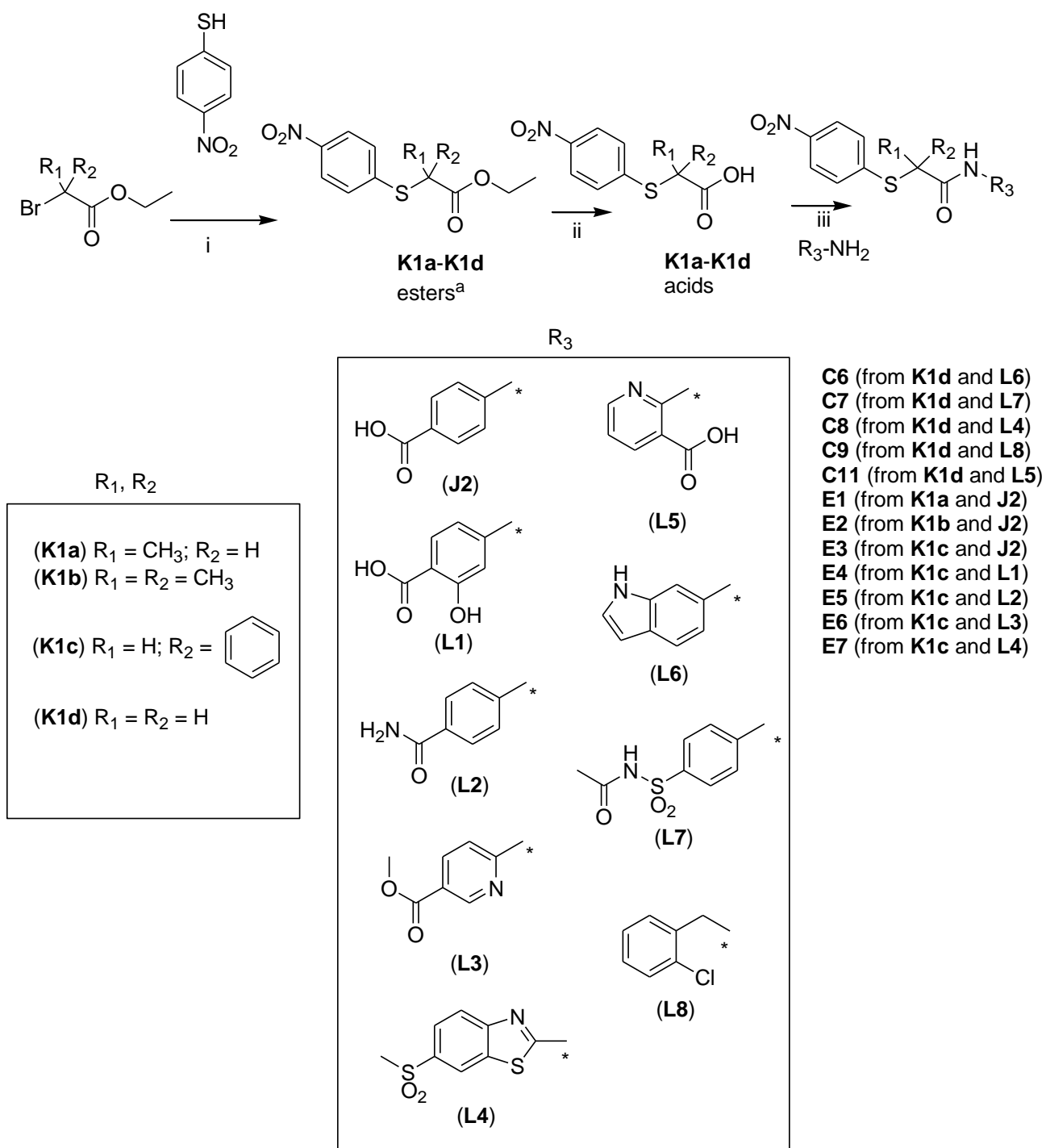


Figure S5. Synthesis of D9 and D10. (i): H₂/Pd:C, CH₃OH.



C6 (from **K1d** and **L6**)
C7 (from **K1d** and **L7**)
C8 (from **K1d** and **L4**)
C9 (from **K1d** and **L8**)
C11 (from **K1d** and **L5**)
E1 (from **K1a** and **J2**)
E2 (from **K1b** and **J2**)
E3 (from **K1c** and **J2**)
E4 (from **K1c** and **L1**)
E5 (from **K1c** and **L2**)
E6 (from **K1c** and **L3**)
E7 (from **K1c** and **L4**)

Figure S6. Synthesis of compounds C6-C9 and C11, E1-E7. (i): $\text{K}_2\text{CO}_3/\text{acetone}$. In the case of **K1d**, methylbromoacetate was used instead of ethylbromoacetate ; (ii): NaOH/EtOH ; (iii): $(\text{COCl})_2/\text{THF}$ then TEA (for **E1-E6, C6, C7, C9, C11**) or WSC/DMF (for **C8, E7**).

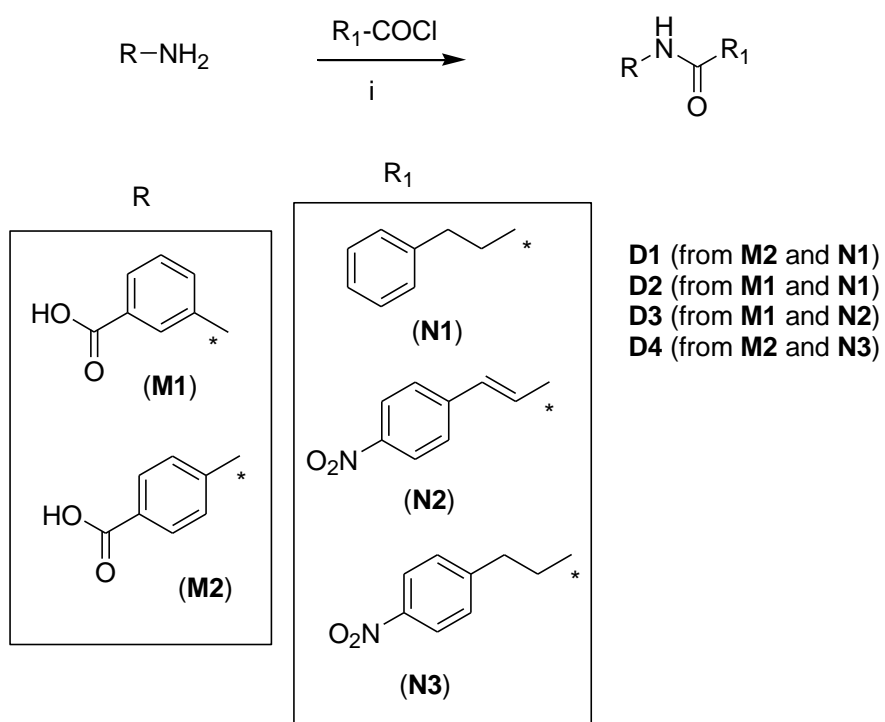


Figure S7. Synthesis of compounds D1-D4. (i): TEA/CH₂Cl₂

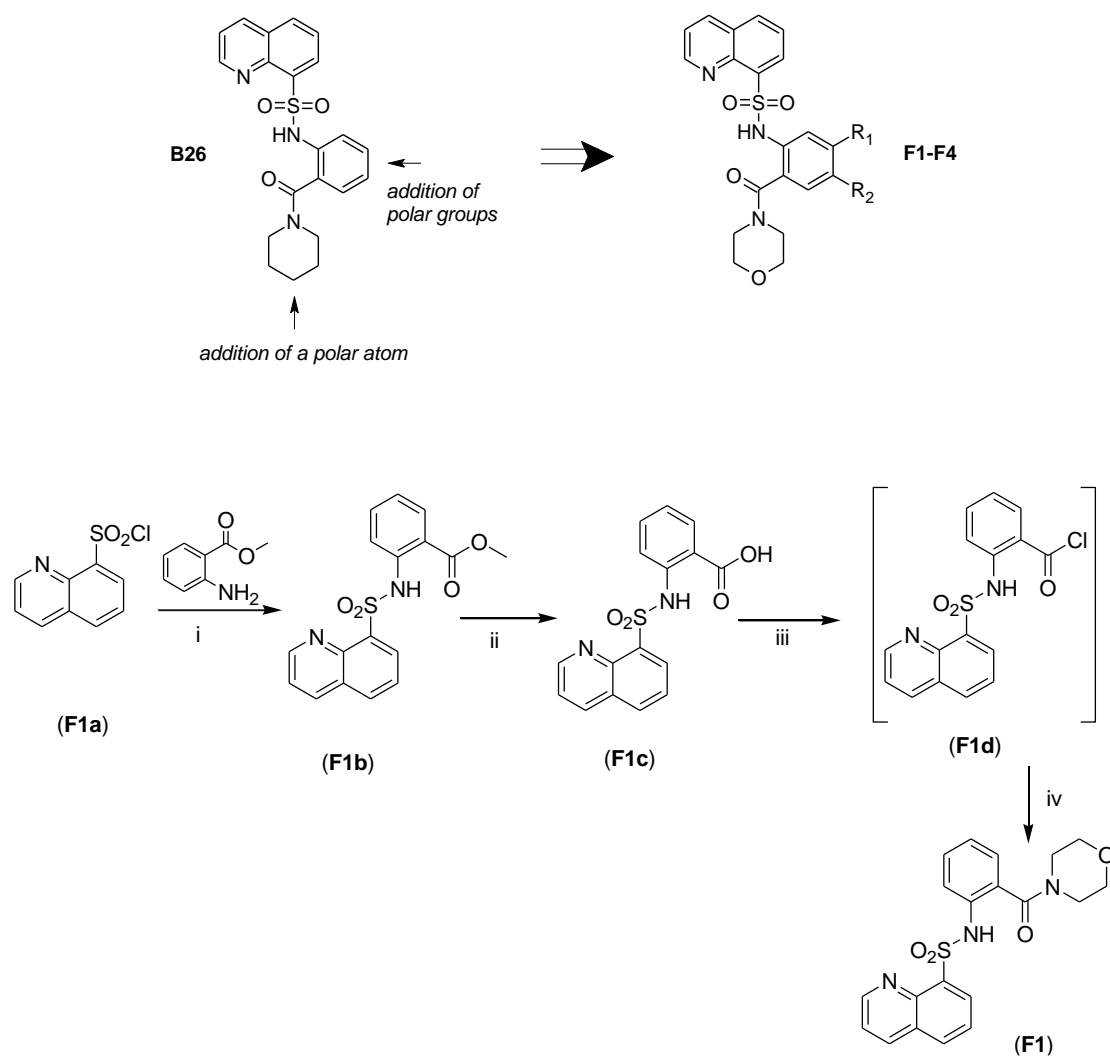


Figure S8. Design of compound F (upper panel). Synthesis of compound F1 (bottom panel). (i): CH₂Cl₂/pyridine/DMAP, RT; (ii): THF/LiOH 2M; (iii): THF/DMF, (COCl)₂; (iv): morpholine, CH₂Cl₂/TEA 0°C.

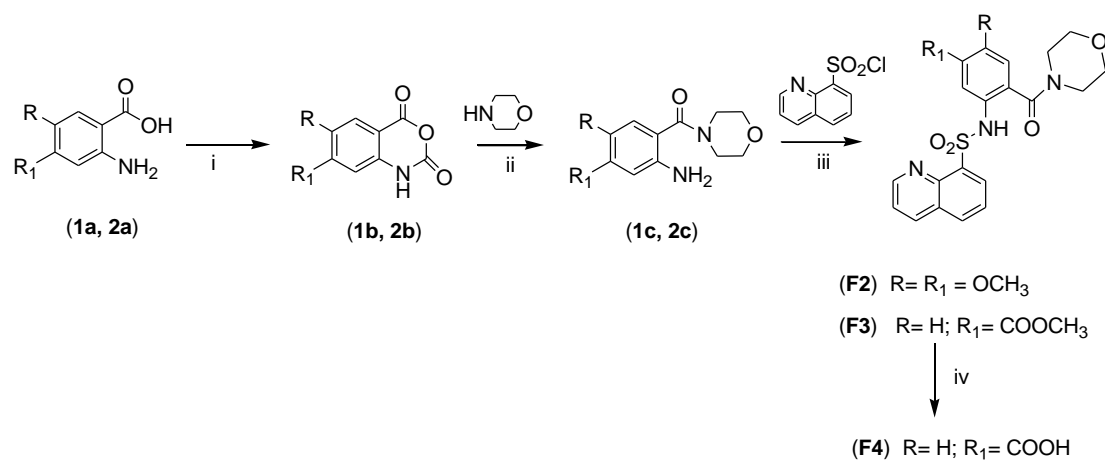


Figure S9. Synthesis of compounds F2-F4. (i): THF/triphosgene, r.t.; (ii): DMF/DMAP; (iii): CH₂Cl₂/pyridine/DMAP; (iv): THF/LiOH 2M.

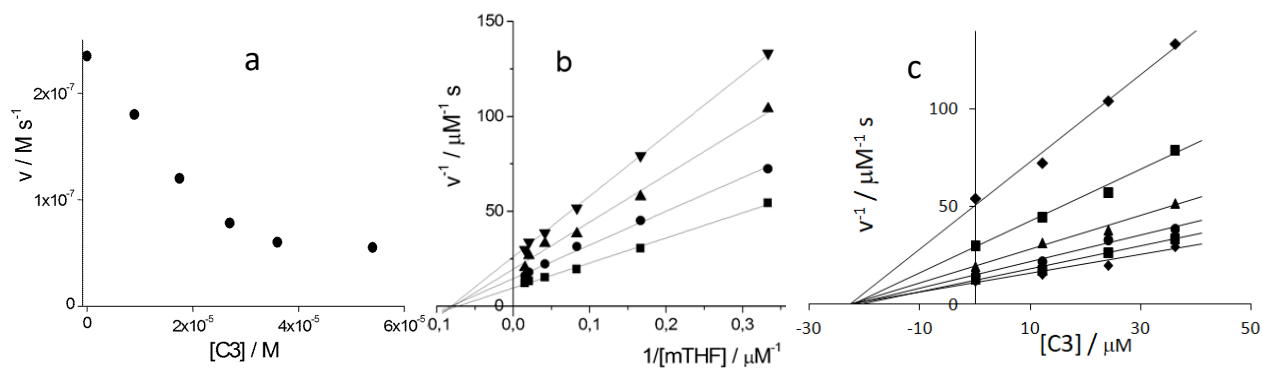


Figure S10. Inhibition of hTS by compound C3. **a**, Dependence of the initial reaction rate on **C3** concentration. $[E_T] = 300$ nM (M = moles of dimer per liter), $[dUMP] = 120$ μM , $[MTHF] = 60$ μM ; **b**, double reciprocal and, **c**, Dixon plots. In both plots, $[E_T] = 300$ nM, $[dUMP] = 120$ μM , $[MTHF]$ was between 3 and 65 μM and $[C3] = 0, 12, 24$ and 36 μM . In all plots, v is the initial reaction rate.

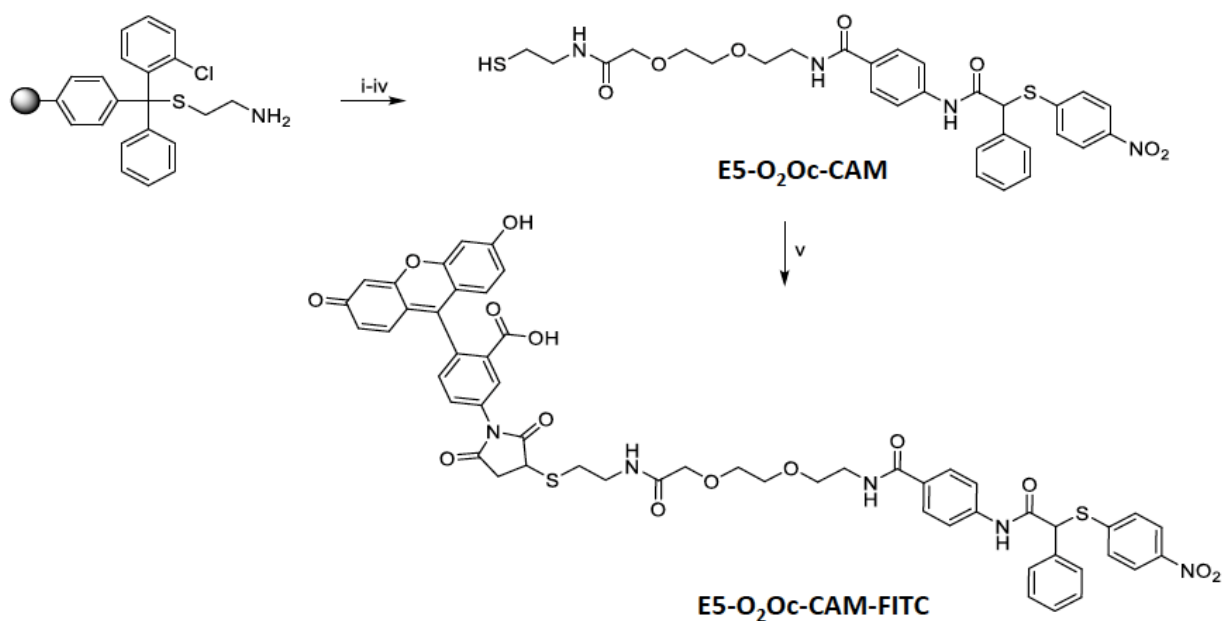


Figure S11. Synthesis of compounds E5-O₂Oc-CAM-FITC. (i) cysteamine 2-chlorotrityl resin (1 eq.), Fmoc-O₂Oc-OH (4 eq.), DIC (4 eq.), HOBt (4 eq.), DMF, r.t., 30 min; (ii) 40% piperidine in DMF, r.t., 5 min; (iii) **E3** (2 eq.), HATU (3 eq.) DIPEA (2 eq.), DMF, r.t., 3 h; (iv) trifluoroacetic acid (TFA)/H₂O/phenol/triisopropylsilane 88:5:5:2 v/v (10 mL / 0.2 g of resin); r.t., 30 min; (v) E5-(O₂Oc)-CAM (1 eq.), Fluorescein-5-Maleimide (0.06 eq.), CH₃CN/H₂O, r.t., 5 min. (Figs.S12 and Fig.S13.)

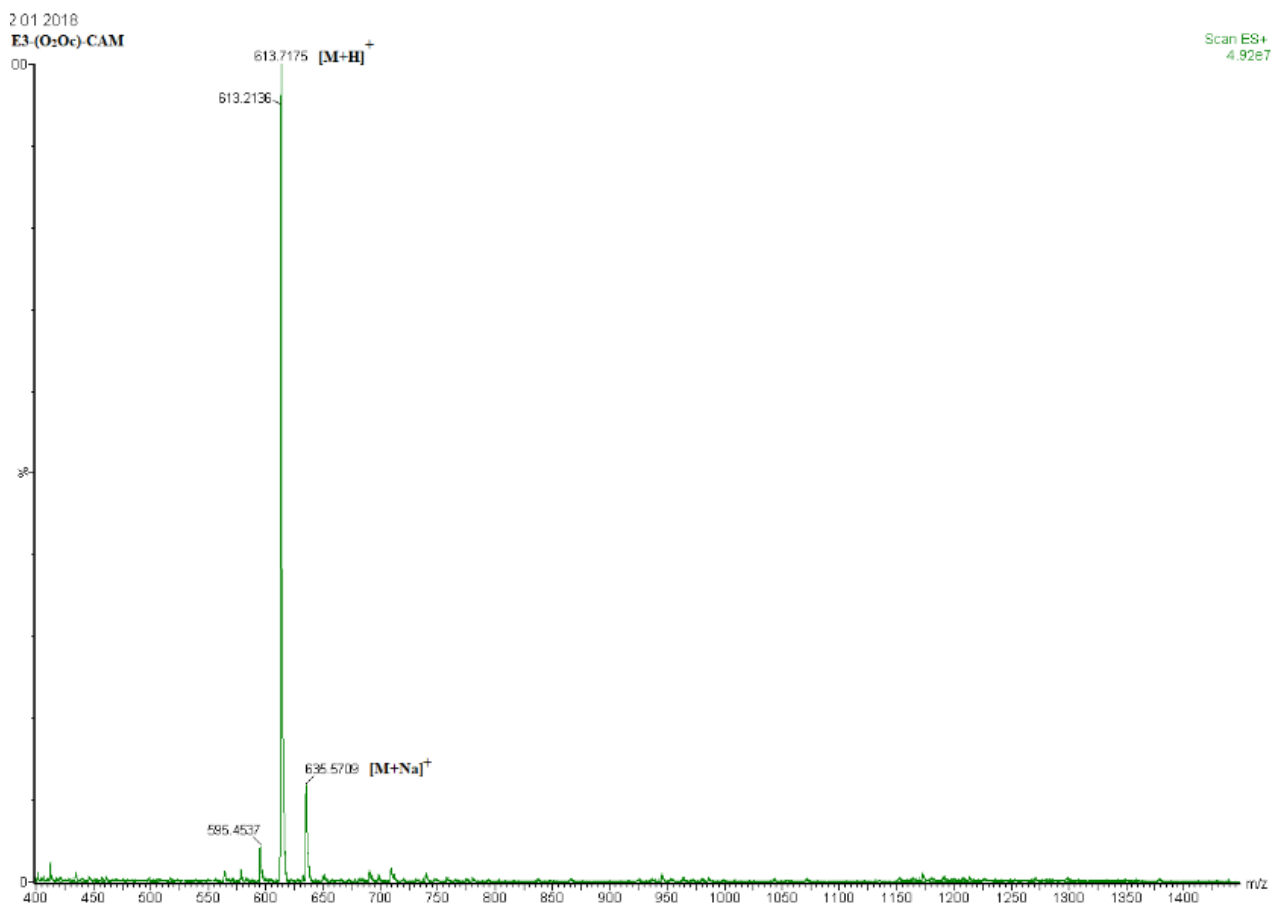


Figure S12. Mass spectrum of E5-(O₂Oc)-CAM ESI-HRMS calcd for C₂₉H₃₃N₄O₇S₂⁺ (M+H⁺):
613.1785.

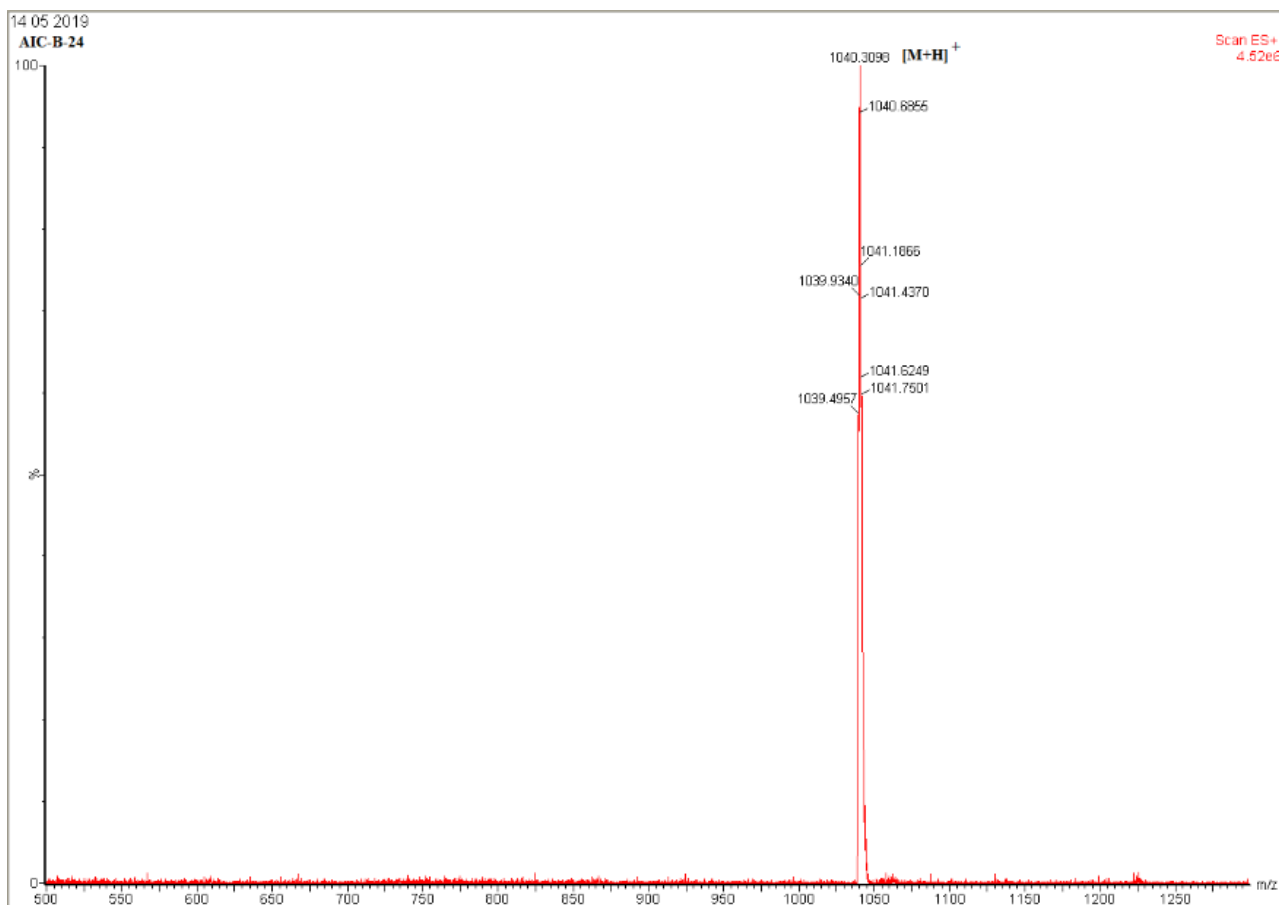


Figure S13. Mass spectrum of E5-(O₂Oc)-CAM-FITC. ESI-HRMS calcd for C₅₃H₄₆N₅O₁₄S₂⁺ (M+H⁺):1040.2477.

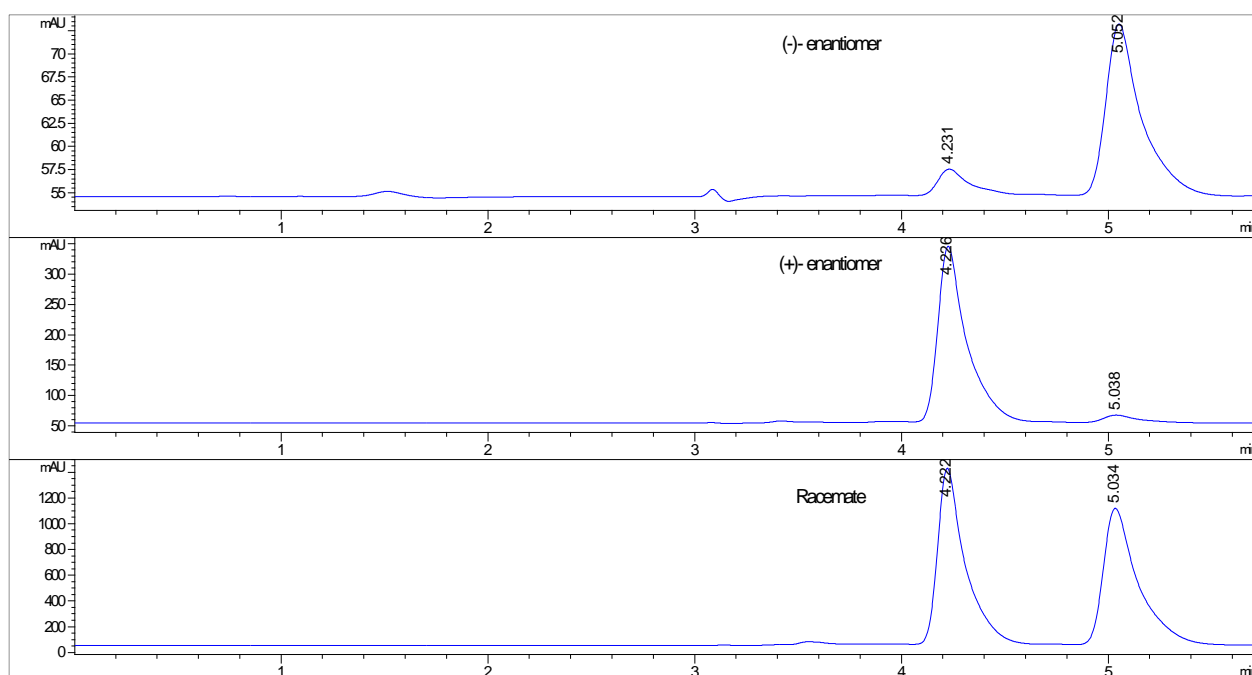


Figure S14. Chromatograms of single (\pm)-E7 enantiomers. Column: Chiralcel® OD (250 \times 4.6 mm I.D., 5 μ m), mobile phase: water:acetonitrile 2:98 (v/v), flow rate: 1 mL/min; λ = 254 nm.

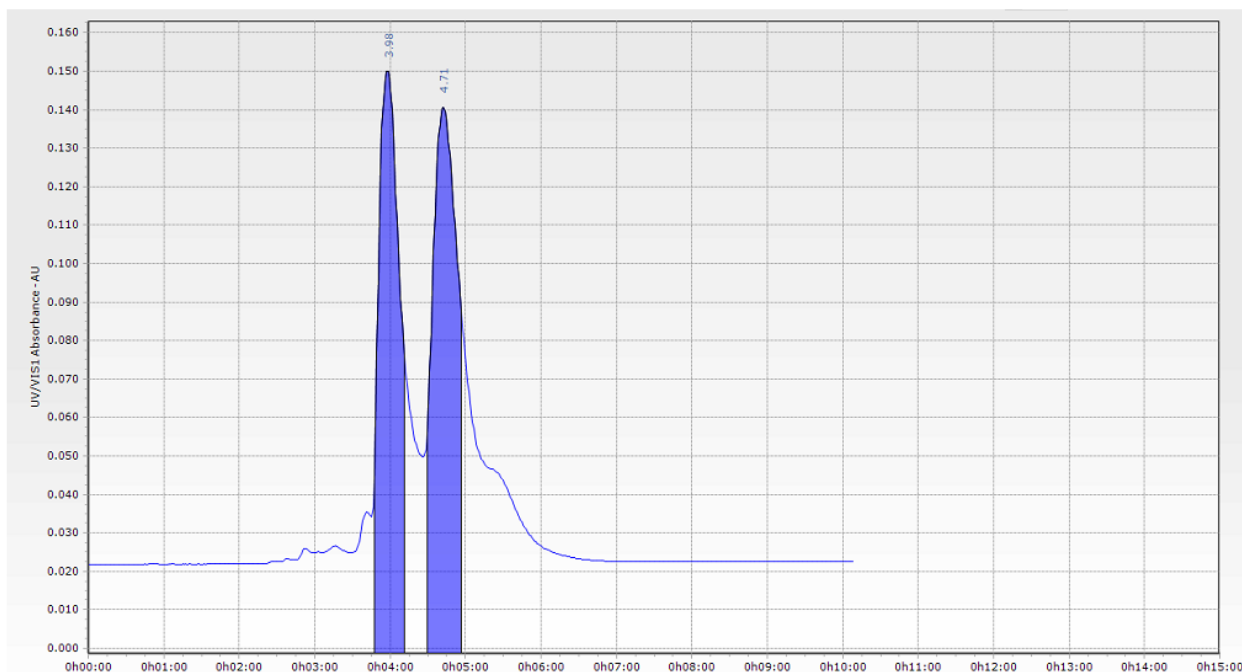


Figure S15. Semipreparative enantioseparation of (±)-E7. Column: Chirasphere OD, mobile phase water:acetonitrile 2:98 (v/v), flow rate: 5 ml/min, λ : 254 nm, room temperature.

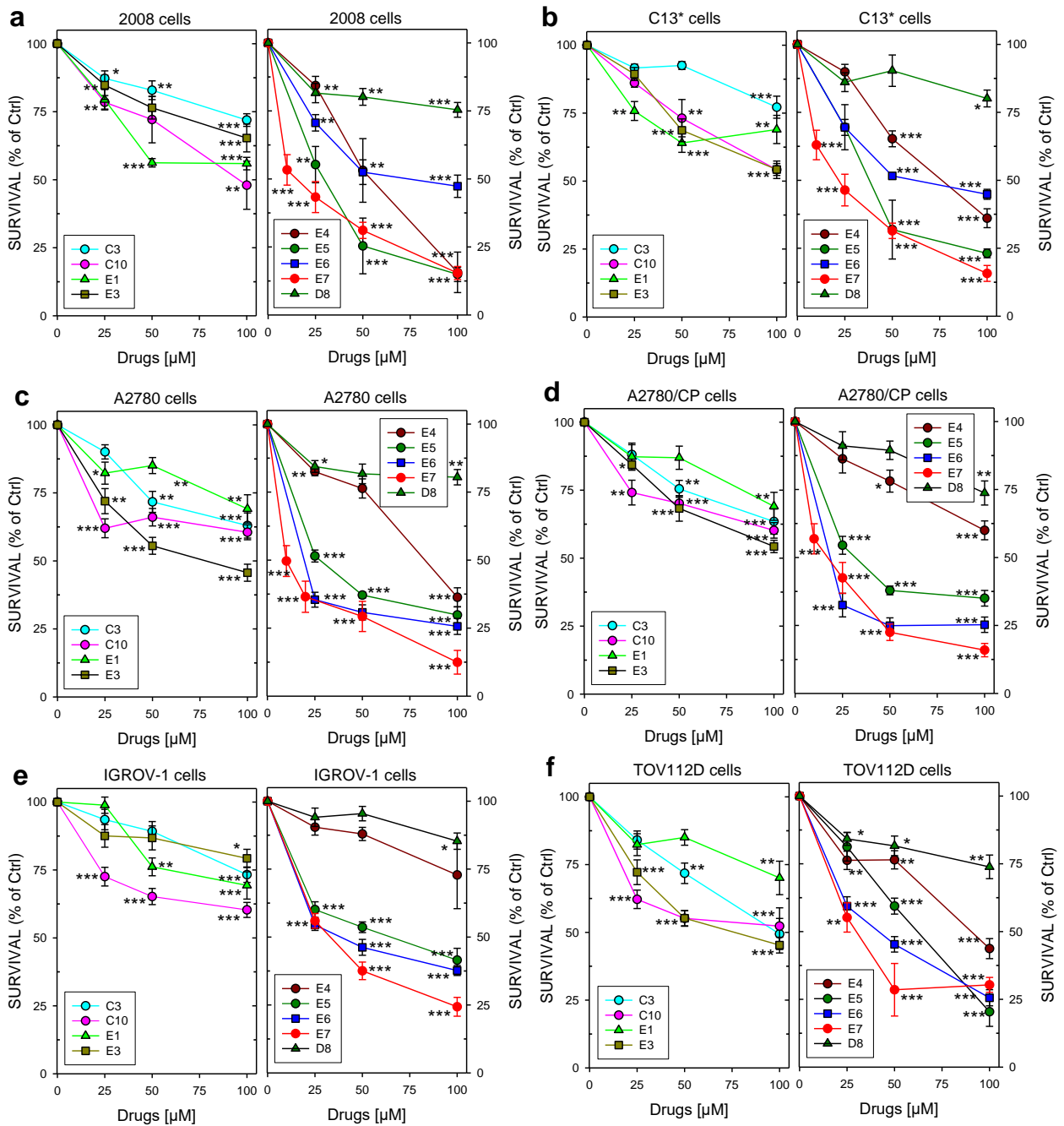


Figure S16. Ovarian cancer cell growth inhibition. Cell survival percentages are the mean \pm S.E.M. of two separate experiments performed in duplicate. **a**, 2008 cells. **b**, C13* cells. **c**, A2780 cells. **d**, A2780/CP cells. **e**, IGROV-1 cells. **f**, TOV1120 cells. Data indicate mean values and standard deviation from three experiments performed in duplicate. P values were calculated with two-sided Student's *t*-test and ANOVA followed by the Tukey's multiple comparison. * $p < 0.05$; ** $p < 0.01$; *** $p < 0.001$, $n=3$

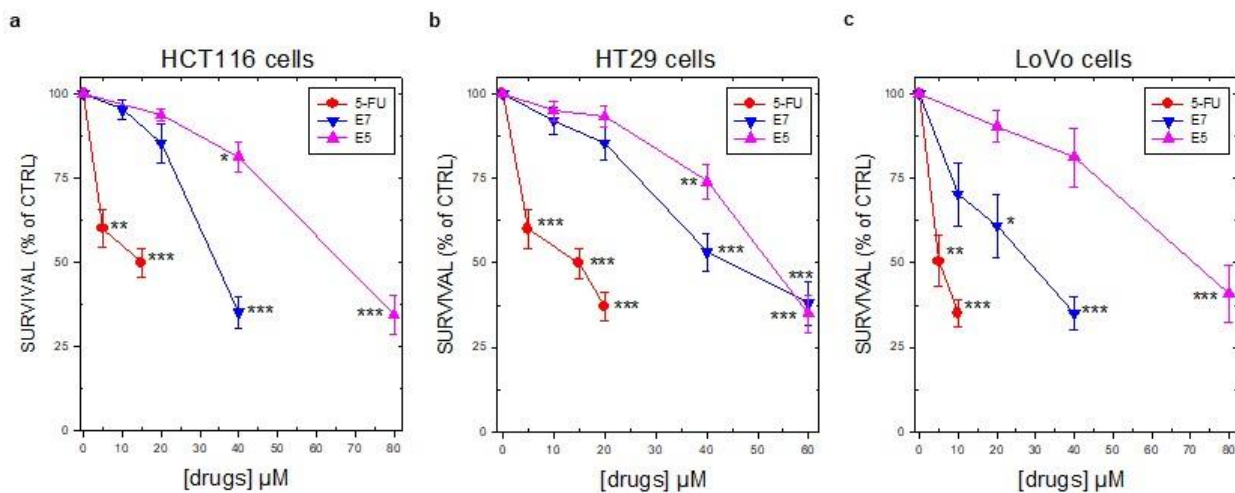


Figure S17. Colon cancer cell growth inhibition. Cell survival percentages are the mean \pm S.E.M. of three separate experiments performed in duplicate. **a**, HCT116 cells. **b**, HT29 cells. **c**, LoVo cells. Data indicate mean values and standard deviation from three experiments performed in duplicate. P values were calculated with two-sided Student's *t*-test and ANOVA followed by the Tukey's multiple comparison. * $p < 0.05$; ** $p < 0.01$; *** $p < 0.001$, $n=3$.

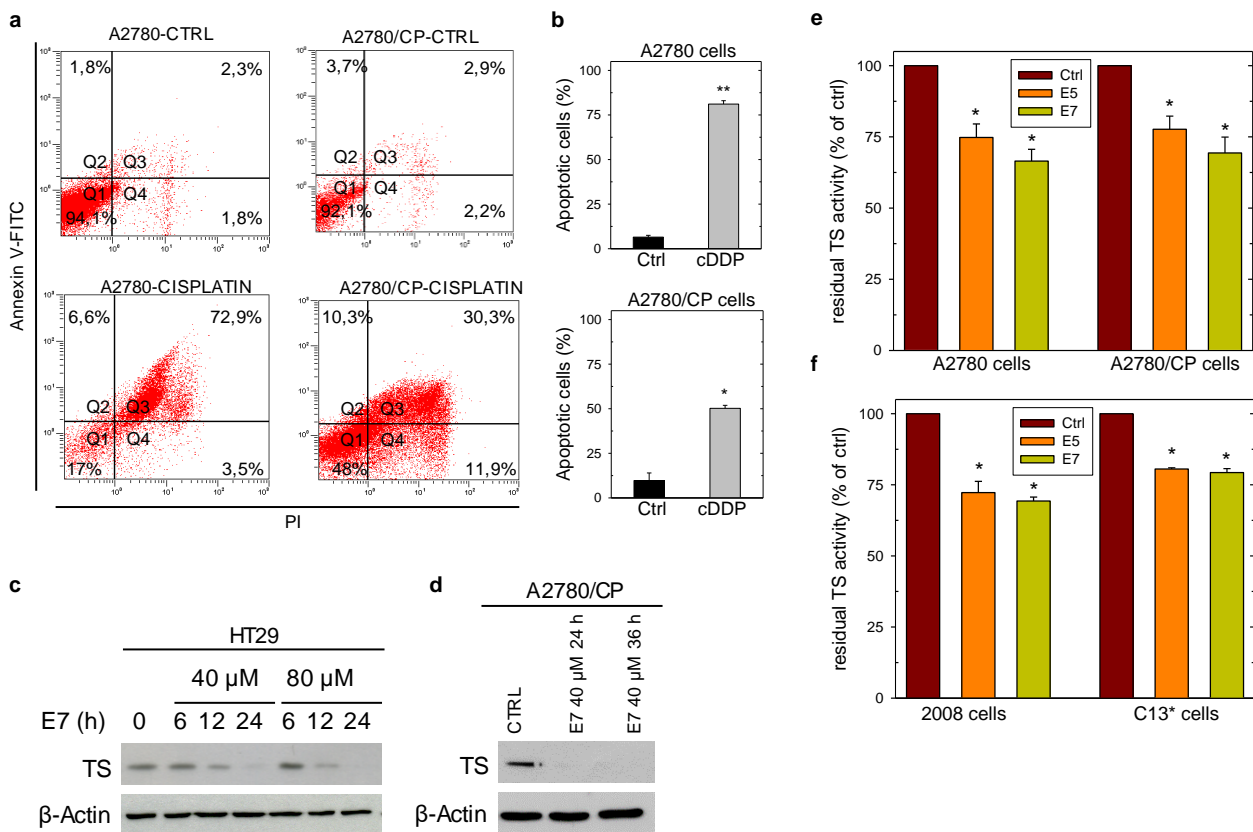
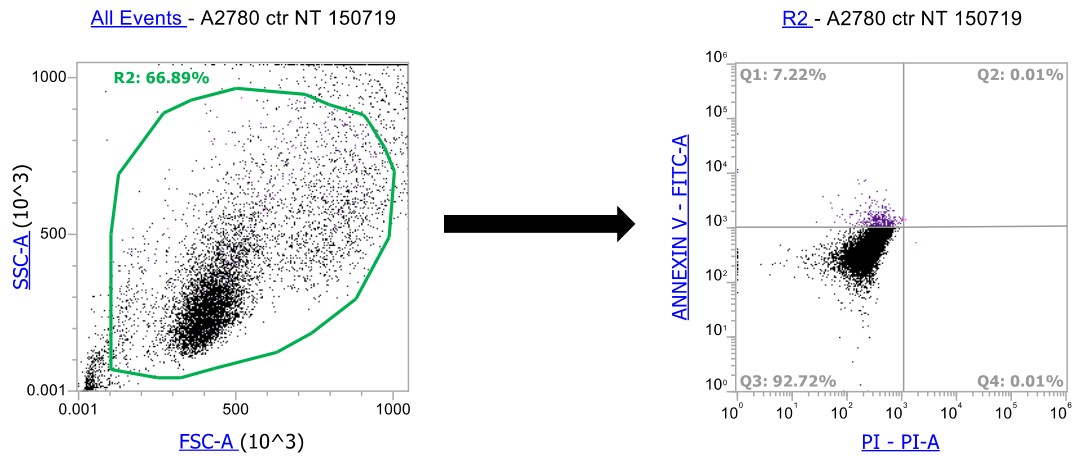


Figure S18. Effect of cisplatin on cell death, and effect of dimer disrupters on hTS activity and hTS protein levels in cells. **a**, flow cytometric analysis of apoptosis of A2780 and A2780/CP cells treated with cisplatin (13 μ M, 72h) (Annexin V-/PI-: live cells, Annexin V+/PI-: early apoptotic cells, Annexin V+/PI+: late apoptotic cells, Annexin V-/PI+: necrotic cells). **b**, quantification of Annexin V-positive cells (Q2+Q3) was performed using Annexin V/PI kit. **c**, effects of **E7** (different times) on hTS protein level in HT29 cells, and **d**, A2780/CP cells. **e**, cellular extracts from A2780 and A2780/CP cell lines processed for TS activity after incubation with **E5** and **E7** at concentrations corresponding to IC_{50} values (see Table S12). **f**, cellular extracts from 2008 and C13* cell lines processed for TS activity after incubation with **E5** and **E7** at concentrations corresponding to IC_{50} values. All the results are the mean of three experiments performed in duplicate. Data indicate mean values and standard deviation. P values were calculated with two-sided Student's *t*-test and ANOVA followed by the Tukey's multiple comparison. * $p < 0.05$; ** $p < 0.01$; *** $p < 0.001$.

a



b

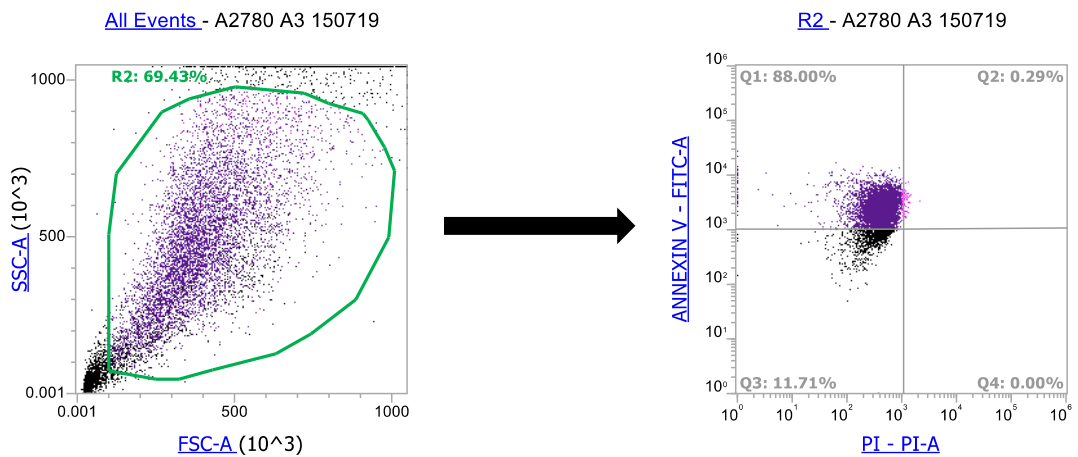


Figure S19. Example of gating strategy used for cell analysis. Gating strategy used to assess the percentage of apoptotic cells (Annexin V/PI) shown in Fig. 6b and Fig. S18a. **a**, Untreated (ctr) cells. Left panel, FSC-A vs SSC-A. Right panel, representative flow cytometry analysis plots of Annexin V/PI staining (Parameters: PI-PI-BL2-A vs ANNEXIN V-FITC-BL1-A; Gate: all events). **b**, Treated cells. Left panel, FSC-A vs SSC-A. Right panel, representative flow cytometry analysis plots of Annexin V/PI staining (Parameters: PI-PI-BL2-A vs ANNEXIN V-FITC-BL1-A; Gate: all events).

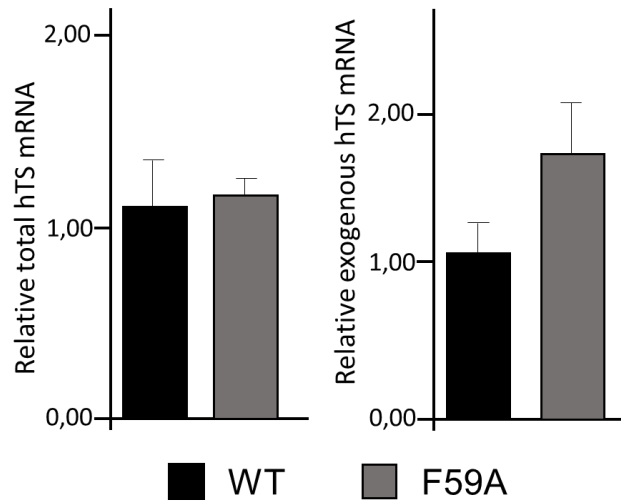


Figure S20. Expression levels of total (exogenous plus endogenous) and exogenous hTS mRNAs 24 hours after transfection of HCT116 cells with wild-type hTS-Myc-DDK tagged or mutant hTS-Myc-DDK-F59A vectors. Quantitative Real Time RT-PCR results showing the expression of total and exogenous hTS mRNAs in HCT116 cells transfected with wild-type hTS-Myc-DDK tagged (WT) or mutant hTS-Myc-DDK-F59A vectors. The mRNA expression was calculated with the $\Delta\Delta C_t$ method (calibrator: average of HCT116 cells transfected with WT hTS-Myc-DDK-tagged vector) with GAPDH as endogenous control. Columns and bars indicate mean values + S.E.M. (n= 6 for two independent experiments).

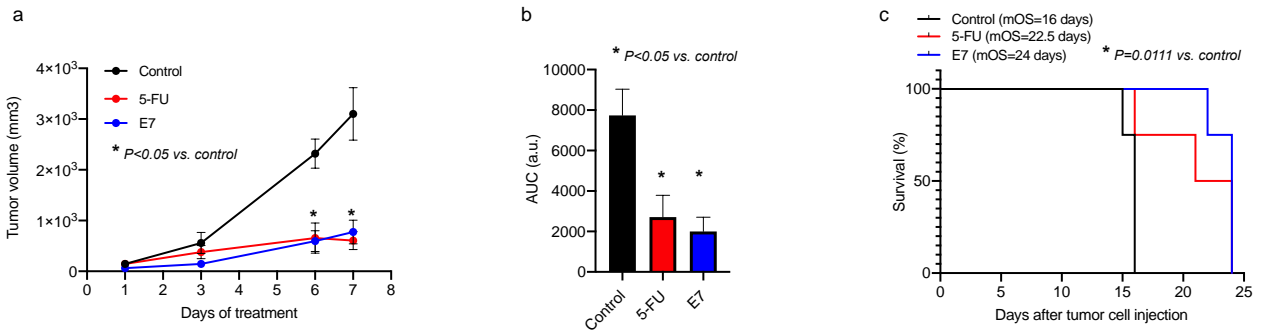


Figure S21. Effects of E7 *in vivo*. **a**, tumor growth kinetics at the indicated time points. Athymic Nude-Foxn1nu female mice were subcutaneously inoculated with 2×10^6 A2780 cells. Implanted xenotransplanted mice, chosen randomly, were subjected to **E7**, 5FU and vehicle treatment, as indicated in the materials and methods section; $n = 4$ mice per group. * **E7**-treatment is statistically different to control (vehicle) for the tumor volume at 6th and 7th day (t-test $p < 0.05$). Error bars indicate SEM. **b**, quantitative analysis of the AUC of tumor growth kinetics in control, **E7** and 5FU-treated mice. Bars are representative of the mean \pm SEM obtained from all mice treated (t-test, * $p < 0.05$). **c**, survival curves (Kaplan Meier) showing the percentage of survival of xenotransplanted mice, placebo control versus **E7** and 5FU-treated mice (Log-rank (Mantel-Cox) test P value=0.0024; $n=4$).

Supplementary Tables

Table S1.

Pockets found at the dimer interface of the active hTS (PDB ID: 1HVY). During the MD simulations, all pockets were dynamic and changed size, some disappeared or reappeared (see Table S2).

Pocket	Residues forming the pocket	Size (Å ³) ^a	RNA binding residues ^b	Other properties
<i>Pockets found in the crystal structure (monomer, A chain)</i>				
Y202	R64, Q200, F201 ^c , Y202, S209, C210 ^c , Q211, D247, I249	22	No	Not found in the dimeric structure since F59' of the other monomer fills the pocket. (Fig. S1). Interactions with polar, hydrophobic and aromatic residues are possible.
K47a	K47, D49, R50, T51, T55, S57, Y258, D254, H256, S216, G217	n.d. ^d	Yes: K47, D254 ^e	This pocket is part of the active site (Fig. S1). In a dimer, it is filled with R175' from the other monomer. Interactions with polar, hydrophobic and aromatic residues are possible. There are several energetically favorable water binding sites in front of the active site (PDB ID: 1HVY).
K47b	K47, S57, F59, D254	19.4	Yes: K47, F59, D254 ^e	This pocket is at the left side of the active site front (Fig. S1). It is not found in the dimer because it is filled with Y202' of the other monomer. Interactions with polar, aromatic and especially hydrophobic residues are possible.
I178	Q160, R163, V164, T167, R176, I177, I178, M179	32.7	Yes: R176	This pocket can also be found in the dimer. Interactions with polar, hydrophobic and aromatic residues are possible. Especially water probe was favored, consistent with the crystal water found in the site.
Y213	A197, L198, Q211, Y213	3.9	Yes: A197, Y213 ^f	In the dimer this pocket is partially filled with the Y213' from the other monomer. It is a very hydrophobic pocket.
<i>Pockets that appeared during the MD simulations (monomer, A chain)</i>				

W182	F137, Q138, F142, G143, A144, Q160, C180, W182, N183, R185, D186 ^g	101.4 ^g	Yes: F142, R185	W182 is within the active site loop (residues 181-197) that twists around 180° when hTS is activated/inactivated. Residue F142 divides the pocket into two compartments. A narrow region for favorable polar or aromatic interactions is found in the middle of the pocket and a large region for hydrophobic interaction at the mouth of the pocket.
C195	W182, P194, C195, H196, A197, R215 ^h	59.6 ^h	Yes: C195, A197, R215	C195 is the catalytic residue and resides on the other side of the active site loop than W182.
<i>Pockets found in the crystal structure (dimer)</i>				
A ⁱ	V158, Q160, R163, V164, T167, D174, R176, I177, I178, W182 ^j , P184', L187', P188', P193'	232/362	Yes: V158, R176, P184	These pockets reside between the active site loop and the 'R175 bump' (residues 170-175) in the dimeric form of hTS and the I178 pocket of the monomeric hTS is part of it.
B ⁱ	H39, C43, G44, V45, S57, V58, F59, R64', R68', Y202', V204', E207', S209', D247', I249'	38/210	Yes: H39, C43, G44, V45, V58, F59	These pockets reside between the beta sheet kink and the 'C20 peptide' ^k (residues 198-217). The region below the main Y202 pocket is part of these pockets.
C	F142, F142', C180, W182, W182', P184	25	Yes: F142, P184	This symmetric pocket resides at the crossroads of the interface loops (residues 141-159) and active site loops (i.e., between the A pockets). In the inactive hTS, this pocket is deeper and larger than in the active hTS due to the conformational change of the active site loops upon inactivation.
D ⁱ	K47, D48, D49, T55, S57, F59, D254, H256, P172', D173', D174', R175', I177', Q200', Y202', F201', V203'	143/149	Yes: K47, F59, D254 ^e	These are groups of small pockets in front of the dUMP phosphate binding site. They line the K47 pockets of the monomeric hTS and are favorable binding sites for water.

^aSize as calculated by CASTp;

^bRNA binding residues as predicted with the KYG server (both active and inactive hTS conformations);

^cBackbone atoms only;

^dNot possible to determine the size as the pocket is part of the active site cavity;

^eIn the inactive conformation (PDB ID: 1YPV);

^fOnly in the active conformation;

^gAt 7 ns of the explicit water MD simulation (with crystal water included);

^hAt 4 ns of the explicit water MD simulation (with crystal water included);

ⁱTwo similar pockets found due to symmetry.

^j(') after a residue name refers to the residue in the opposite monomer;

^kA 20-mer peptide at the hTS dimer interface (17).

Table S2.

Interface pockets at the 1HVY monomer during the explicit water simulation with crystal water molecules included (without dUMP). Pockets are named according to the data in Table S1.

Time (ns)	Size of a pocket (\AA^3) determined by CASTp ^a					
	Y202 pocket (& around) ^b	I178 pocket	Y213 pocket	K47b pocket ^c	W182 pocket	C195 pocket
0	169.4	32.7	3.9	19.4	-	-
1	37.1	237	-	-	22.8	14.5
2	271.6	11.6	46.3	24	11.8	24.6
3	392.5	42.7	59.6	-	14.5	19.8
4	510.6	63.1	53.1	-	17.4	59.6
5	276.3	42.2	-	93.1	-	34
6	584.3	14.8	-	-	-	-
7	101.5	-	-	-	101.4	-

^aSizes of the pockets depend on the method CASTp uses for their calculation. In principle, according to CASTp, a phenyl ring can fit into a pocket of ca. 20\AA^3 , as e.g. for the K47b pocket in the crystal structure).

^bThe region surrounding the Y202 pocket is included here; thus the volumes are much larger than the pocket itself (Table S1). Y202 can block the main pocket by moving its side chain (in the monomer simulations).

^cThe K47a pocket is always part of the large active site cavity, so its size cannot be followed separately. (see Fig. S1).

Table S3. Data collection and refinement statistics (data in parenthesis refer to the highest resolution shell).

Protein	hTS mutant Y202C	hTS mutant C195S-Y202C
PDB code	4O1U	4O1X
DATA COLLECTION STATISTICS		
Beamline, $\lambda(\text{\AA})$	ESRF ID29, 0.9360	ESRF ID23-2, 0.873
Space group	P3 ₁	P2 ₁ 2 ₁ 2 ₁
$\Delta\phi$ (°)	1	0.5
Cell dimensions (\AA , °)		
a	96.23	94.93
b	96.23	95.52
c	83.77	131.59
Resolution (\AA)	48.12 - 2.26 (2.38 - 2.26)	38.65 - 2.32 (2.45 - 2.32)
N mol/asym. unit	2 (1 dimer)	4 (2 dimers)
Observed reflections	151047 (22511)	212942 (30276)
Unique reflections	39688 (5882)	51794 (7464)
Completeness (%)	97.6 (98.6)	99.0 (99.0)
Rmerge (%)	6.7 (37.8)	8.5 (36.6)
I/ σ (I)	12.0 (3.7)	10.4 (4.0)
Multiplicity	3.8 (3.8)	4.1 (4.1)
REFINEMENT STATISTICS		
Resolution range (\AA)	48.12 - 2.26 (2.32 - 2.26)	38.49 - 2.32 (2.38 - 2.32)
R _{cryst} (%)	17.2 (22.7)	20.6 (27.5)
n. of ref. in R _{free} set, R _{free} (%)	1972, 21.0 (27.7)	2628, 26.0 (39.4)
Total atoms	4475	9482
protein	4240	9169
waters	186	250
sulfate ions	30	40
other (ethylene glycol, chloride)	19	23
Mean B value (\AA^2)	54.17	32.89
RMSD bond lengths (\AA)	0.010	0.011
RMSD bond angles (°)	1.435	1.532
RMSD chiral volumes	0.099	0.097
RMSD planes (\AA)	0.006	0.007
Est. error on coord. based on R value (\AA)	0.19	0.45
Ramachandran plot (%)		
Favored	90.8	89.6
Allowed	9.2	10.4
Not allowed	0.0	0.0

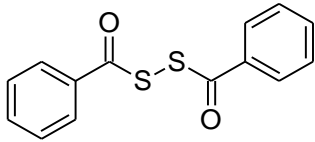
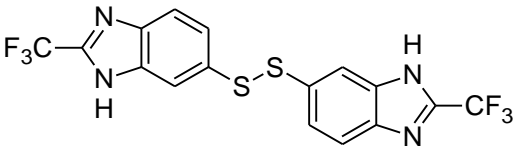
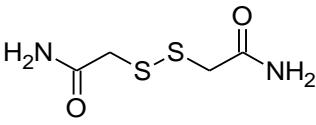
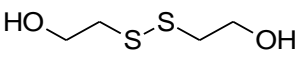
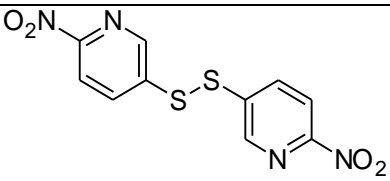
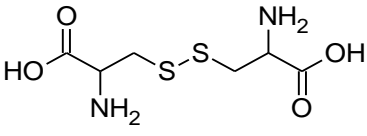
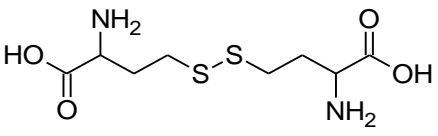
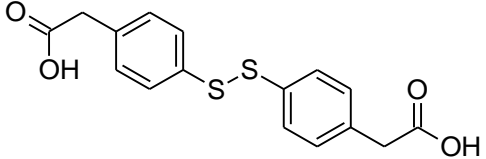
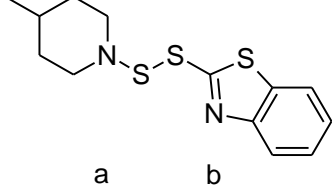
Table S4.

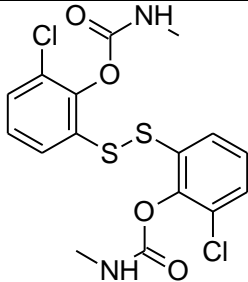
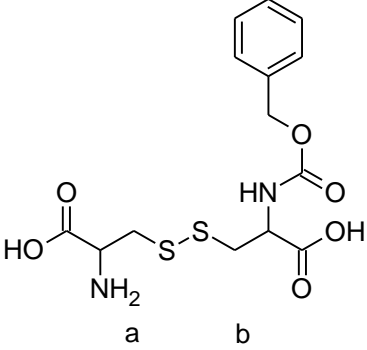
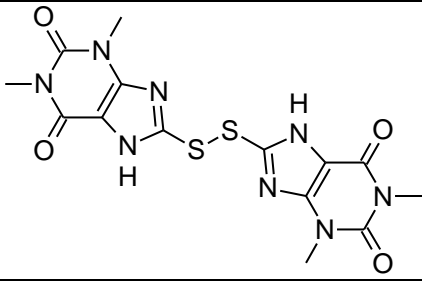
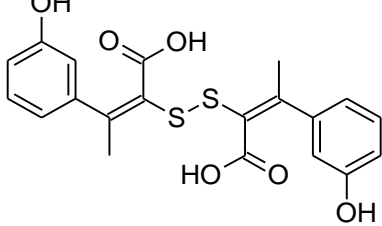
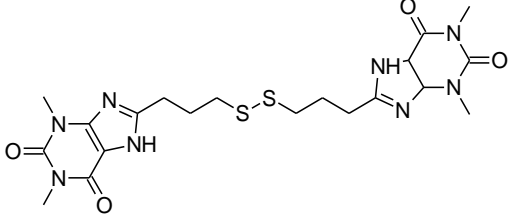
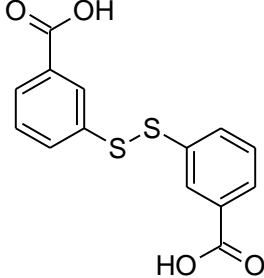
Solvent accessibility of the cysteine residues in hTS mutants and their chemical modifications upon reaction with β -mercaptoethanol. SCH = S-methyl-thio-cysteine; CME = S,S-(2-hydroxyethyl) thiocysteine.

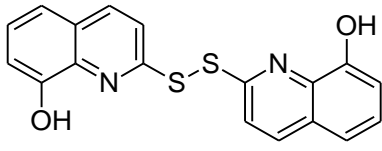
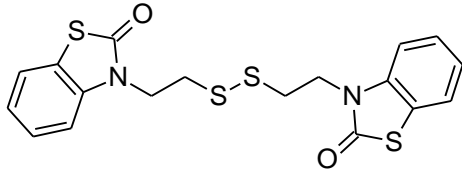
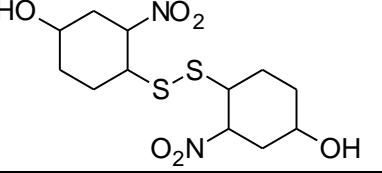
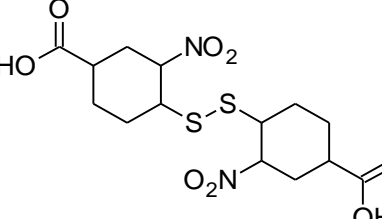
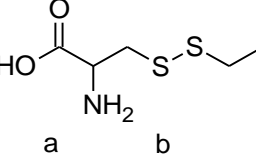
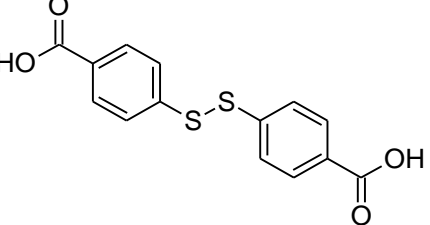
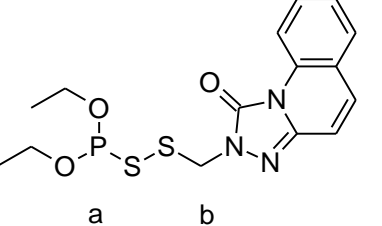
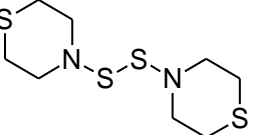
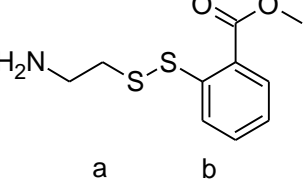
Decreasing solvent accessibility	Solvent accessibility	Cysteine residue number	Chemical Modification	
			Y202C	C195S_Y202C
	Fully accessible	43	SCH	CME
	Partially accessible	180	SCH	Cys (possibly modified: weak electron density beyond S)
	Partially accessible	195	SCH	Ser
	Partially accessible	202	CME	CME
	Almost buried	199	CME	CME
	Completely buried	210	Cys	Cys

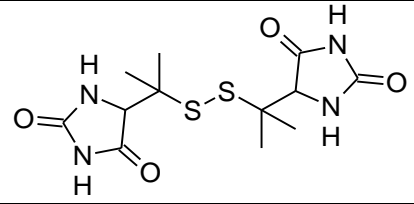
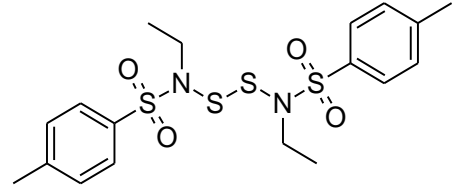
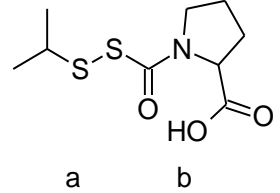
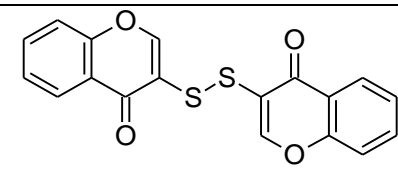
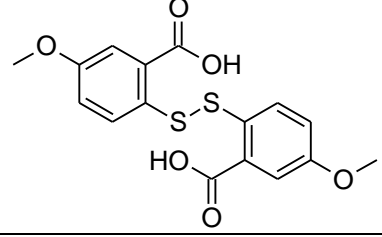
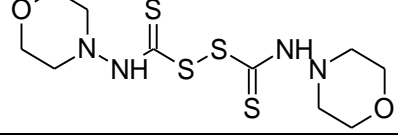
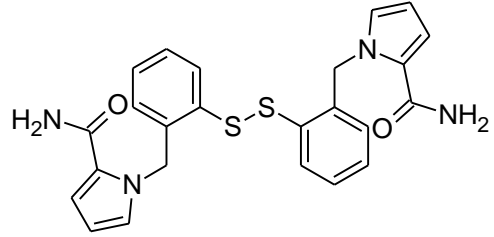
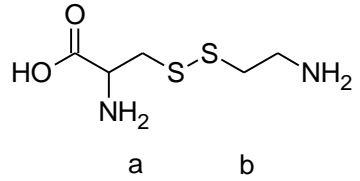
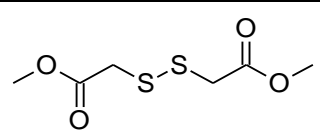
Table S5.

Library screened through mass spectrometry.

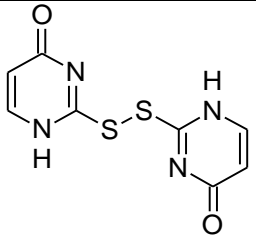
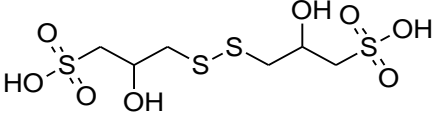
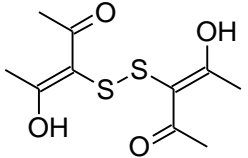
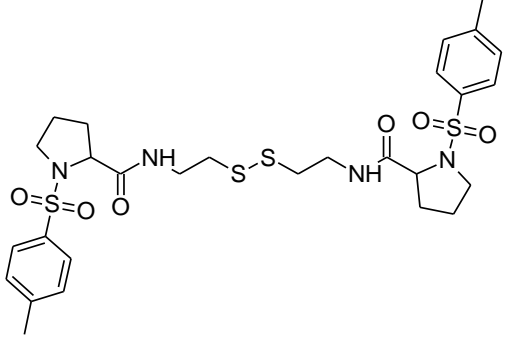
Compound	Properties	Commercial Codes	Structures
A1	MW: 274.358 Log P: 3.110 N Heavy Atoms: 9+9	NCI: NSC209 ZINC: 1555356	
A2	MW: 435.39 Log P: 4.964 N Heavy Atoms: 13+13	NCI: NSC659162 ZINC: 1636936	
A3	MW: 180.248 Log P: -1.014 N Heavy Atoms: 5+5	NCI: NSC28727 ZINC: 1646639	
A4	MW: 154.251 Log P: 0.380 N Heavy Atoms: 4+4	NCI: NSC33920 ZINC: 1665970	
A5	MW: 312.325 Log P: 2.780 N Heavy Atoms: 10+10	NCI: NSC149336 ZINC: 1734461	
A6	MW: 240.300 Log P: -5.196 N Heavy Atoms: 7+7	NCI: NSC13203 ZINC: 1529198	
A7	MW: 268.354 Log P: -4.214 N Heavy Atoms: 8+8	NCI: NSC11337 ZINC: 1529294	
A8	MW: 332.394 Log P: 2.768 N Heavy Atoms: 11+11	NCI: NSC211 ZINC: 1555358	
A9 ^a	MW: 296.474 Log P: 3.992 N Heavy Atoms: 8+10	NCI: NSC261199 ZINC: 1558189	 a b

A19	MW: 433.329 Log P: 3.812 N Heavy Atoms: 13+13	NCI: NSC39633 ZINC: 1671480	
A20 ^a	MW: 373.424 Log P: -0.922 N Heavy Atoms: 7+17	NCI: NSC43135 ZINC: 1675892	
A21	MW: 424.458 Log P: 0.462 N Heavy Atoms: 14+14	NCI: NSC71895 ZINC: 1697318	
A22	MW: 416.467 Log P: 4.628 N Heavy Atoms: 14+14	NCI: NSC108934 ZINC: 1701075	
A23	MW: 508.617 Log P: 1.992 N Heavy Atoms: 17+17	NCI: NSC110311 ZINC: 1702746	
A24	MW: 304.341 Log P: 3.668 N Heavy Atoms: 10+10	NCI: NSC110311 ZINC: 1704344	

A25	MW: 353.438 Log P: 4.974 N Heavy Atoms: 12+12	NCI: NSC125034 ZINC: 1714235	
A26	MW: 420.592 Log P: 4.408 N Heavy Atoms: 13+13	NCI: NSC125828 ZINC: 1714842	
A27	MW: 352.427 Log P: 2.342 N Heavy Atoms: 11+11	NCI: NSC175829 ZINC: 1716349	
A28	MW: 406.431 Log P: 2.400 N Heavy Atoms: 13+13	NCI: NSC175830 ZINC: 1716350	
A29 ^a	MW: 181.276 Log P: -1.22 N Heavy Atoms: 3+7	NCI: NSC135126 ZINC: 1721731	
A30	MW: 304.341 Log P: 3.64 N Heavy Atoms: 10+10	NCI: NSC210281 ZINC: 1745667	
A31 ^a	MW: 383.425 Log P: 4.847 N Heavy Atoms: 8+16	NCI: NSC213718 ZINC: 1752388	
A32	MW: 268.486 Log P: 0.502 N Heavy Atoms: 7+7	NCI: NSC18421 ZINC: 1769219	
A33 ^a	MW: 244.354 Log P: 1.979 N Heavy Atoms: 4+11	NCI: NSC342027 ZINC: 1579497	

A34	MW: 346.426 Log P: -0.122 N Heavy Atoms: 11+11	NCI: NSC350993 ZINC: 1581670	
A35	MW: 460.654 Log P: 4.418 N Heavy Atoms: 14+14	NCI: NSC363956 ZINC: 1585472	
A36 ^a	MW: 248.342 Log P: 2.330 N Heavy Atoms: 4+11	NCI: NSC369423 ZINC: 1587145	
A37	MW: 354.400 Log P: 3.734 N Heavy Atoms: 12+12	NCI: NSC370926 ZINC: 1587470	
A38	MW: 364.393 Log P: 4.058 N Heavy Atoms: 12+12	NCI: NSC372683 ZINC: 1588809	
A39	MW: 354.535 Log P: -0.49 N Heavy Atoms: 10+10	NCI: NSC403854 ZINC: 1596138	
A40	MW: 462.587 Log P: 3.728 N Heavy Atoms: 16+16	NCI: NSC611506 ZINC: 1611876	
A41 ^a	MW: 197.299 Log P: -3.390 N Heavy Atoms: 4+7	NCI: NSC161601 ZINC: 1623380	
A42	MW: 210.271 Log P: 1.608 N Heavy Atoms: 6+6	NCI: NSC638710 ZINC: 1625711	

A43 ^a	MW: 178.272 Log P: 2.648 N Heavy Atoms: 4+6	NCI: NSC96660 ZINC: 1626922	
A44 ^a	MW: 303.292 Log P: 2.194 N Heavy Atoms: 6+13	NCI: NSC96669 ZINC: 1626930	
A45 ^a	MW: 362.443 Log P: 4.087 N Heavy Atoms: 10+14	NCI: NSC96696 ZINC: 1626956	
A46	MW: 404.548 Log P: 5.792 N Heavy Atoms: 12+12	NCI: NSC97416 ZINC: 1632630	
A47	MW: 289.203 Log P: 4.406 N Heavy Atoms: 8+8	NCI: NSC98831 ZINC: 1648618	
A48	MW: 238.324 Log P: 1.828 N Heavy Atoms: 7+7	NCI: NSC308782 ZINC: 1568750	
A49	MW: 460.654 Log P: 4.346 N Heavy Atoms: 14+14	NCI: NSC342021 ZINC: 1579493	
A50 ^a	MW: 270.412 Log P: -2.552 N Heavy Atoms: 7+8	NCI: NSC342029 ZINC: 1579499	
A51	MW: 442.551 Log P: 2.012 N Heavy Atoms: 15+15	NCI: NSC405812 ZINC: 1598776	
A52	MW: 272.432 Log P: -0.834 N Heavy Atoms: 7+7	NCI: NSC14558 ZINC: 1653104	

A53	MW: 254.289 Log P: -1.58 N Heavy Atoms: 8+8	NCI: NSC106685 ZINC: 1697982	
A54	MW: 340.415 Log P: -2.662 N Heavy Atoms: 8+8	NCI: NSC126672 ZINC: 1715307	
A55	MW: 262.346 Log P: 4.702 N Heavy Atoms: 8+8	NCI: NSC15869 ZINC: 1733696	
TCP	MW: 654.884 Log P: 4.088 N Heavy Atoms: 21+21		

^a For asymmetric disulphide compounds the two possible binding fragments are indicated by “a” and “b”.

Table S6.

Mass spectrometry screening results: compounds detected bound to hTS C195S-Y202C.

Compound	MALDI	ESI-QToF
A2	detected	not detected
A4	detected	detected
A5	detected	detected
A6	detected	detected
A7	detected	not detected
A9	detected	not detected
A10	detected	detected
A11	detected	not detected
A14	detected (both fragments)	detected (both fragments)
A15	detected (both fragments)	detected (both fragments)
A16	not detected	detected
A20	detected (fragment b)	detected (fragment b)
A21	detected	not detected
A22	detected	not detected
A25	detected	not detected
A26	detected	not detected
A27	detected	not detected
A28	detected	not detected
A29	detected (both fragments)	detected (both fragments)
A30	detected	detected
A36	detected (both fragments)	detected (fragment b)
A37	detected	not detected
A38	detected	detected
A41	detected	not detected
A42	detected	not detected
A43	detected	detected (both fragments)
A47	detected	detected
A49	detected	not detected
A55	detected	not detected
TCP	detected	detected

Table S7.

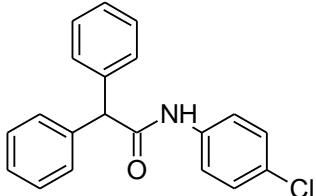
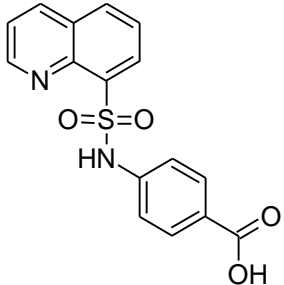
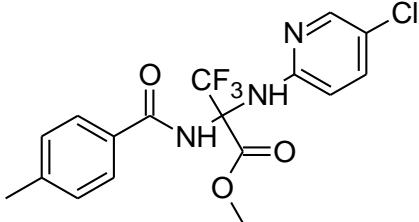
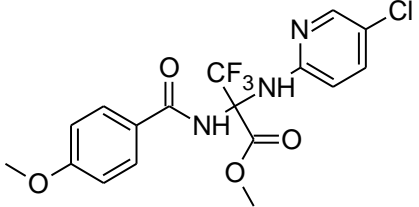
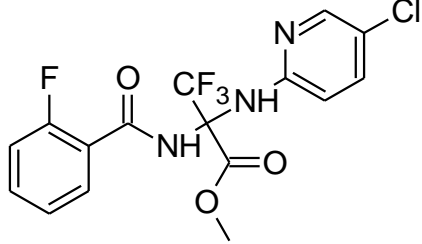
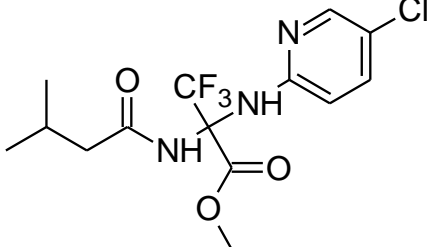
Results of the mass spectrometry experiments on C195S-Y202C hTS protein-ligand complexes digested with trypsin and analyzed by MALDI (M) and ESI (E) MS. If the ligand is not identified through E it is indicated as (E-).

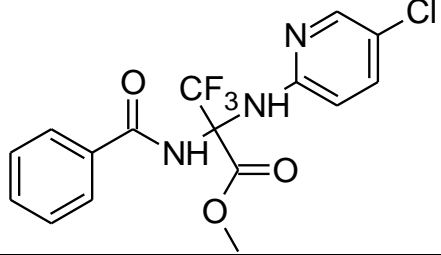
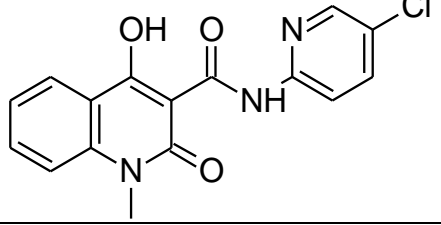
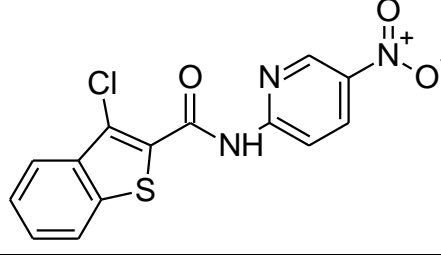
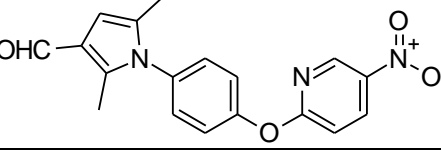
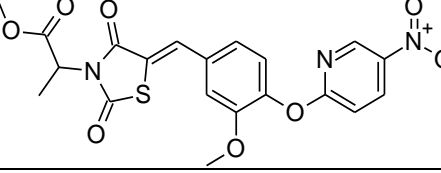
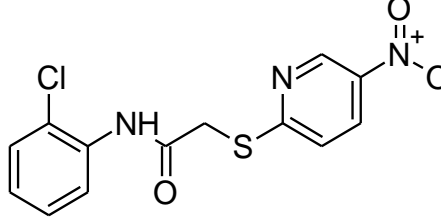
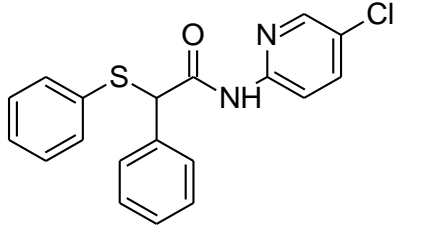
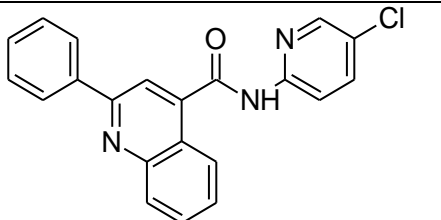
Compound	CYS 180				CYS 199, 202, 210	
	(177)- (185) IIMCAWNPR (sequence A)		(176) –(185) RIIMCAWNPR (sequence B)		(186)- (215) DLPLMALPPSHALCQFCVV NSELSCQLYQR (sequence C)	
	Cam (1x) 1160.57 08 Da	Lig (1x) ^a	Cam (1x) 1316.6720 Da	Lig (1x) ^a	Cam (3x) 3546.7006 Da	Lig (1x) Cam (2x) ^a
A5	M E	M E	ND ^b	ND ^b	M E	M
A6	M E	ND ^b	ND ^b	M E	M E-	ND ^b
A10	M E	M	E	ND ^b	M E	M
A15 (both fragments)	M E	E(a)	ND ^b	M(a)- E(ab)	M E-	ND ^b
A20 (fragment b)	M E	M(b) E(ab)	E	ND ^b	M E-	M(b) E(b)
A38	M E	ND ^b	ND ^b	M E	M E	ND ^b
TCP	M E	M E	ND ^b	ND ^b	M E	M

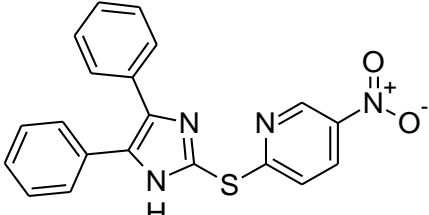
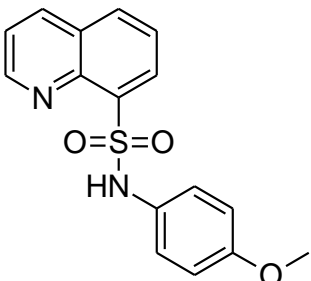
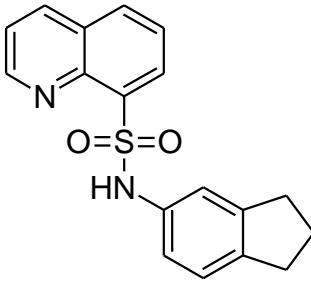
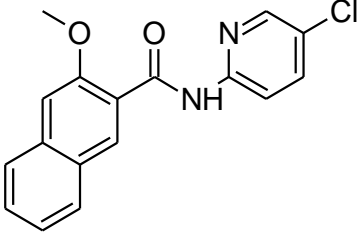
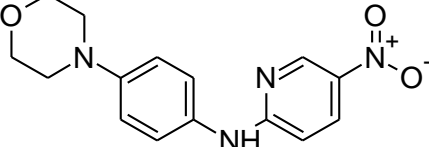
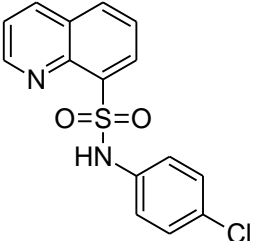
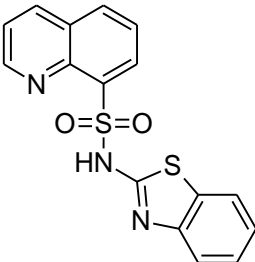
^aThe ligands bound to the Cys-containing peptides were identified by replacing the MW of the carbamidomethyl group (56 Da) with the MW of the thiol originated from the disulphides on the prototypic reporter ions 1160.5, 1316.7, 3546.7. For symmetric disulphides, the MW of the tethered-ligand corresponds to half of the MW of the molecule; for asymmetric disulphides, the MW of the tethered-ligand corresponds to the MW of either the **a** or **b** portions of the molecule; ^b ND= not detected

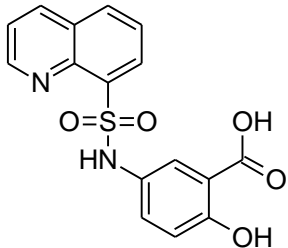
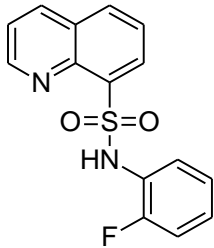
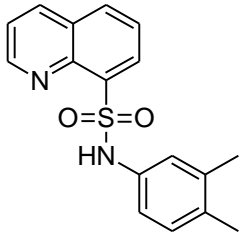
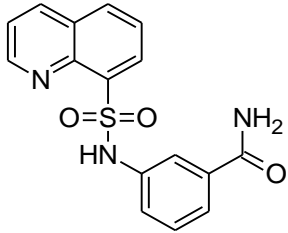
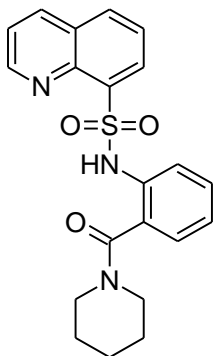
Table S8.

FRET analysis and kinetic inhibition data for compounds **B1-B26** against hTS. $\Delta\Phi_{\text{fret}}$ = change in FRET efficiency with respect to untreated hTS.

Compound	Formula	% enzyme activity inhibition ^a	$\Delta\Phi_{\text{fret}}^b$
B1		20	0
B2		20	0
B3		15	0
B4		ND ^c	0
B5		ND	0
B6		ND	0

B7		ND	0
B8		30	0
B9		40	0
B10		15	0
B11		85	0
B12		15	-0.13
B13		25	0
B14		25	0

B15		45	0
B16		ND	0
B17		35	0
B18		35	0
B19		15	0
B20		40	0
B21		15	0

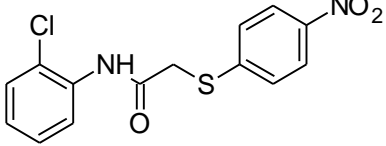
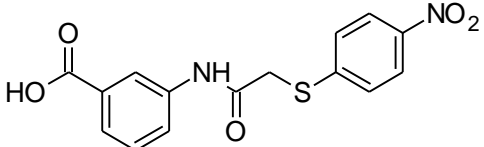
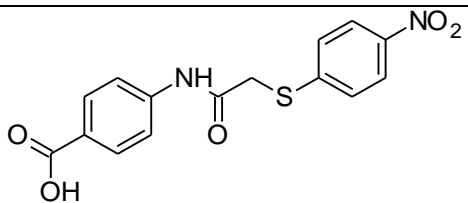
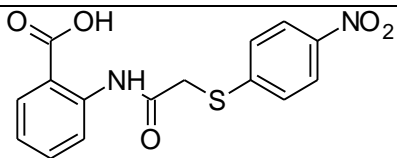
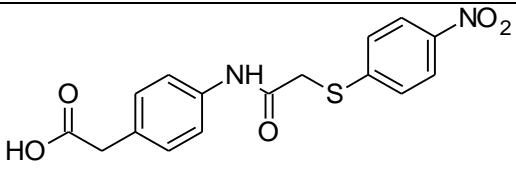
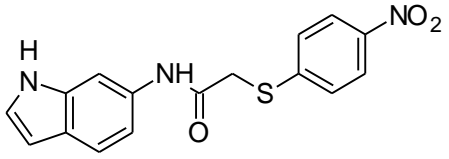
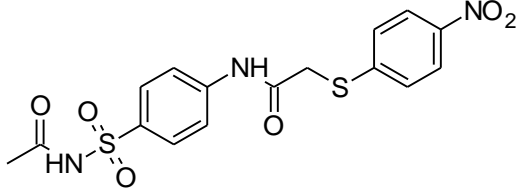
B22		40	0
B23		ND	0
B24		30	0
B25		15	0
B26		ND	-0.02

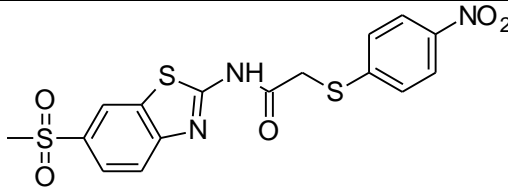
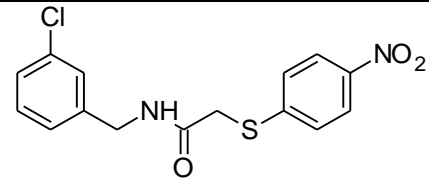
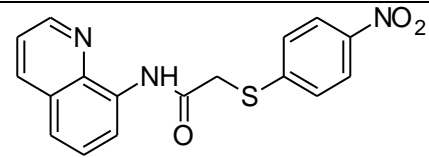
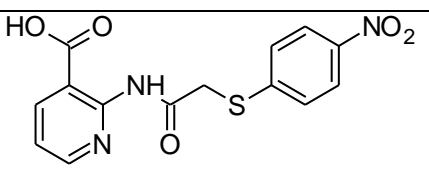
^a % inhibition was measured at 50 μM conc., unless otherwise stated; standard error (SE) +/-20% of the displayed value.

^b measured at 50 μM ; the value is the result of the subtraction of the $\Delta\Phi_{\text{fret}}$ value obtained in the presence of DMSO alone (-0.1) from that obtained in the presence of the tested compounds; standard error (SE) +/-15% of the displayed value;

^c ND not active at the concentrations tested.

Table S9.FRET analysis and kinetic inhibition data for compounds **C1-C11** against hTS.

Compound		Synthetic Scheme	IC_{50} (μM) ^b	$\Delta\Phi_{fret}$ ^b
C1		2	ND ^c	-0.31
C2		1	83	-0.37
C3		1	5.25	-0.5
C4		1	246	-0.30
C5		1	76	-0.33
C6		3	ND	-0.09
C7		3	ND	-0.10

C8		3	30	-0.67 ^d
C9		3	ND	-0.05
C10		2	ND	-0.56
C11		3	75	-0.21

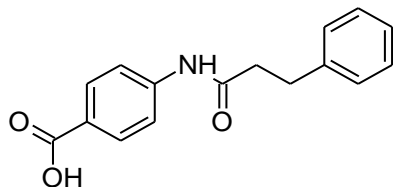
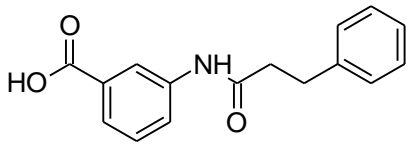
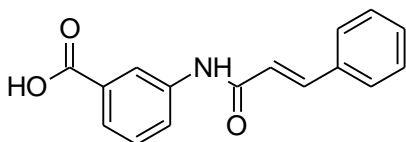
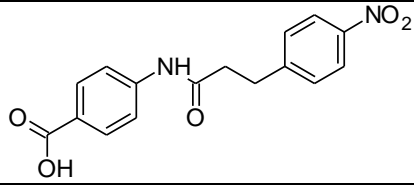
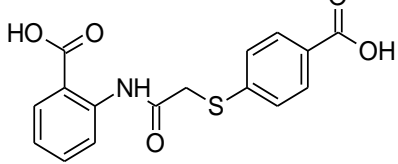
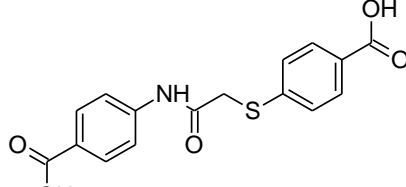
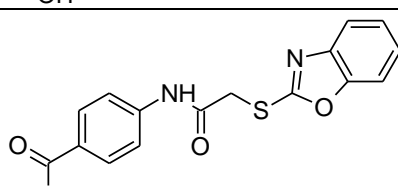
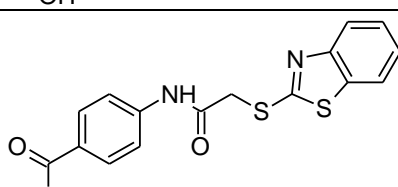
^a IC₅₀ data unless otherwise stated show a standard error (SE) +/-20% of the displayed value.

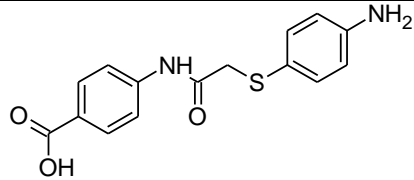
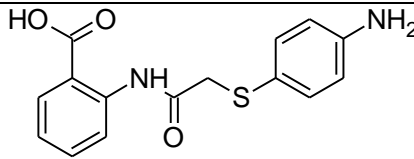
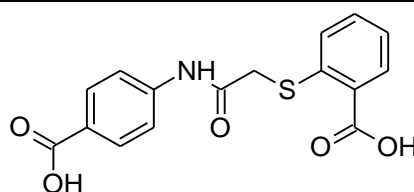
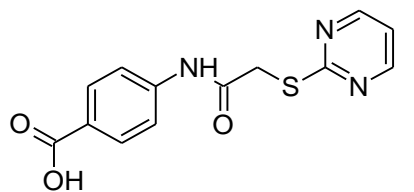
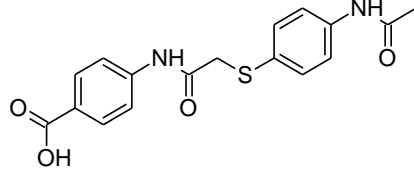
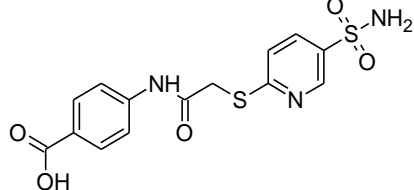
^b measured at 50 μM; the value is the result of the subtraction of the ΔΦ_{fret} value obtained in the presence of DMSO alone (-0.1) from that obtained in the presence of the tested compounds; standard error (SE) +/-15% of the displayed value;

^c ND not active at 50 μM ;

^d measured at 100 μM.

Table S10.FRET analysis and kinetic inhibition data for compounds **D1-D14** against hTS.

Compound	R	Synthetic Scheme	IC_{50} (μM) ^a	$\Delta\Phi_{fret}$ ^b
D1		4	ND ^c	0
D2		4	ND	0
D3		4	ND	0
D4		4	ND	-0.09
D5		1	40	-0.24
D6		1	53	-0.22
D7		1	42	-0.33
D8		1	47	-0.14

D9		2	60	-0.36 ^d
D10		2	85	-0.26
D11		1	ND	0
D12		1	105	-0.22
D13		1	ND	0
D14		1	ND	0

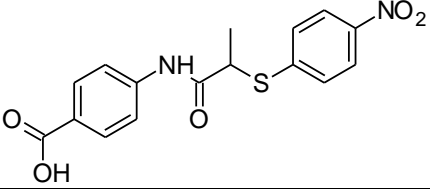
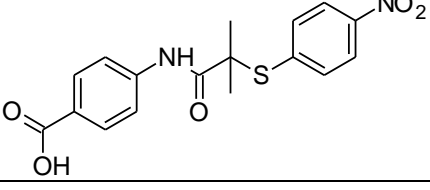
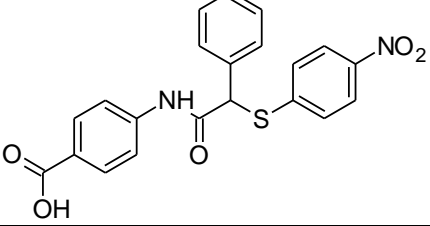
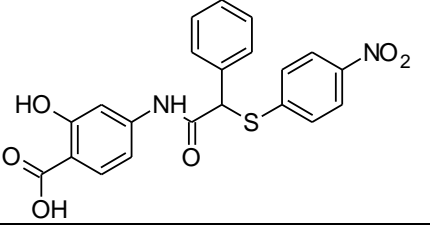
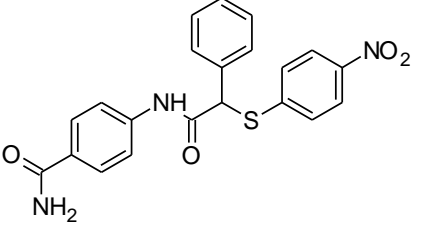
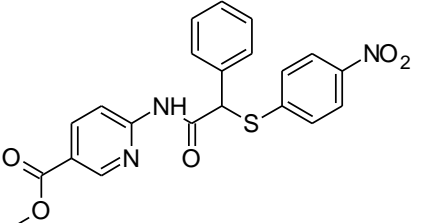
^a IC₅₀ data unless otherwise stated show a standard error (SE) +/-20% of the displayed value.

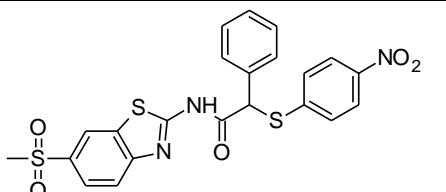
^b measured at 50 μM; the value is the result of the subtraction of the ΔΦ_{free} value obtained in the presence of DMSO alone (-0.1) from that obtained in the presence of the tested compounds; standard error (SE) +/-15% of the displayed value;

^c ND not active at 50 μM ;

^d measured at 100 μM.

Table S11.FRET analysis and kinetic inhibition data for compounds **E1-E7** against hTS.

Compound		Synthetic Scheme	IC_{50} (μM) ^a	$\Delta\Phi_{fret}$ ^b
E1		3	44	-0.32
E2		3	ND ^c	0
E3		3	23	-0.56
E4		3	40	-0.87 ^d
E5		3	40	-0.24
E6		3	10	-0.24

E7		3	7 ^e	-0.1 at 10 μM ^f
-----------	---	---	----------------	---------------------------------------

^a IC_{50} data unless otherwise stated show a standard error (SE) +/-20% of the displayed value.

^b measured at 50 μM ; the value is the result of the subtraction of the $\Delta\Phi_{\text{fret}}$ value obtained in the presence of DMSO alone (-0.1) from that obtained in the presence of the tested compounds; standard error (SE) +/-15% of the displayed value; all experiments were repeated 3 times.

^c ND not active at 50 μM ;

^d measured at 100 μM ;

^e IC_{50} apparent value, due to low solubility;

^f $\Delta\Phi_{\text{fret}}$ only detectable at 10 μM , due to low solubility.

Table S12.

Enzyme inhibition data (hTS) and hTS dimer interaction inhibitors (evaluated by FRET decrease, $\Delta\Phi_{\text{fret}}$) of compounds **F1-F4**

Compound	R ₁	R ₂	Scheme	IC ₅₀ (μM)	$\Delta\Phi_{\text{fret}}^a$
F1	-H	-H	5	ND ^b	-0.02
F2	-OCH ₃	-OCH ₃	6	ND	-0.35
F3	-COOCH ₃	-H	6	ND	-0.13
F4	-COOH	-H	6	ND	-0.04

^a measured at 50 μM ; the value is the result of the subtraction of the $\Delta\Phi_{\text{fret}}$ value obtained in the presence of DMSO alone (-0.1) from that obtained in the presence of the tested compounds; standard error (SE) +/-15% of the displayed value; all experiments were repeated at least 3 times.

^b ND not active at 50 μM .

Table S13

Racemization rate constants of (+)-**E7** and (-)-**E7** determined in buffer solutions. Time intervals for enantiomerization kinetics analysis: 0', 10', 20', 30', 40' and 50'. T = 37.5 °C.

	(+)- E7	(-)- E7
k (s ⁻¹)	$2.03 \pm 0.18 \times 10^{-4}$	$2.10 \pm 0.16 \times 10^{-4}$
$t_{1/2}$ (min)	56.80	54.98

Table S14.

IC50 values ($\mu\text{M} \pm \text{SE}$) for selected compounds obtained after 72 h treatment of 2008, C13*, A2780, A2780/CP, IGROV1 and TOV112D human ovarian cancer cells. Data indicate mean values and standard deviation from at least two experiments performed in duplicate. P values were calculated with two-sided Student's *t*-test and ANOVA followed by the Tukey's multiple comparison. * $p < 0.05$; ** $p < 0.01$; *** $p < 0.001$ (n=3-5)

Compounds	2008 cells	C13* cells	A2780 cells	A2780/CP cells	IGROV1 cells	TOV112D cells
5-FU	6.4±0.7	9.3±1	8.5±0.8	11.6±1.2	16.9±1	ND
C2	>100	>100	>100	>100	>100	>100
C3	>100	>100	>100	>100	>100	99.1±11
C4	>100	>100	>100	>100	>100	>100
C5	>100	>100	>100	>100	>100	>100
C8	98±7	>100	>100	>100	>100	>100
C11	>100	>100	>100	>100	>100	>100
D5	>100	>100	>100	>100	>100	>100
D6	>100	>100	>100	>100	>100	>100
D7	>100	>100	>100	>100	>100	>100
D8	>100	>100	>100	>100	>100	>100
D9	>100	>100	>100	>100	>100	>100
D12	>100	>100	>100	>100	>100	>100
E1	77±4	>100	>100	>100	>100	>100
E3	>100	>100	76.6±9	>100	>100	72.2±9
E4	55.8±7	76.3±9	88.3±11	>100	>100	88.5±9
E5	29.8±4	38.3±5	28.8±4	34.3±5	63.9±8	60.5±7

E6	61±6	50.5±2	19.5±2	18.7±1	39.1±3	41.5±7
E7	14.6±1	21.1±2	10.1±0.3	21.5±3	37.4±6	31.±2

Table S15.

IC50 values ($\mu\text{M} \pm \text{SE}$) for compounds **E5**, **E7**, obtained after 72 h treatment of PDAC-2 and PDAC-5 pancreatic cancer cells, HT29, HCT116 and LoVo human colorectal cancer cells. Data indicate mean values and standard deviation from at least two experiments performed in duplicate. P values were calculated with two-sided Student's *t*-test and ANOVA followed by the Tukey's multiple comparison.

* $p < 0.05$; ** $p < 0.01$; *** $p < 0.001$ (n=3).

Compounds	PDAC-2	PDAC.5	HT29 cells	HCT116 cells	LoVo cells
5-FU	3.00 \pm 0.7	4.37 \pm 2.1	14.2 \pm 3.0	13.5 \pm 1.5	7.9 \pm 1.2
E5	32.5 \pm 6.5	17.9 \pm 1.0	70.5 \pm 1.6	61.8 \pm 1.8	52.1 \pm 9.7
E7	9.1 \pm 0.4	11.6 \pm 1.6	34.5 \pm 3.0	35.5 \pm 0.3	23.3 \pm 9.0

Table S16. PK parameters for **E7** after single intravenous (IV) or oral administration (PO). C_{max} (maximum plasma concentration); T_{max} (time of maximum plasma concentration); AUC (area under the curve); T_{half} (plasma half time); MRT (mean residence time); V_z (Volume of distribution); V_{ss} (Steady state volume of distribution); C_{last} (last observed plasma concentration); T_{last} (Last time point with observable concentration).

Parameter	Dose	C _{max}	T _{max}	AUC _{last}	AUC _{tot}	Extrapolated AUC	T _{half}	MRT	Clearance	V _z	V _{ss}
Unit	mg/kg	ng/mL	h	ng/mL*h	ng/mL*h	%	H	H	mL/min/kg	L/kg	L/kg
E5	1 (IV)	1345	0.08	1875	2312	0.02	5.0	2.1	7.21	3.12	0.90
E7	1 (IV)	3113	0.08	38577	42312	1.6	13.6	16.2	0.39	0.46	0.38
E5	20(P)	230.3	2	3001	3003	0.1	7.5	8.5	111.01	72.5	56.9
E7	20(P)	5340	3	143763	146235	1.7	13.7	20.8	2.28	2.7	2.8

SI Reference

1. J. Phan, S. Koli, W. Minor, R. B. Dunlap, S. H. Berger, L. Lebioda, Human thymidylate synthase is in the closed conformation when complexed with dUMP and raltitrexed, an antifolate drug. *Biochemistry* **40**, 1897-1902 (2001).
2. G. Brady, P. Stouten, Fast prediction and visualization of protein binding pockets with PASS. *J. Comput. Aided Mol. Des.* **14**, 383-401 (2000).
3. J. Dundas, Z. Ouyang, J. Tseng, A. Binkowski, Y. Turpaz, J. Liang, CASTp: computed atlas of surface topography of proteins with structural and topographical mapping of functionally annotated residues. *Nucleic Acids Res.* **34**, W116-W118 (2006).
4. R. C. Wade, P. J. Goodford, Further development of hydrogen bond functions for use in determining energetically favorable binding sites on molecules of known structure. 2. Ligand probe groups with the ability to form more than two hydrogen bonds. *J. Med. Chem.* **36**, 148-156 (1993).
5. D. A. Case, T. E. Cheatham III, T. Darden, H. Gohlke, R. Luo, K. M. Merz Jr, A. Onufriev, C. Simmerling, B. Wang, R. J. Woods, The Amber biomolecular simulation programs. *J. Comput. Chem.* **26**, 1668-1688 (2005).
6. Y. Duan, C. Wu, S. Chowdhury, M. C. Lee, G. Xiong, W. Zhang, R. Yang, P. Cieplak, R. Luo, T. Lee, J. Caldwell, J. Wang, P. Kollman, A point-charge force field for molecular mechanics simulations of proteins based on condensed-phase quantum mechanical calculations. *J. Comput. Chem.* **24**, 1999-2012 (2003).
7. T. Wang, R. C. Wade, Implicit solvent models for flexible protein-protein docking by molecular dynamics simulation. *Proteins* **50**, 158-169 (2003).
8. W. L. Jorgensen, J. Chandrasekhar, J. D. Madura, R. W. Impey, M. L. Klein, Comparison of simple potential functions for simulating liquid water. *J. Chem. Phys.* **79**, 926-935 (1983).

9. K. Henrick, J. M. Thornton, PQS: a protein quaternary structure file server. *Trends Biochem Sci.* **199823**, 358-361 (1998).
10. M. Anirban, C. Charusita, Effect of the Berendsen thermostat on the dynamical properties of water. *Molecular Physics*, **102**, 681-685 (2004).
11. U. Essmann, L. Perera, M.L Berkowitz, T. Darden, H. Lee, L.G. Pedersen, A smooth particle mesh Ewald method. *J Chem Phys* **103**, 8577-8593 (1995).
12. J.P. Ryckaert, G. Ciccotti, H.J.C. Berendsen. Numerical integration of cartesian equations of motion of a system with constraints - molecular dynamics of N-alkanes. *Journal of Computational Physics*. **23**, 327-341 (1977).
13. O.M. Salo-Ahen, A. Tochowicz, C. Pozzi, D. Cardinale, S. Ferrari, Y. Boum, S. Mangani, R. M Stroud, P. Saxena, H. Myllykallio, M. P. Costi, G. Ponterini, R. C Wade. Hotspots in an obligate homodimeric anticancer target. Structural and functional effects of interfacial mutations in human thymidylate synthase. *J. Med. Chem.* **58**, 3572-3581 (2015).
14. A. G. Leslie, The integration of macromolecular diffraction data. *ActaCrystallogr. D Biol. Crystallogr.* **62**, 48-57 (2006).
15. P. Evans, Scaling and assessment of data quality. *ActaCrystallogr. D Biol. Crystallogr.* **62**, 72-82 (2006).
16. M. D. Winn, C. C. Ballard, K. D. Cowtan, E. J. Dodson, P. Emsley, P. R. Evans, R. M. Keegan, E. B. Krissinel, A. G. W. Leslie, A. McCoy, S. J. McNicholas, G. N. Murshudov, N. S. Pannu, E. A Potterton, H. R. Powell, R. J. Read, A. Vagin, K. S. Wilson, Overview of the CCP4 suite and current developments. *Acta Crystallogr. D Biol. Crystallogr.* **67**, 235-242 (2011).
17. A. Vagin, A. Teplyakov, MOLREP: an automated program for molecular replacement. *J. Appl. Crystallogr.* **30**, 1022-1025 (1997).
18. D. Cardinale, G. Guaitoli, D. Tondi, R. Luciani, S. Henrich, O. M. H. Salo-Ahen, S. Ferrari, G. Marverti, D. Guerrieri, A. Ligabue, C. Frassinetti, C. Pozzi, S. Mangani, D. Fessas, R. Guerrini,

- G. Ponterini, R. C. Wade, M.P Costi, Protein-protein interface-binding peptides inhibit the cancer therapy target human thymidylate synthase. *Proc. Natl. Acad. Sci. U SA* **108**, E542-E549 (2011).
19. J. Phan, S. Koli, W. Minor, R. B. Dunlap, S. H. Berger, L. Lebioda, Human thymidylate synthase is in the closed conformation when complexed with dUMP and raltitrexed, an antifolate drug. *Biochemistry* **40**, 1897-1902 (2001).
20. M. D. Winn, G. N. Murshudov, M. Z. Papiz, Macromolecular TLS refinement in REFMAC at moderate resolutions. *Methods Enzymol.* **374**, 300-321 (2003).
21. G. N. Murshudov, A. A. Vagin, E. J. Dodson, Refinement of macromolecular structures by the maximum-likelihood method. *Acta Crystallogr. D Biol. Crystallogr.* **53**, 240-255 (1997).
22. P. Emsley, B. Lohkamp, W. G. Scott, K. Cowtan, Features and development of Coot. *Acta Crystallogr. D Biol. Crystallogr.* **66**, 486-501 (2010).
23. G. Langer, S. X. Cohen, V. S. Lamzin, A. Perrakis, Automated macromolecular model building for X-ray crystallography using ARP/wARP version 7. *Nat. Protoc.* **3**, 1171-1179 (2008).
24. A. Vagin, A. Teplyakov, MOLREP: an automated program for molecular replacement. *J. Appl. Crystallogr.* **30**, 1022-1025 (1997).
25. P. D. Adams, P. V. Afonine, G. Bunkóczi, V. B. Chen, N. Echols, J. J. Headd, Li-W. Hung, S. Jain, G. J. Kapral, R. W. G. Kuntzle, A. J. McCoy, N. W. Moriarty, R. D. Oeffner, R. J. Read, D. C. Richardson, J. S. Richardson, T. C. Terwilliger, P. H. Zwart, The Phenix software for automated determination of macromolecular structures. *Methods.* **55**, 94-106 (2011).
26. R. A. Laskowski, M. W. MacArthur, D. S. Moss, J. M. Thornton, PROCHECK - a program to check the stereochemical quality of protein structures. *J. App. Cryst.* **26**, 283-291 (1993).
27. S. McNicholas, E. Potterton, K. S. Wilson, M. E. M. Noble, Presenting your structures: the CCP4mg molecular-graphics software. *Acta Cryst. D***67**, 386-394 (2011).
28. J. J. Irwin, B. K. Shoichet, ZINC – A free database of commercially available compounds for virtual screening. *J. Chem. Inf. Model.* **45**, 177-182 (2005).

29. G. Cruciani, P. Crivori, P. A. Carrupt, B. Testa, Molecular fields in quantitative structure-permeation relationships: the VolSurf approach. *J. Mol. Struct. Theo. Chem.* **503**, 17-30 (2000).
30. Simon Cross, Massimo Baroni, Emanuele Carosati, Paolo Benedetti, and Sergio Clementi, FLAP: GRID Molecular Interaction Fields in Virtual Screening. Validation using the DUD Data Set. *J. Chem. Inf. Model.* **50**, 1442-1450 (2010).
31. G. M. Morris, D. S. Goodsell, R. S. Halliday, R. Huey, W. E. Hart, R. Belew, A. J. Olson, Automated docking using a lamarckian genetic algorithm and empirical binding free energy function. *J. Comput. Chem.* **19**, 1639-1662 (1998).
32. F. Genovese, S. Ferrari, G. Guaitoli, M. Caselli M. P. Costi, G. Ponterini, Dimer-monomer equilibrium of human thymidylate synthase monitored by fluorescence resonance energy transfer. *Protein Sci.* **19**, 1023-1030 (2010).
33. G. Marverti, Ligabue A, Lombardi P, Ferrari S, Monti MG, Frassinetti C, Costi MP. Modulation of the expression of folate cycle enzymes and polyamine metabolism by berberine in cisplatin-sensitive and -resistant human ovarian cancer cells. *Int. J. Oncol.* **43**,1269-1280 (2013).
34. B.M. Beaufort, J.C.A. Helmijr, A.M. Piskorz, M. Hoogstraat, K. Ruigrok-Ritstier, N. Besselink, M. Murtaza, W.F.J. van IJcken, A.A.J. Heine, M. Smid, M.J. Koudijs, J.D. Brenton, E.M.J.J. Berns, J. Helleman, Ovarian Cancer Cell Line Panel (OCCP): Clinical Importance of In Vitro Morphological Subtypes. *PLoS ONE* **9**, e103988 (2014).
35. E. Giovannetti, Q. Wang, A. Avan, N. Funel, T. Lagerweij, Jih-H. Lee, V. Caretti, A. van der Velde, U. Boggi, Y. Wang, Role of CYB5A in Pancreatic Cancer Prognosis and Autophagy Modulation. *Journal of the National Cancer Institute*, **106** (2014), djt346, <https://doi.org/10.1093/jnci/djt346>
36. G. Marverti, Ligabue, A., Paglietti, G., Corona, P., Piras, S., Vitale, G., Guerrieri, D., Luciani, R., Costi, M.P., Frassinetti, C., and Moruzzi, M.S. Collateral sensitivity to novel thymidylate synthase

inhibitors correlates with folate cycle enzymes impairment in cisplatin-resistant human ovarian cancer cells. *Eur. J. Pharmacol.* **615**, 17-26 (2009).

37. J-M. Shi, J. Pei, E-Q. Liu, L. Zhang, Bis(sulfosuccinimidyl) suberate (BS3) crosslinking analysis of the behavior of amyloid- β peptide in solution and in phospholipid membranes. *PLoS ONE* **12**(3), e0173871 (2017). <https://doi.org/10.1371/journal.pone.0173871>
38. C. Li, B. Liu, J. Chang, T. Groessl, M. Zimmerman, Y. Q. He, J. Isbell, T. Tuntland T, A modern in vivo pharmacokinetic paradigm: combining snapshot, rapid and full PK approaches to optimize and expedite early early drug discovery. *Drug Discov Today* **18**, 71-78 (2013).
39. Thomas Wurdinger, Christian Badr, Lisa Pike, Ruben de Kleine, Ralph Weissleder, Xandra O Breakefield Bakhos A Tannous A secreted luciferase for *ex vivo* monitoring of *in vivo* processes. *Nature Methods* **5**, 171–173 (2008).